Special Contract SPC-94-4086

MICROWAVE AND MILLIMETER WAVE TEMPERATURE AND HUMIDITY ATMOSPHERIC SOUNDING

FINAL REPORT:

THE ANALYSIS OF THE INFORMATION CONTENT OF OUTGOING MICROWAVE RADIATION MEASUREMENTS AND ACCURACY OF TEMPERATURE AND HUMIDITY MICROWAVE SOUNDING OF THE ATMOSPHERE

YU.M.TIMOFEYEV
E.M.SHULGINA
A.V.POLYAKOV
A.V.VASILYEV
YU.V.PLOCHENKO
A.B.USPENSKY

Research Institute of Physics
St.Petersburg State University
Ulyanovskaya, 1
St.Petersburg-Petrodvorets
198904 Russia

November 1995

St.Petersburg
Russia

REPORT DOCUMENTATION PAGE

Form Approved OMB No. 0704-0188

1. AGENCY USE ONLY (Leave blank)	2. REPORT DATE	3. REPORT TYPE AND DATES COVERED
	November 1995	Final Report

4. TITLE AND SUBTITLE

Microwave and Millimeter Wave Temperature and Humidity Atmospheric Sounding

5. FUNDING NUMBERS

F6170894W0784

6. AUTHOR(S)

Prof. Yuri Timofeyev

7. PERFORMING ORGANIZATION NAME(S) AND ADDRESS(ES)

St Petersburg State University
Atmospheric Physics Department
Ulyanovsaya 1
St Petersburg 198904
Russia

8. PERFORMING ORGANIZATION REPORT NUMBER

N/A

9. SPONSORING/MONITORING AGENCY NAME(S) AND ADDRESS(ES)

EOARD
PSC 802 BOX 14
FPO 09499-0200

10. SPONSORING/MONITORING AGENCY REPORT NUMBER

SPC 94-4086

11. SUPPLEMENTARY NOTES

12a. DISTRIBUTION/AVAILABILITY STATEMENT

Approved for public release; distribution is unlimited.

12b. DISTRIBUTION CODE

A

13. ABSTRACT (Maximum 200 words)

This report results from a contract tasking St Petersburg State University as follows: Analyze the characteristics of SSM/T1&2 sounding systems, analyze accuracy of present DMSP sounding systems and investigate the information content and optimal microwave instrument design or temperature and humidity profiling.

14. SUBJECT TERMS

EOARD

15. NUMBER OF PAGES

93

16. PRICE CODE

N/A

17. SECURITY CLASSIFICATION OF REPORT	18. SECURITY CLASSIFICATION OF THIS PAGE	19. SECURITY CLASSIFICATION OF ABSTRACT	20. LIMITATION OF ABSTRACT
UNCLASSIFIED	UNCLASSIFIED	UNCLASSIFIED	UL

ABSTRACT

The study is dedicated to analysis of the information content of outgoing microwave radiation measurements and the potential accuracy of atmospheric temperature and humidity profile retrieval for different designs of experiment.

It has been shown that, in principle, outgoing microwave radiance measurements in the 1-200 GHz spectral range contain a considerable quantity of independent components of the information (up to 30) about temperature and humidity profiles. Extracting all these information from outgoing radiance spectra (that can be achieved using optimal microwave radiometer) makes possible to retrieve the temperature and humidity profiles with errors of 0.5-1.0K and 5-10% of the H_2O mixing ratio, respectively.

CONTENT

1.INTRODUCTION

At present, satellites are an integral part of the operational atmospheric observing system. Remote sensing of meteorological parameters is a source of the information for analysis and numerical weather prediction. In spite of evident progress in elaboration of microwave atmospheric sounding systems achieved during past decades, these systems do not meet the recent requirements to the accuracy and vertical resolution of temperature and water vapor profiles, remotely retrieved.

The accuracy and vertical resolution of remote sounding microwave methods depend on many factors:

1.Measurement system characteristics - spectral region used, number and positions of the spectral intervals, their spectral resolution, instrumental noise, absolute calibration quality of outgoing radiance measurements.

2.The accuracy of radiative transfer microwave models used for description of radiation generation and transformation in the "atmosphere - underlying surface" system with due regard for molecular absorption, scattering in clouds, polarization of radiation in scattering and reflecting processes, etc.

3.The accuracy of used quantitative characteristics of the interaction between microwave radiation and atmosphere and underlying surface, namely - the O_2 and H_2O absorption coefficients, radiative characteristics of clouds and surface, etc.

4.The nature of the retrieval algorithms, i.e. the methods of the inverse problem solution.

5.The quality and volume of *a priori* information about parameters to be retrieved.

6.The state of atmosphere.

7.The methods of processing the sounding product from satellites.

All above factors can influence on a quality of retrieved data to the different degree. But undoubtedly, in our opinion, the measurement sounding system characteristics are the most effective factor. In this connection, it seems to be very important to analyze an information content of outgoing microwave radiance measurements, i.e. to determine a maximal quantity of information about atmospheric temperature and humidity profiles, being in radiance measurements , and to estimate the maximal potential accuracy of remote sensing.

To solve these problems, there has been developed a new radiative code for calculations of outgoing brightness temperature and its variational derivatives with respect to different atmospheric and surface parameters in the 1-200 GHz spectral range (MIT-SPbSU program). The program was successfully debugged and run

on the PC.

By use of this program, the dependencies of variational derivatives (temperature and humidity weighting functions) on atmospheric and surface states have been analyzed. The calculations of the covariance matrices of outgoing microwave radiance for 1500 measurement frequencies in the 1-200 GHz spectral range, simulated the "complete radiance transfer experiment", and for SSM/T, SSM/T-2 radiometers of DMSP satellite sounding system have been carried out for a case of the global statistics of the atmospheric temperature and humidity profiles. The quantities of independent information characteristics contained in radiance measurements at different measurement error levels for the above designs of the experiments have been determined by the calculations of the eigenvalues for covariance matrix of outgoing microwave radiance.

The information content of outgoing microwave radiance measurements was estimated for the complete radiance experiment and for SSM/T, SSM/T-2 radiometers (individually and in combination). The potential accuracies of atmospheric temperature and humidity profile retrievals were calculated for different measurement schemes and errors, *a priori* statistics, vertical averaging in the atmosphere.

The examples of the numerical experiments on atmospheric temperature and humidity profile retrievals are given for all examined measurement schemes. The above studies have been carried out for the cloudless atmosphere and two types of underlying surface - sea and land.

2.RADIATIVE TRANSFER MODEL OF CLOUDLESS ATMOSPHERE OVER UNDERLYING SURFACE IN THE 1-200 GHZ RANGE

2.1. Atmosphere

These studies of information content of outgoing microwave radiative measurements and potential accuracy of the temperature and humidity atmospheric sounding are based on the integral form of the radiative transfer equation. In the case of the cloudless atmosphere, outgoing radiation intensity, a radiance, can be expressed by the following form:

$$J(f) = e_f B_f[T_s]\cdot P_f(0,p_0) + \int_0^{p_0} B_f[T(p)]\cdot\frac{\delta P_f(0,p))}{\delta p}dp +$$

$$(1-e_f)\cdot P_f(0,p_0)\cdot\int_0^{p_0} B_f[T(p)]\cdot\frac{\delta P_f(p_0,p))}{\delta p}dp \qquad (2.1)$$

where e_f is a surface emissivity, B_f is the Planck function, P_f is the transmittance function, T_s and $T(p)$ are the surface temperature and the atmospheric temperature profile, respectively, p_0 is a pressure near Earth surface.

For the studied microwave spectral range, using Rayleigh-Jeans approach, the equation (3.1) can be written in terms of the brightness temperature of outgoing radiance T_B:

$$T_B(\nu) = e_f T_s\cdot P_f(0,p_0) + \int_0^{p_0} T(p)\cdot\frac{\delta P_f(0,p))}{\delta p}dp +$$

$$(1-e_f)\cdot P_f(0,p_0)\cdot\int_0^{p_0} T(p)\cdot\frac{\delta P_f(p_0,p))}{\delta p}dp \qquad (2.2)$$

The microwave atmospheric absorption spectrum (and emission spectrum) is characterized by the absorption due to molecular oxygen, water vapor, cloud and precipitation (Ulaby et.al.,1982; Stepanenko et.al.,1987; Hollweg et.al., 1994). Another minor gases in the microwave domain such as ozone, nitric acid, hydrochloric acid and chemical radicals do not influence seriously on the propagation of the radiation in the case of the nadir geometry, but they are important for slant geometry (Waters and Wofsy, 1978).

Molecular oxygen strongly absorbs due to magnetic dipole rotational transitions near 60 and 118 GHz. At altitudes below about 50 km, the pressure broadening of the lines dominates the Doppler effect, which becomes important in the middle atmosphere. At higher altitudes (>50 km), the Zeeman splitting of the oxygen becomes important.

The water vapor lines in the microwave domain are due to electric dipole rotational transitions extending into sub-millimeter region.

The resonant transition center frequencies for some of the oxygen and water vapor absorption lines are presented in table 2.1.

Table 2.1

The resonant transition center frequencies for O_2 and H_2O

(from Liebe, 1988)

Line number	Water vapor	Oxygen
	Absorption line center frequency (GHz)	
1	22.235	tens of
2	183.31	lines
3	323	at
4	325.15	50-70 GHz
5	380.20	
6	390	one line
7	436	at
8	438	118.75
9	442	
10	448	

Non-resonant (continuum) interactions of the dry air add a small contribution at high pressure in the lower atmosphere due to the Debye spectrum of oxygen below 10 GHz and pressure-induced nitrogen absorption above 100 GHz (Mingelgin,1974; Stankevich, 1974; Liebe, 1985, 1989).

To accomplish the planned studies of the information content and sounding accuracy, it is necessary to have available of a radiative transfer model for the required spectral range. In the general case, the radiative model is due to provide the calculations of the following radiation characteristics for arbitrary atmospheric and surface models in given spectral interval and with defined spectral slit function:

a).Outgoing radiance, $J_{\Delta f}(\bar{f})$ and brightness temperature $T_B(\bar{f})$;

b).Variational (functional) derivatives of outgoing radiance (and brightness temperature) with respect to the vertical profiles and parameters of the

atmospheric and surface state $\frac{\delta J_{\Delta f}(\bar{f})}{\delta X_i}\Big|_{\bar{X}_i} = A[\bar{f},p]$ and $\frac{\delta T_B(\bar{f})}{\delta X_i}\Big|_{\bar{X}_i}$.

Here Δf is considered spectral interval, $\bar{f}$ - its reference (usually, central) frequency, $\bar{X}_i$ -the vectors describing atmospheric and surface physical state, p - pressure chosen as independent spatial variable (as well as in the majority of the studies on discussed problem).

Thanks to kindness of Dr. R.McClatchey (Phillips Laboratory, Atmospheric Science Division), we have available the RADTRAN and FASCOD3P codes permitting calculations of $J_{\Delta f}(\bar{f})$ and $T_B(\bar{f})$. In the above radiative transfer codes, the blocks for variational derivative computing are absent. But keeping in mind the opportunities of variational derivative calculations by numerical methods, we have tried to use FASCOD3P and RADTRAN codes for the $J_{\Delta f}(\bar{f})$ and $T_B(\bar{f})$ calculations.

In the first stage, we would have to make sure, that our versions of these codes give the correct values of $J_{\Delta f}(\bar{f})$ or $T_B(\bar{f})$ and their variations for different atmospheric models in the given spectral range. As "a standard", we used the data of International comparisons (Chedin et al., 1988). We compared the results of calculations using FASCOD3P, RADTRAN codes and the above data (Chedin et al., 1988).

Calculations of the transmittance functions and brightness temperatures by FASCOD3P and RADTRAN codes were carried out for the following conditions:

a).Spectral range from 0.645 to 6.8 cm^{-1} with step of 0.03 cm^{-1};

b).The vertical radiation transfer, i.e. calculations of the transmittance for the whole of the atmosphere and the brightness temperature at the upper atmospheric boundary;

c).Cloudless atmosphere;

d).Surface temperature is equal to atmospheric one at the lowest level.

In the FASCOD3P program, O_2 and H_2O absorption and Voigt profile of spectral absorption line up to 64 half-width have been taken into account.

The comparisons were conducted for 4 atmospheric models (1-middle latitudes,summer; 2-middle latitudes, winter; 3-subarctic,winter; 4-tropical atmosphere) and 2 values of the emissivity (e=0.5 and 1.0).

In the Table 2.2, as an example, the results of calculated transmittance (P) and brightness temperature (T_B) comparisons for "middle latitude, summer" model and different emissivity are given.

In the Table 2.2, the differences $\delta P=P_F-P_R$ and $\delta T_B=T_F-T_R$ for a number of

frequencies are given. The subscripts F and R denote FASCOD3P and RADTRAN codes, respectively.

It can be seen from Table 2.2, for some frequencies the differences between P and T_B calculations by two codes may amount to marked values, namely, δP reaches to 0.167, and δT_B may be larger than 50K. For illustration, in Fig.2.1 a)-c) the spectral dependencies of δP and δT_B (for different emissivities) are given. The ranges of maximal transmittance and brightness temperature differences are located at about 60, 120 GHz and at some other spectral ranges.

Table 2.2

Comparison of P and T_B calculated by FASCOD3P and RADTRAN codes

Frequency,GHz	δP	$\delta T_B(e=1)$	$\delta T_B(e=0.5)$
19.34	-0.06395	-3.12	-3.45
25.63	-0.04479	-2.47	-9.47
31.93	-0.01712	-1.35	-8.84
36.42	-0.01791	-1.45	-10.28
45.42	-0.06707	-4.79	-14.62
47.22	-0.07530	-5.88	-17.76
51.71	-0.16176	-15.94	-26.44
53.51	-0.07556	-17.48	-21.42
55.31	-0.00008	1.45	1.43
58.01	0.00000	11.48	11.48
60.71	0.00000	12.79	12.79
62.51	0.00000	-13.61	-13.61
64.31	-0.00008	0.31	0.31
67.90	-0.13585	-20.51	-31.19
71.50	-0.02049	-9.21	-40.07
77.80	0.05063	-3.21	-42.04
84.09	0.10499	0.01	-46.43
92.19	0.13508	1.71	-50.03
99.38	0.15020	2.49	-52.57
105.68	0.13423	1.87	-51.79
111.97	0.08774	-0.30	-47.93
117.37	-0.12776	-23.37	-28.52
119.17	0.00341	0.64	-0.05
120.07	-0.10868	-23.42	-28.83
132.66	0.13579	1.67	-52.76
143.45	0.13574	2.02	-50.85
155.14	0.13283	2.29	-46.40
162.34	0.11527	2.25	-39.18
170.43	0.06415	2.02	-20.45
173.13	0.03771	1.89	-10.70
176.73	0.00589	1.31	-0.35
181.23	0.00000	-0.32	-0.32
185.72	0.00000	-0.04	-0.04
198.31	0.05553	2.10	-14.81
203.71	0.12962	3.12	-27.78

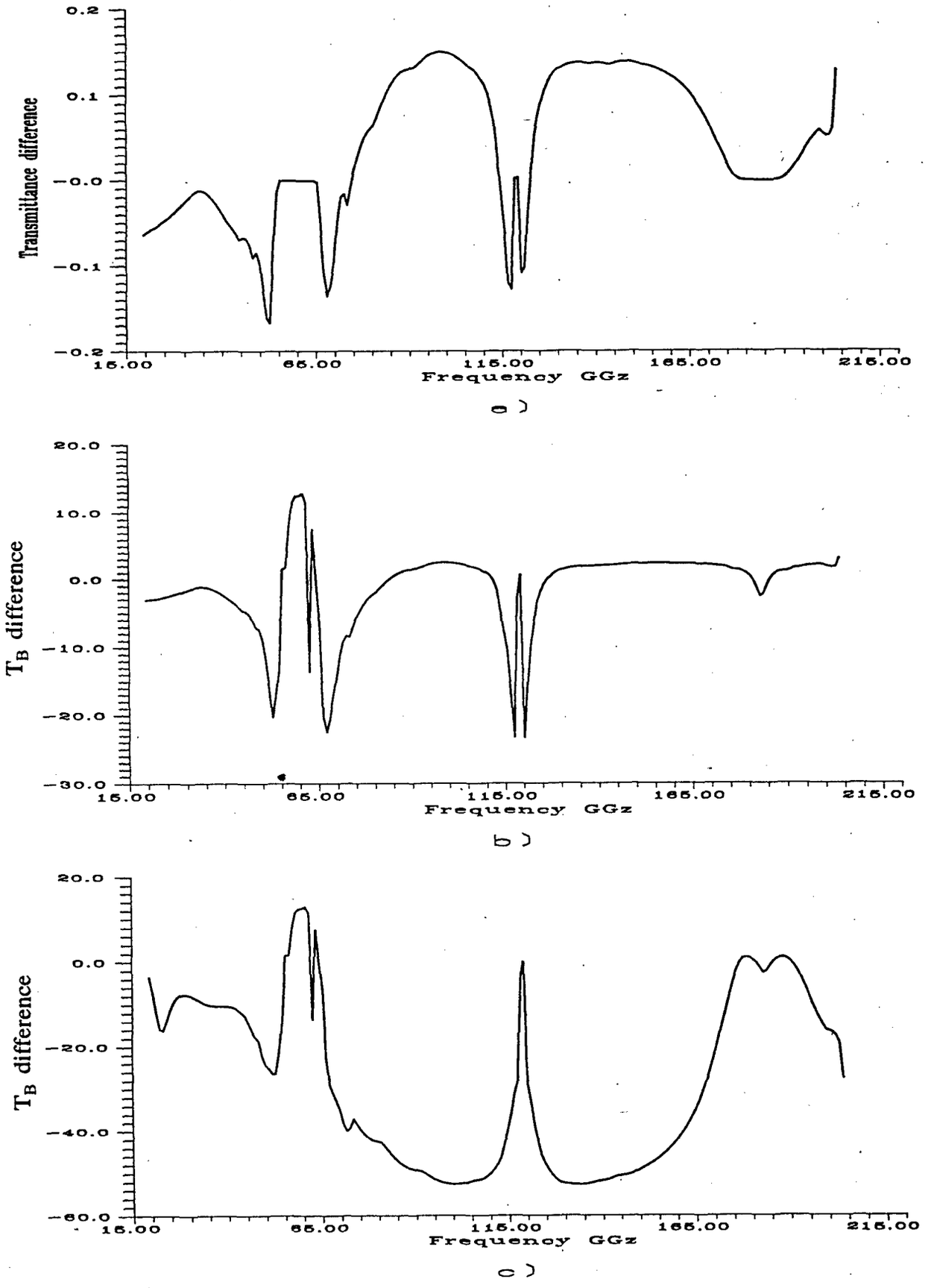

Fig.2.1.Spectral behavior of the transmittance (a) and brightness temperature (b,c) differences at surface emissivities e.
b-e=1.0; c-e=0.5.

The above analysis has demonstrated, that available FASCOD3P and RADTRAN versions give the results differing very considerably for a number cases. It testified to the necessity of additional comparisons with independent data. In Table 2.3, the comparisons between data calculated by FASCOD3P and RADTRAN codes and the results of the report about International comparisons of different codes (Chedin et al., 1988) are cited.

Table 2.3

Comparison of monochromatic brightness temperatures calculated by FASCOD3P, RADTRAN codes and the results of different participants of the ITRA (Intercomparison of Transmittance and Radiance Algorithms)

Chann.	AFGL	IAP	CNRS	MIT	FASCOD3P	RADTRAN
1		274.80	274.92		264.49	275.03
2		274.21	274.40		263.48	274.29
3		272.93	272.90		263.15	272.32
4		264.99	264.68		225.80	263.21
5		250.15	250.70		223.67	260.60
6		238.23	237.80		222.40	237.59
7		228.47	228.03		222.06	228.58
8	222.4	221.69	221.77	221.2	221.90	222.16
9	218.2	218.09	218.31	217.9	223.13	218.14
10	219.7	220.02	220.41	219.5	223.17	220.43
11	223.7	224.31	224.45	223.7	222.23	224.77
12	230.5	231.40	231.70	230.3	223.28	234.50
13	241.1	242.04	242.23	240.8	223.26	249.95
14	253.4	254.30	253.58	253.7	223.30	281.33
15,16		275.52	275.90		255.33	275.67
17		278.14	277.64		271.03	278.30
18	245.0	244.26	244.34	244.0	248.45	250.39
19	258.3	257.41	257.58	257.3	254.47	261.14
20		271.00	270.60		265.64	271.97

The channels are numbered in accordance with AMSU (Advanced Microwave Sounding Unit) channels.

Data in the table comes from the following participants of the Comparisons:

AFGL - Air Force Geophysical Laboratory, USA;

IAP - Institute of Applied Physics, University of Bern, Switzerland;

CNRS - Laboratoire De Meteorologie Dynamique Du Cent.Nat.de la Rech. Scient., France;

MIT - Massachusetts Institute of Technology, USA

It is necessary to note the evidently incorrect results of the brightness temperature (T_B) calculations for a number of frequencies by the version of

RADTRAN code, available to us:

For example:

Frequency, GHz	T_B, K
56.9678	428.76
57.6122	457.24
57.6167	289.96

It is evident, that the first two T_B values make no physical sense.

The above analysis of data calculated by available FASCOD3P and RADTRAN versions demonstrates an impossibility of their utilization (or our inability to use them) for our studies.

Therefore we developed the new own code MIT-SPbSU for $J_{\Delta f}(\bar{f})$ and $T_B(\bar{f})$ calculations on the basis of detailed radiative transfer model MIT description (Liebe et al., 1993). Simultaneously we have not only repeated the Liebe algorithm, but also have added a block for variational derivative calculations. The latter results in the suitability of our program for inverse problem modeling.

Radiative transfer model MIT is one of the latest version of MPM code (Millimeter wave Propagation Model), most widely used in practice and originally described by Liebe (1981). It has been updated several times (Liebe, 1985, 1988, 1989; Liebe and Hufford, 1989a; Liebe et al., 1989b; Liebe et al., 1991; Liebe et al., 1993) to match spectroscopic measurements of absorption, propagation delay and emission of molecular oxygen, water vapor and atmosphere. Liebe (MPM) integrates oxygen and water-vapor lines up to 1 GHz assuming Van Vleck-Weisskopf line shapes with line overlap corrections according to Rosenkranz (1975). He adds dry air and water-vapor continue which are mainly based on own laboratory measurements. A strong negative temperature dependence of the continuum absorption is included. Below 300 GHz a modified continuum reduces the line parameter base to a smaller amount of spectroscopic parameters to be considered thus reducing the computational effort when calculating transmittances and radiances.

MIT code (Liebe et al., 1993) models of the propagation characteristics of the atmosphere for the frequency range from 1 to 1000 GHz (1THz). Refractivity spectra of the main natural absorbers (i.e. oxygen, water-vapor, suspended droplets and ice particles) are computed from known meteorological variables. The primary contributions of dry air come from 44 O_2 lines. Results from extensive 60 GHz laboratory measurements of the pressure-broadened O_2 spectrum were applied to update the line data base. The water-vapor module considers 34 local H_2O lines plus continuum contributions from the H_2O spectrum above 1 THz, which are formulated as wing response of a pseudoline centered at 1.8 THz.

The authors have maintained that the new code MPM-93 reproduces the spectral characteristics of the clear atmosphere (O_2, H_2O) between 18 and 930 GHz within the in certainty limits of five reported controlled experiments (Becker and Autler,1946; Liebe, 1987; Furashov et al., 1989; Bauer and Godon, 1991; Godon et al., 1992).

The comparisons of brightness temperatures calculated by MIT-SPbSU program with the results represented in the report (Chedin et al., 1988) for a number frequencies are given in Table 2.4.

Table 2.4

Comparisons of data calculated by MIT-SPbSU program with the results of the report (Chedin et al., 1988)

Chann.	AFGL	IAP	CNRS	MIT	MIT-SPbSU(1)	MIT-SPbSU(2)
1		274.80	274.92		274.69	274.69
2		274.21	274.40		274.15	274.15
3		272.93	272.90		272.41	272.41
4		264.99	264.68		264.31	264.31
5		250.15	250.70		249.62	249.62
6		238.23	237.80		237.82	237.82
7		228.47	228.03		228.36	228.36
8	222.4	221.69	221.77	221.2	221.74	221.75
9	218.2	218.09	218.31	217.9	218.30	218.30
10	219.7	220.02	220.41	219.5	220.33	220.33
11	223.7	224.31	224.45	223.7	224.77	224.77
12	230.5	231.40	231.70	230.3	232.14	232.15
13	241.1	242.04	242.23	240.8	242.83	242.83
14	253.4	254.30	253.58	253.7	253.94	253.94
15,16		275.52	275.90		275.45	275.43
17		278.14	277.64		277.18	277.16
18	245.0	244.26	244.34	244.0	243.89	243.89
19	258.3	257.41	257.58	257.3	256.51	256.51
20		271.00	270.60		269.53	269.53

In the tab.2.4, the monochromatic value for nonmonochromatic channels is the mean of all brightness temperatures calculated for the sideband center frequencies. MIT SPbSU(1) and MIT SPbSU(2) are the values of radiance and brightness temperature, respectively, calculated by (1.1) and (2.2). Other designations are in keeping with those in tab.2.3.

It can be seen that the accordance of our results with the independent data is very satisfactory. As a rule, the differences do not exceed 1K, and those are the tenths of Kelvin in the most cases.

Developed MIT-SPbSU code was further used for studying the information content of outgoing microwave radiation measurements and to analyze a remote sensing accuracy under different designs of satellite experiments.

2.2.Surface emissivity

Most emissivity models used in practice are empirical or semiempirical ones. The review of these model has been given in our "Feasibility Study" (Timofeyev et al., 1994).

Though the use of theoretical models is more desirable, in the most cases their applying is impossible as their mathematical formulations are very complex and actual values of employing numerous parameters are unknown.

Pure empirical models are developed by fitting different functions of measurable ground truth parameters into the observed emissivity data. Unfortunately, as we have mentioned in the "Feasibility Study" (Timofeyev et al., 1994), experimental emissivity data in the examined frequency range are very limited. Semiempirical models use also some theoretical dependencies in addition to emissivity observations.

Since empirical models are received from measurements at certain conditions (frequencies, polarization, etc.), their usability is restricted. By applying semiempirical models, the range of their practical implementation may be enlargened to necessary measurement conditions.

To estimate a range of emissivity variations for different natural surfaces, we have used the semiempirical models of land and sea in available microwave frequency domain and have developed the computer programs for calculations. Only summer conditions have been examined .

2.2.1.Sea emissivity

For calm sea surface, a penetration depth is less than a half centimeter at the lowest examined frequency (Ulaby et al.,1986), and much less in the higher ones. So emission behavior of open sea water in the absence of foam is exclusively determined by the surface layer and can be calculated from the power reflection coefficients (Fresnel ones) of the surface. Their dependence on salinity, surface temperature and frequency have been well defined (e.g. Stogryn,1971; Klein and Swift,1977).

The main conclusion from the studies of calm sea surface emissivity is the following. Above 6 GHz, the only effecting parameter (in addition to angle of incidence, polarization and operation frequency) is the surface temperature.

The emissivity of wind roughened sea surface increases, that is caused by surface roughness and foam cover appearing on surface at wind speed of about 7m/c. The foam cover influence on emissivity prevails and depends on wind speed. For foam

cover influence accounting, we used a parameterization proposed by Wilheit (1979) and developed by Wilheit and Chang(1980).

Wilheit model can be applied up to 37 GHz. But since the model is based on the use of a real surface geometry, it probably can be applied within the whole of examined frequency range. Besides, a comparison of different ocean surface emissivity models with measurements given in the papers of Sasaki et al. (1987; 1988) confirmed that Wilheit model seems to be more accurate at the higher frequencies (Pulliainen et al., 1990).

In Fig.2.2 the data of sea surface emissivity calculations are given for calm sea and sea driven by wind with speeds of 20 and 40 m/c. It can be seen, that the variations of sea surface emissivity are fairly large and range from 0.07 at 3 GHz to 0.2 at 43 GHz. It seems possible to parameterize a spectral dependence of sea emissivity at high frequencies by linear function for inversion purposes. This conclusion coincides with the result of formerly study (Ferraro et al., 1986).

2.2.2.Land emissivity

To estimate the land emissivity, we have used the models of surface differing with soil texture (sand or clay), categories of roughness (smooth; low, medium or high roughness) and types of vegetation (short grass, agricultures, forest).

The emissivity of bare smooth soil is determined by dielectric properties of the target. Spectral behavior of soil dielectric constants depends, in the main, on soil moisture and, to small degree, on texture.

For our calculations we have used the laboratory data on soil dielectric constant given by Leschansky et al. (1971).

Frequency dependencies of bare smooth sand and clay surface emissivity at different moistures are given in Fig.2.3. As seen, the emissivity variations, depending on volumetric soil moisture increase from 5 to 20%, range from 0.05 at low frequencies to 0.12 at high ones.

Surface roughness results in an increase in emissivity over that of an equivalent smooth surface. One of the first practical quantitative semiempirical approaches to dealing with surface roughness was presented Choudhury et al. (1979). Emissivity of roughness surface is calculated from smooth surface emissivity using an empirically determined roughness parameter, that is proportional to the RMS height variations of the surface. The variants of this approach were proposed by Wang et al. (1980) and Konyate et al. (1981). More sophisticated models have been also studied but are lacking in verification or practicality.

Developing our computer program, we have preferred the model of Wang et al. (1980)

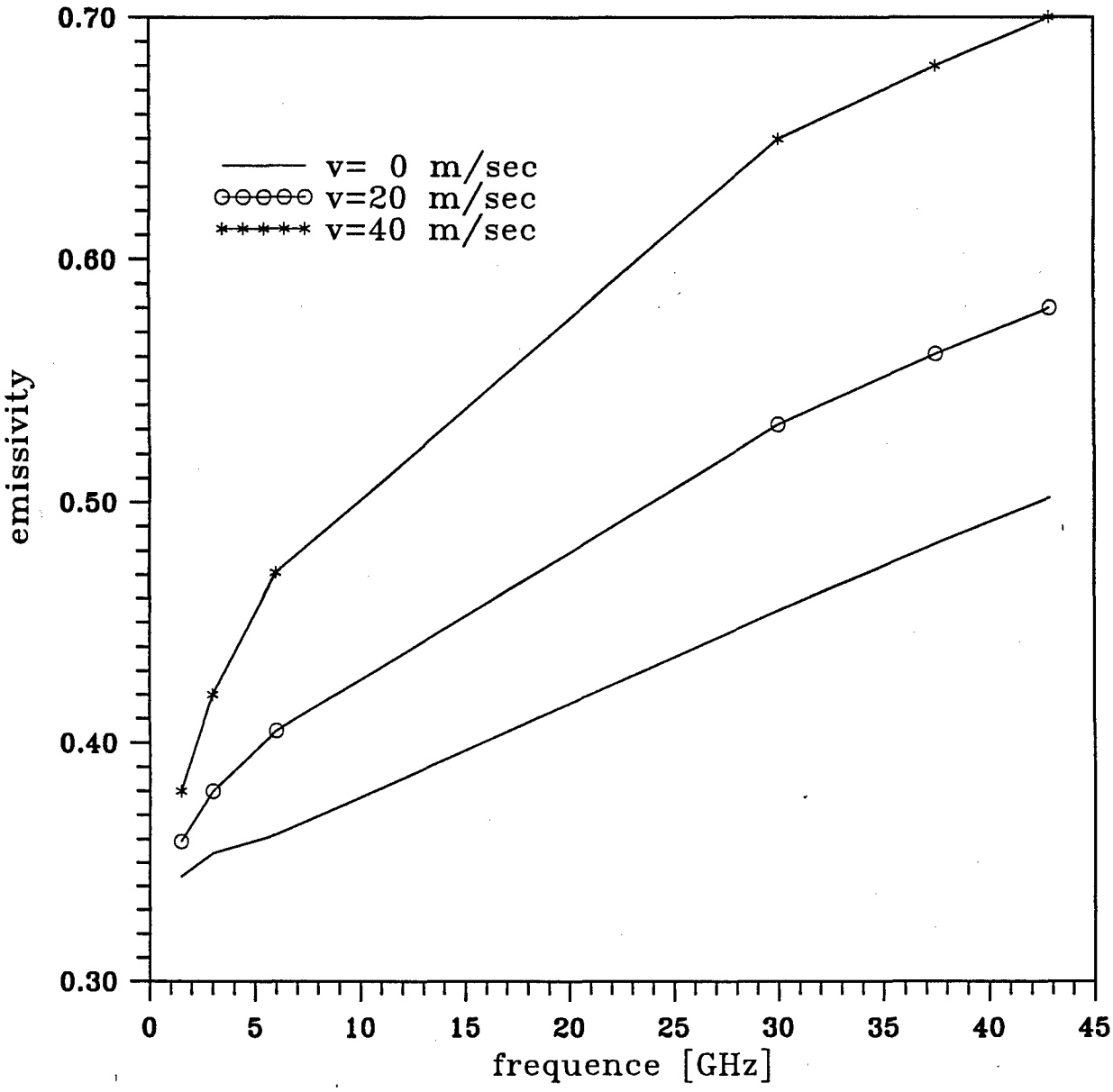

Fig.2.2.Spectral dependence of sea surface emissivity at different wind speeds v.

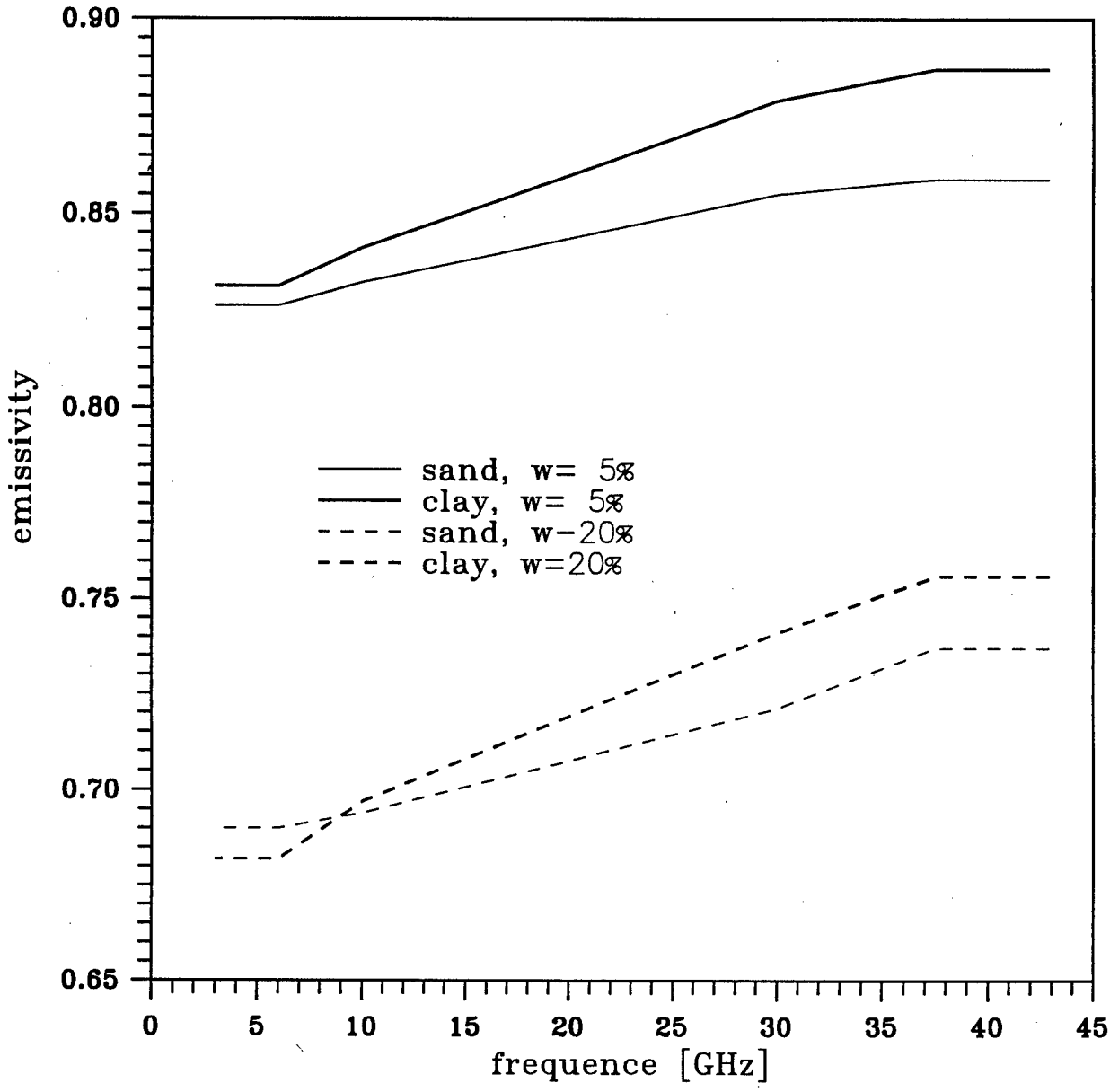

Fig.2.3.Spectral dependence of bare smooth land emissivity at different volumetric soil moisture w.

because of its better correspondence to experimental data (Promes et al., 1988; Tosellini, 1989).

Influence of surface roughness on emissivity of dry and wet sand is given in Fig.2.4. For dry fields, the effect of surface roughness on emissivity is small, but increases with soil moisture growth. Emissivity variations are about 0.04 and reach to 0.1 for dry and wet soils, respectively. At high frequencies (above 10 GHz), the spectral behavior of emissivity can be simulated as linear dependence.

A vegetation canopy over the soil increases the emissivity very strongly. A theoretical model of this process that treats the problem by using the electromagnetic relationships of a two layer incoherent nonscattering medium was developed by Basharinov and Shutko (1975). In this model the vegetation is treated simply an absorbing layer. The nature of the attenuation of this layer was modeled by Kirdiashev et al. (1979) as optical depth and vegetation wet biomass. The plant shape parameter is empirical. Naturally, there are some other studies of vegetation canopy emissivity (for example, Jackson and Schmugge, 1991; Jackson and O'Neill, 1990), but only the study of Kirdiashev give all the data needed to develop the software.

Having in mind that the natural surfaces are usually characterized by both vegetation canopy and roughness, we have developed also a joint model.

In Fig.2.5, as an example, we give the calculated spectral behaviors of surface emissivity for dry and wet roughness land covered with vegetation canopy (short grass). For comparison, the spectral dependencies of bare dry and wet soil emissivity are given in Fig.2.5 too. It can be seen from Fig.2.5, that, as it was in the previous cases, emissivity can be presented by linear spectral dependence at frequencies exceeding 10 GHz.

Summing the above estimates of emissivity variability range, it can be noted the following:

1.Emissivity models of different surfaces have been developed, tested and work well only up to about 40GHz. At higher frequencies, the influence of scattering processes on emissivity of both sea and roughness and vegetated land is very expected. Thus, further theoretical and experimental studies are needed to enhance the models at higher frequencies.

2.The case of calm sea surface is the most clear. The frequency (f) dependence of calm sea emissivity, e, can be given by linear expression (Chedin et al., 1988):

$$e = 0.362 + 0.00272\ f[GHz] \qquad (2.3)$$

3.Emissivity variations caused by wind influence can reach up to 0.2 at f=40 GHz and decrease with frequency growth.

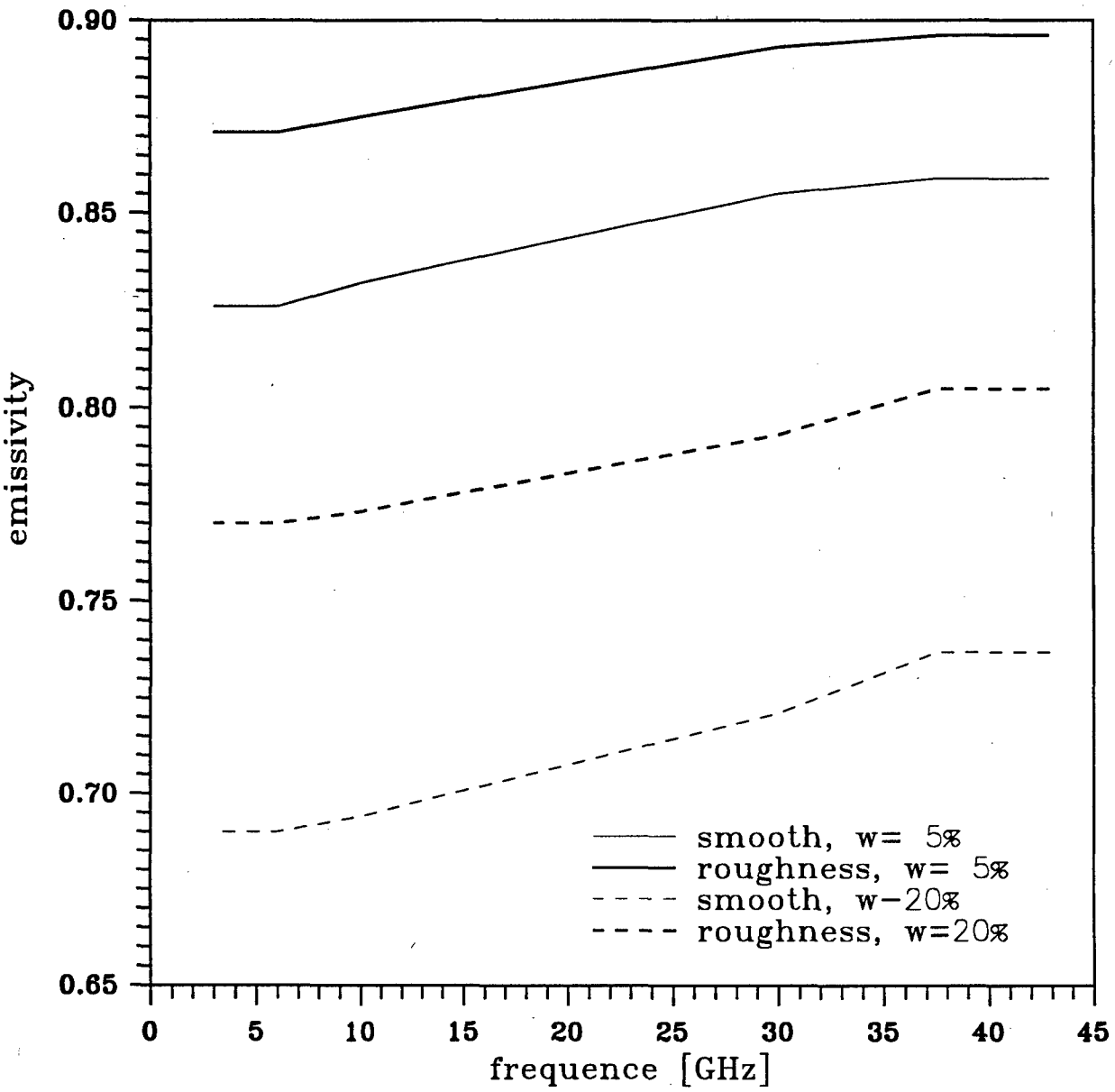

Fig.2.4.Effect of surface roughness on emissivity of dry (w=5%) and wet (w=20%) sand.

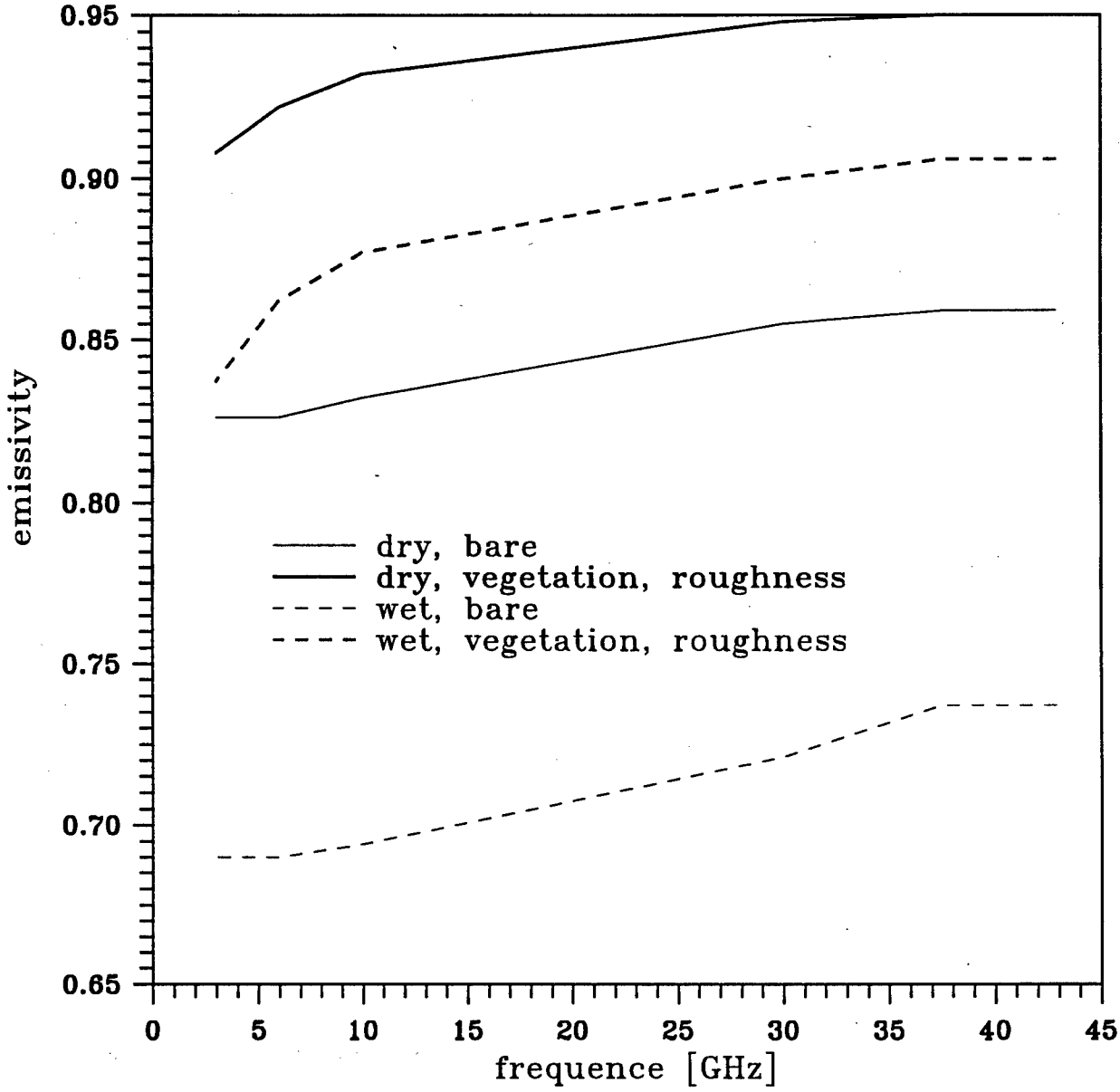

Fig.2.5.Effect of vegetation canopy (short grass) and medium roughness on emissivity of dry (w=5%) and wet (w=20%) sand.

4.Land emissivity ranges from 0.7 to 0.95 depending on soil moisture, roughness and vegetation cover.

5.At frequencies exceeding 10 GHz, spectral behavior of different underlying surfaces can be simulated by linear expressions with different slopes.

It is naturally, that for atmospheric inversion purposes, we ought not model these surface variations in full measure. In our inversion study as a first step, we simulate a spectral sea emissivity dependence by expression (2.3) to have a possibility of comparing our retrieval study with previous ones. Land emissivity is supposed to be constant and equal to 0.95. The choice of this large value of the emissivity is conditioned by desire of well distinguishing of sea and land.

2.3.Examples of variational derivative calculations by MIT-SPbSU code

To demonstrate the potential opportunities of developed MIT-SPbSU code and to analyze the connections between outgoing brightness temperature $T_B(f)$ and atmospheric temperature T(z) or humidity q(z) profiles, we give the examples of calculations of $T_B(f)$ variational derivatives with respect to T(z) and q(z).

Variational derivatives characterize (in linear approach) the sensitivity of outgoing radiance (the brightness temperature) to atmospheric parameter (temperature, humidity) variations at different atmospheric levels. It follows from Taylor-series expansion of $\delta T_B(f)$:

$$\delta T_B(f) = \int_0^{p_0} \frac{\delta T_B(f)}{\delta T(p)} \Big|_{\bar{T}(p)} \cdot \delta T(p) dp + \int_0^{p_0} \frac{\delta T_B(f)}{\delta q(p)} \Big|_{\bar{q}(p)} \cdot \delta q(p) dp \qquad (2.3)$$

which can be rewrite in the operator form as:

$$\delta T_B(f) = A_T \delta T + A_q \delta q \qquad (2.4)$$

It is necessary to note, that variational derivatives differ from so-called "weighting functions" used in some works concerning microwave spectral range (e.g. (Isaacs et al., 1987). The correct expressions for these variational derivatives has been given in paper of Timofeyev (1974). Similar "weighting functions" (those would be more properly termed as the variational derivatives) were applied by Kuo et al.(1994).

Because of numerous wrong representations especially of humidity weighting functions, we adduce here the expression for variational derivative with respect to atmospheric humidity q(z) (Timofeyev, 1974).

In linear approach, the variations of T_B (δT_B), conditioned by the deviations of

q(z), δq, from some average $\bar{q}$, may be expressed as:

$$\delta T_B = \int_0^{p_0} \left.\frac{\delta T_B(f)}{\delta q(p)}\right|_{\bar{q}(p)} \cdot \delta q(p) dp \qquad (2.5)$$

where $\left.\frac{\delta T_B(f)}{\delta q(p)}\right|_{\bar{q}(p)} = \tilde{A}_q$ is humidity variational derivative.

By use of (2.3), one can receive for $\tilde{A}_q$:

$$\tilde{A}_q = \sum_{i=1}^{5} A_{qi} \qquad (2.6)$$

$$A_{q1}(p) = -e\left\{T_s - T(p_0)\right\} \frac{\bar{P}(p_0)k(p)}{g}$$

$$A_{q2}(p) = -\frac{k(p)}{g}\int_p^{p_0} \frac{\delta T(p')}{\delta p} \bar{P}(p')dp'$$

$$A_{q3}(p) = 2(1-e)T(p_0)k(p)\frac{\bar{P}^2(p_0)}{g}$$

$$A_{q4}(p) = (1-e)k(p)\frac{\bar{P}(p_0)}{g}\int_0^{p_0} \frac{\delta T(p)}{\delta p} \bar{P}^*(p)dp$$

$$A_{q5}(p) = (1-e)k(p)\frac{\bar{P}(p_0)}{g}\int_0^{p} \frac{\delta T(p')}{\delta p} \bar{P}^*(p)dp',$$

where

$$P(p) = \exp\left[-\frac{1}{g}\int_0^p k(p)q(p)dp\right];$$

$$P^*(p) = \exp\left[-\frac{1}{g}\int_p^{p_0} k(p)q(p)dp\right];$$

k(p) - the absorption coefficient, e - the emissivity, T_s - the surface temperature, g - free fall acceleration, q(p) - specific atmospheric humidity.

In Fig.2.6, there are shown the monochromatic $T_B(f)$ variational derivatives with respect to T(z) for 7 frequencies corresponding to SSM-T channels. Fig.2.6 demonstrates the vertical opportunities of temperature sounding using outgoing radiative measurements in the O_2 band and fairly uniform covering of all height ranges by variational derivatives for different frequencies.

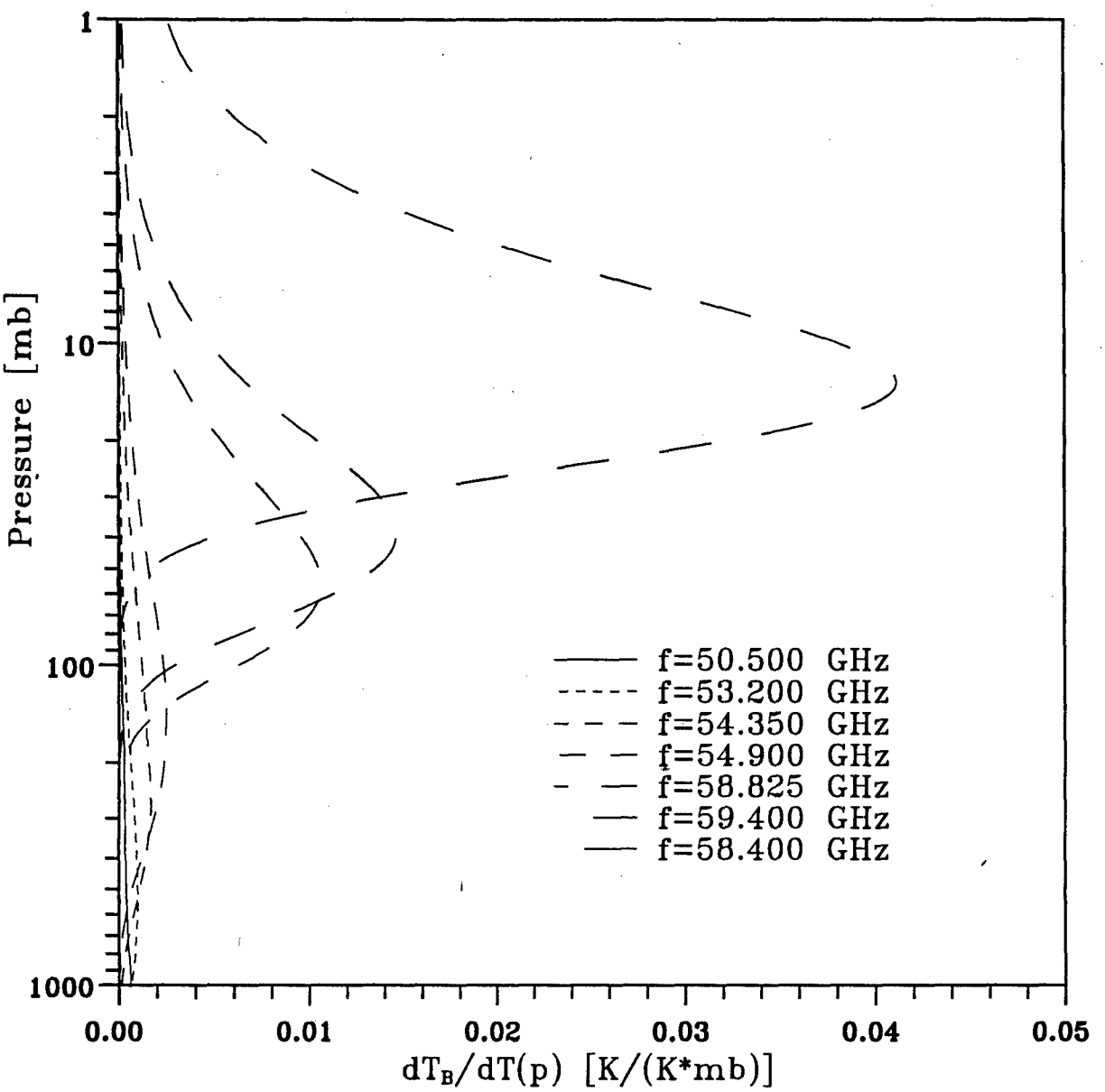

Fig.2.6. Variational derivatives of brightness temperature with respect to atmospheric temperature profile. Atmospheric model – middle latitudes, summer; surface emissivity is 0.95 (land); $T_s=T_{1013}=294.2K$.

It is worth noting a growth of maximal derivative values with pressure decrease. It is caused by choice of pressure as a parameter. To remove an illusory unequivalence of the variational derivatives, those are to be multiplied by the pressure. Then the variational derivatives will be illustrate the influence of parameter variations in the layers of equal thickness (regardless of pressure) on brightness temperature.

To illustrate the above arguments let us compare Fig.2.6 with Fig.2.7 representing the same derivatives but multiplied by corresponding pressures. It is evident, that the latter figure is more informative and all following data concerning both temperature and humidity profiles will be expressed in terms of this product, named by proper "weighting functions".

To illustrate surface influence on $T_B(f)$ derivatives, Fig.2.8 gives a comparison the temperature weighting functions calculated with the values of surface emissivities typical for land and sea. The differences have been observed only for three examined frequencies, therefore in Fig.2.8 the rest curves are absent. As it was expected, the surface influence on the temperature weighting functions is the larger than the derivative maximum is the nearer to the Earth surface. The curve differences are observed only for the pressures which are larger than 100 mb, that let us conclude that the uncertainties in surface emissivity will not influence an accuracy of temperature retrieval in higher atmospheric layers.

It is paid attention an extraordinary, at first sight, behavior of the temperature weighting functions with negative values near surface for the frequency of 50.5 GHz. This appearance is caused by a strong temperature dependence of water vapor absorption near Earth surface. In this spectral range, the absorption, and atmospheric radiance respectively, decreases abruptly with temperature increase. When surface emissivity is equal to 0.95, this effect is masked by dominant contribution of surface emission into outgoing radiance and, as a consequence, into temperature weighting function. It is worth to note, that such strong dependencies of variational derivatives on the atmospheric state testify to poor applicability of purely linear approach for the solution of the inverse problem and to the necessity of using the iterations.

Fig.2.9 describes an influence of the surface temperature or the difference between surface and atmospheric near surface layer temperatures (ΔT) on temperature weighting functions. The results are given for two frequencies only, as the influence is not observed for other examined ones. It is seen the negligible variation of derivative values even for temperature differences of 10K.

To analyze the influence of different atmospheric parameters on the temperature

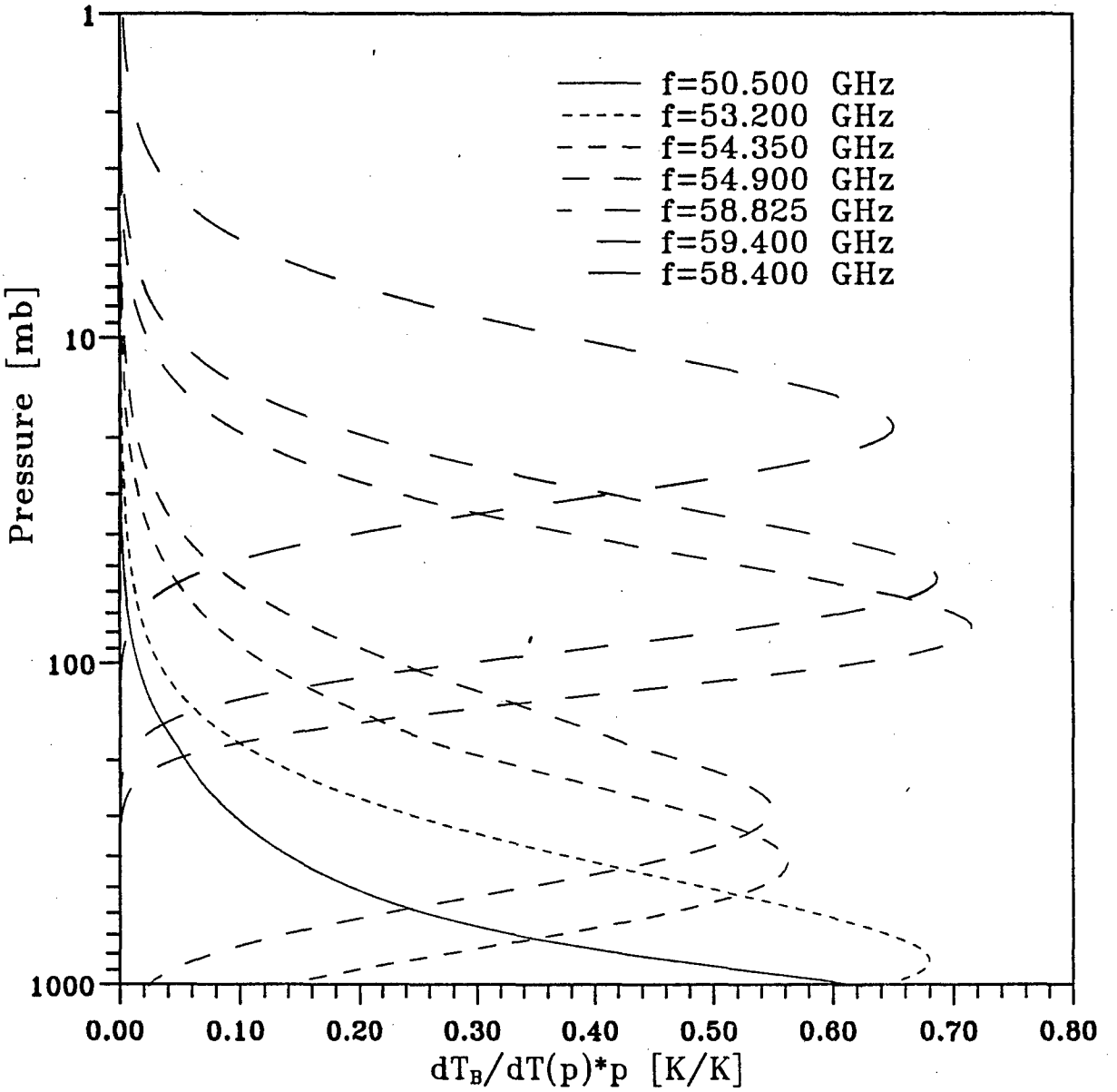

Fig.2.7.Temperature weighting functions for different frequencies.
Atmospheric model – middle altitudes, summer; surface emissivity is 0.95 (land);
$T_s=T_{1013}=294K$.

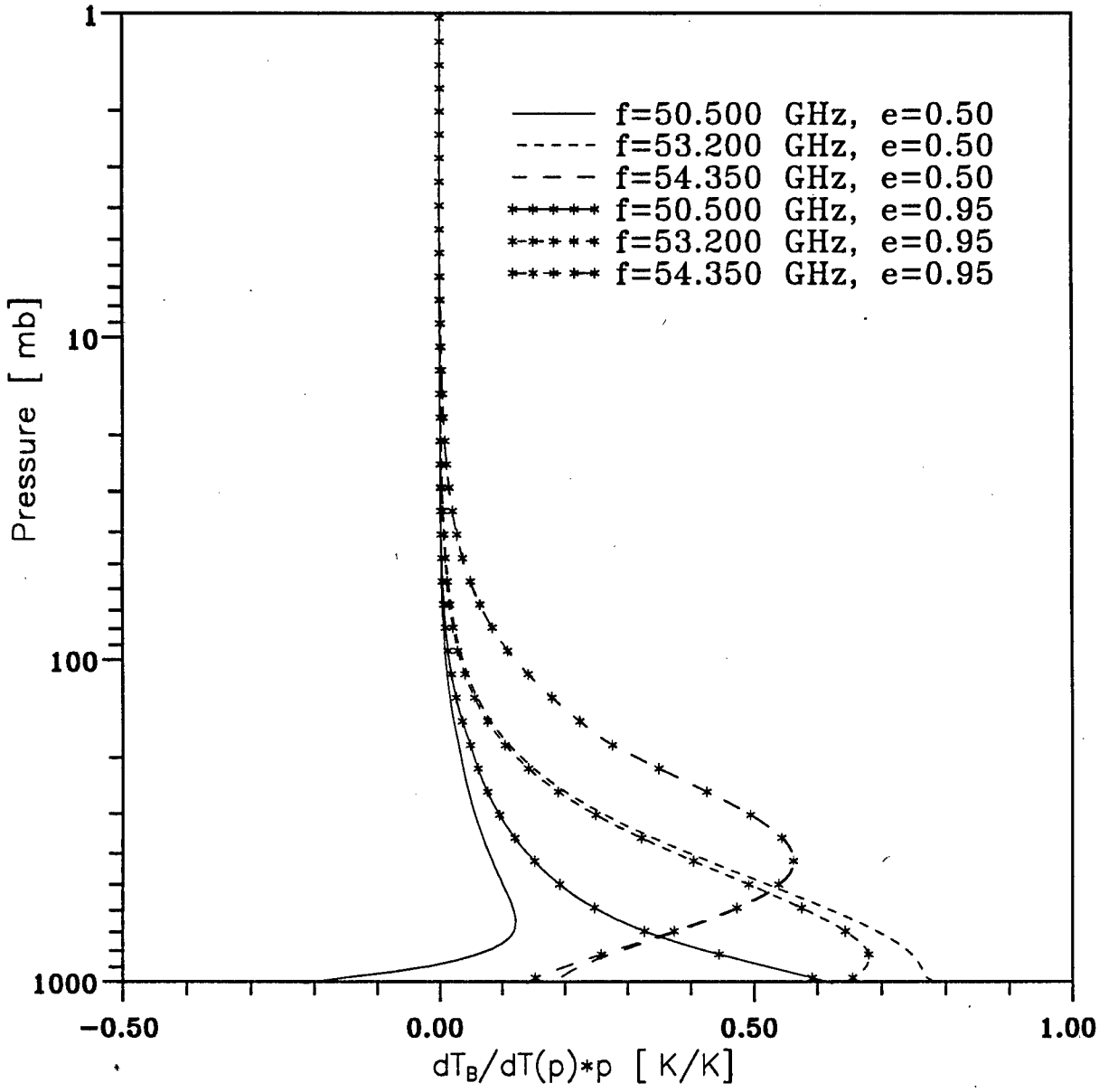

Fig.2.8. Influence of surface emissivity on temperature weighting functions for different frequencies. Atmospheric model – middle latitudes, summer; surface emissivity: 0.95 – land, 0.5 – sea; $T_s=T_{1013}=294.2K$.

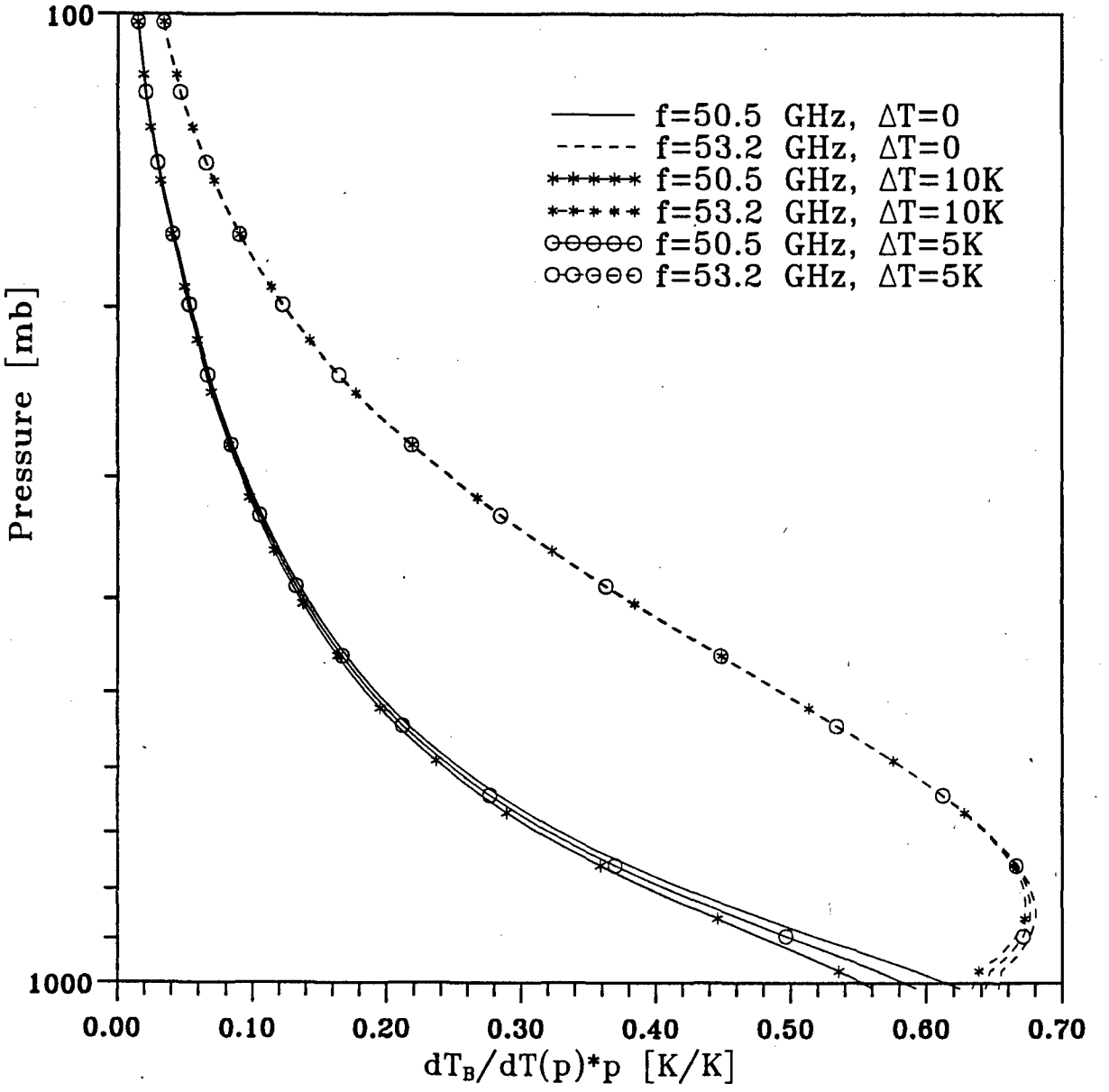

Fig.2.9. Influence of surface temperature on temperature weighting functions for different frequencies. Atmospheric model – middle latitudes, summer; surface emissivity – 0.95 (land); T_{1013}=294.2K.

weighting functions, we carried out the calculations for a number of simulated T(z) and q(z) sets. Fig.2.10 illustrates the influence on temperature weighting functions caused by changing the summer T(z) for middle latitudes by winter one, Fig.2.11 and 2.12 show the effect of the same change of q(z), and both T(z) and q(z) profiles, respectively.

Joint analysis of these three figures makes possible to conclude the following:

1.Temperature profile variations slightly influence the temperature weighting functions because of weak atmospheric transmittance dependence on the temperature.

2.Humidity profile variations effect the temperature weighting functions in the layers below pressure level of 100 mb, and relative variation of derivative values may achieve to about 20%.

3.Under joint changes of temperature and humidity profiles, these effects are added together.

As a whole, the fulfilled analysis let us conclude that temperature weighting functions slightly depend on different parameters of the atmospheric layers with the exception of the near surface atmospheric layers characterizing by the strong influence of surface emissivity and atmospheric humidity on microwave radiance transfer. It means, that the methods based on linearization may be used (taking into account the above remark about near surface layers) for atmospheric temperature profile retrieval.

Analyzing the humidity variational derivatives (variational derivatives with respect to humidity profile) we dealt with those multiplied by the pressure values as it was justified previously. In addition, it is more visual to deal with relative water vapor variations at each level instead of with absolute atmospheric water vapor content. This approach is justified by the proportionality of water vapor variability to average value of mixing ratio (which is strong varies with altitude) at each level. In Fig.2.13 and 2.14 to illustrate these aspects, we give the variational derivatives of outgoing brightness temperature with respect to water vapor mixing ratio profile and those multiplied by the pressure and H_2O mixing ratio and named as "relative humidity weighting functions". The weighting functions, represented here and later, are calculated for frequencies corresponding to three SSM/T-2 channels located near the H_2O absorption line of 183.310091 GHz, to two its channels near 90 and 150 GHz and to the center of the above line. Let us analyze an influence of different parameters on variational derivatives of outgoing brightness temperature with respect to H_2O content profile.

The influence of surface emissivity appears only for two examined frequencies,

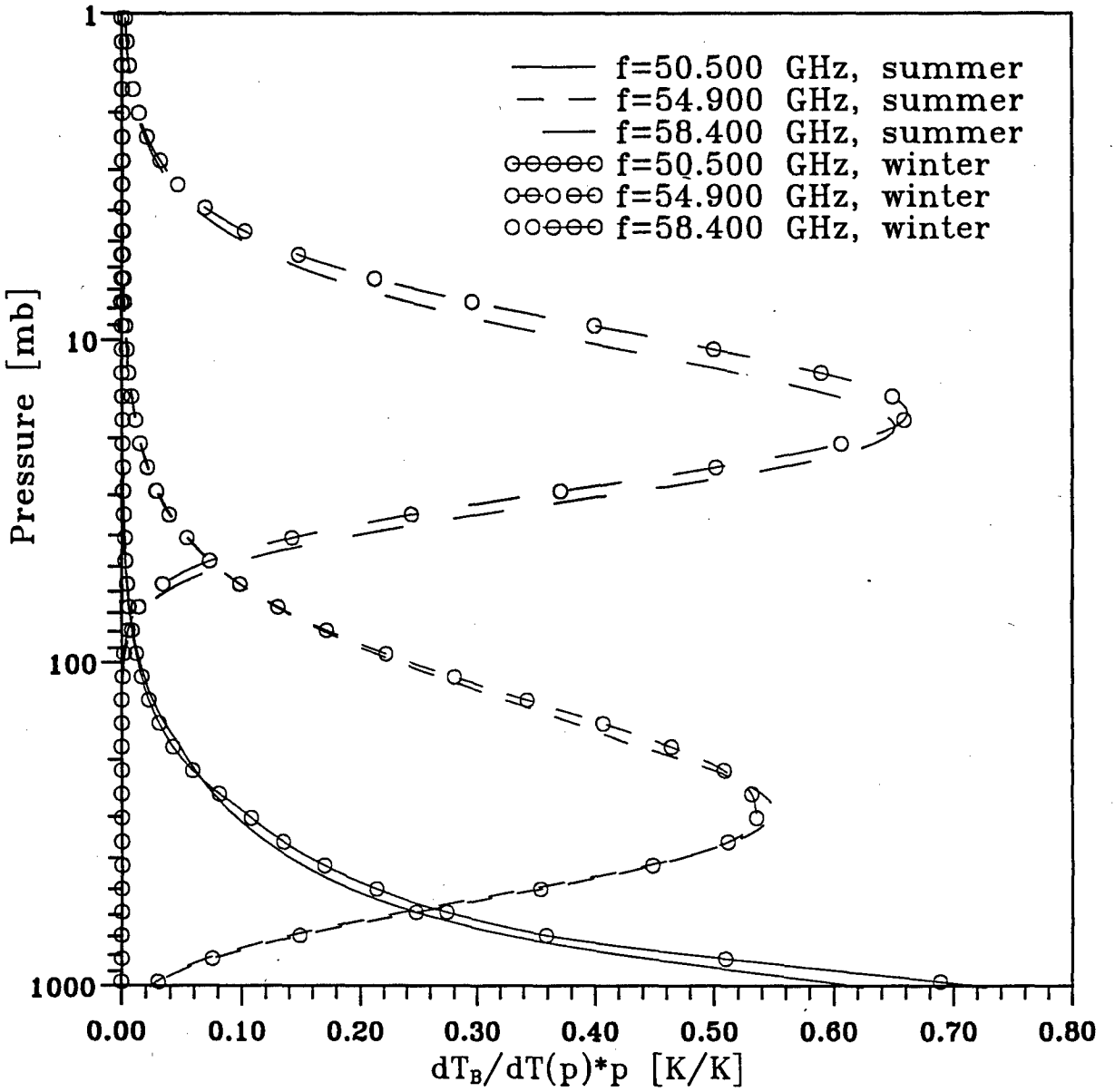

Fig.2.10. Influence of atmospheric temperature profile on temperature weighting functions for different frequencies.
Atmospheric model – middle latitudes, summer; surface emissivity – 0.95 (land);
$T_S = T_{1013}$.
Atmospheric temperature profile corresponds to summer or winter model for middle latitudes.

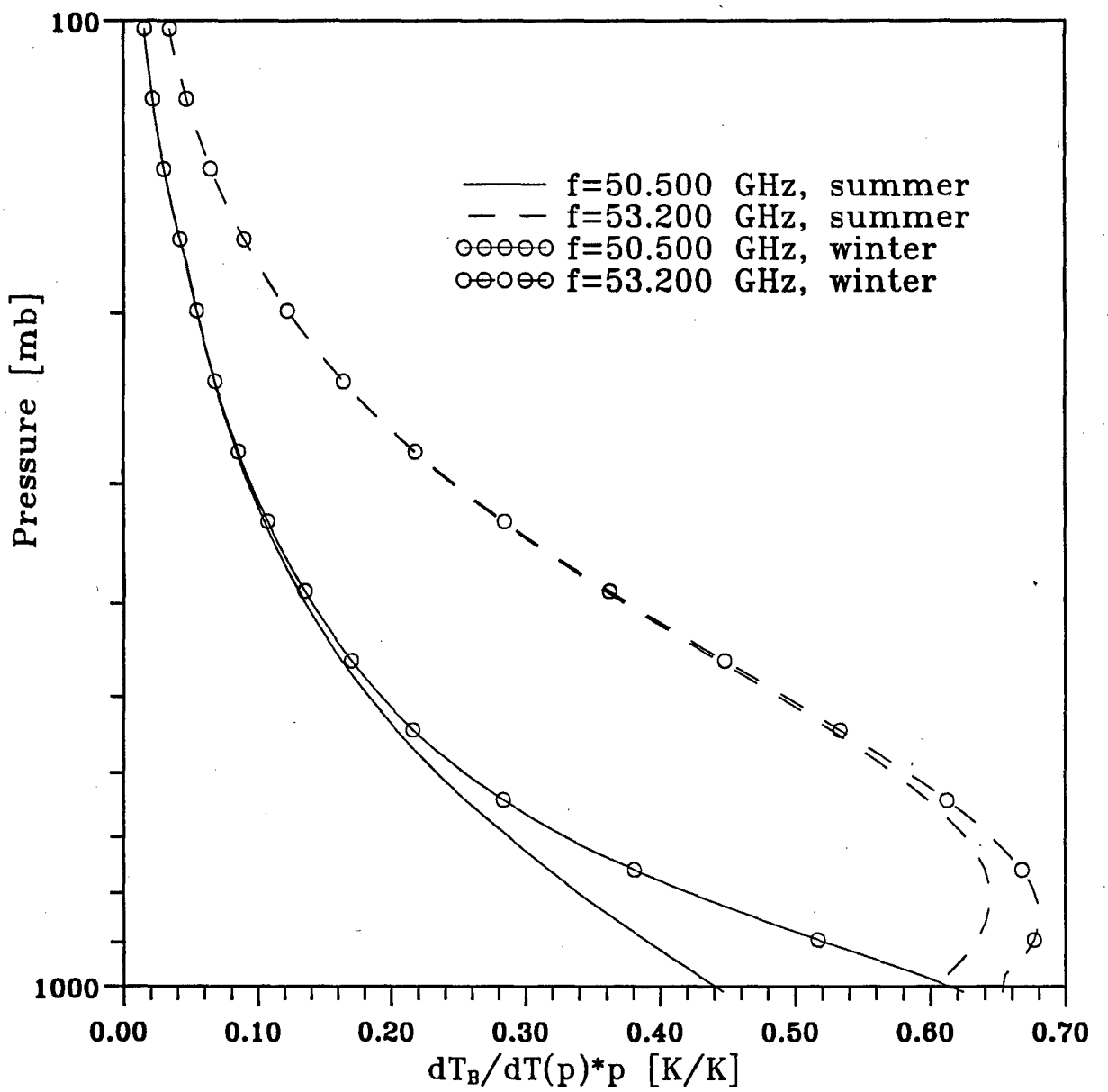

Fig.2.11. Influence of atmospheric humidity profile on temperatu weighting functions for different frequencies. Atmospheric model – middle latitudes, summer; surface emissivity – 0.95 (land); $T_S=T_{1013}$. Atmospheric humidity profile corresponds to summer or winter model for middle latitudes.

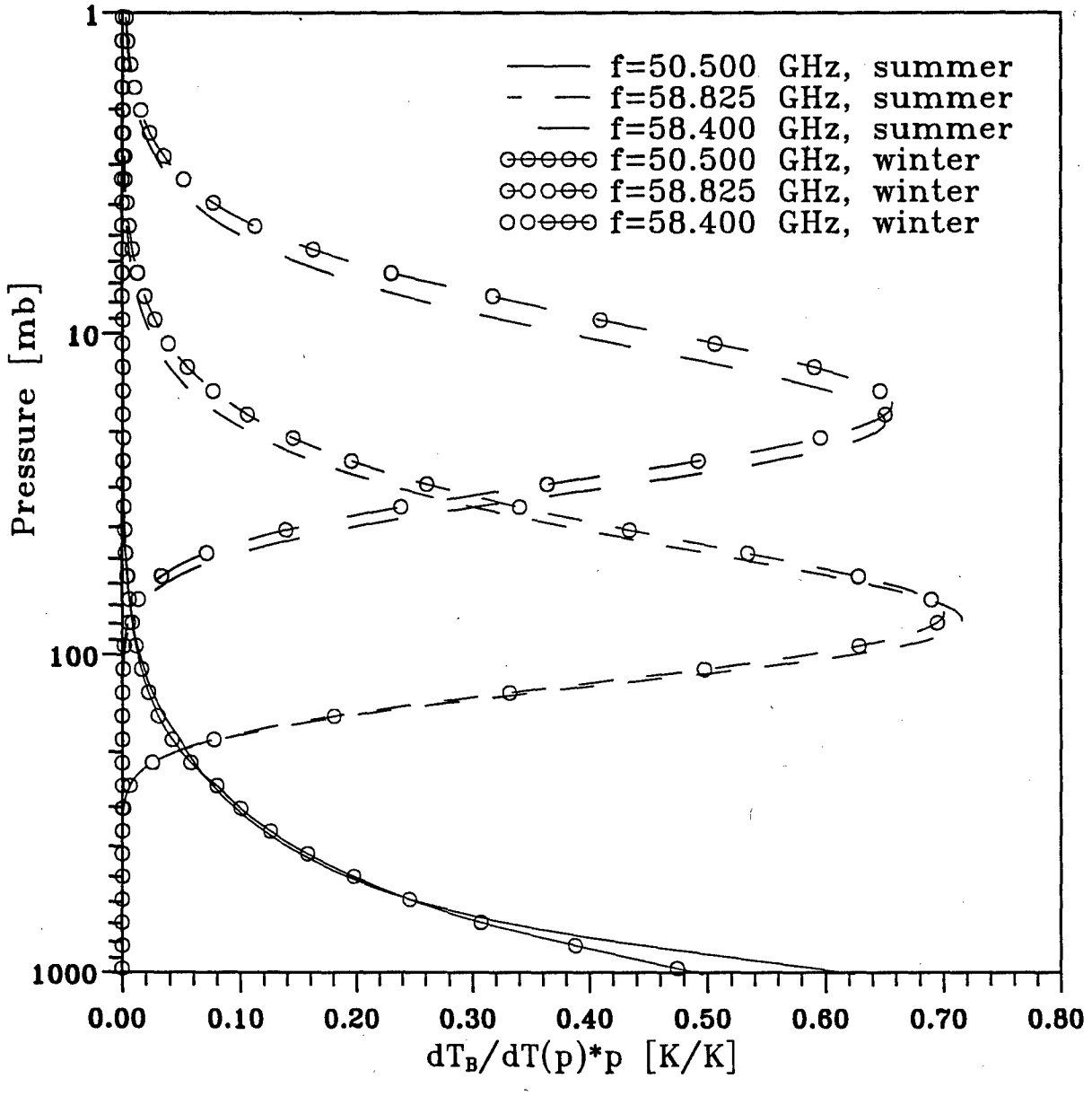

Fig.2.12. Influence of atmospheric state on temperature weighting functions.
Atmospheric models–middle latitudes, summer or winter; surface emissivity – 0.95 (land);
$T_S=T_{1013}$=294.2K (summer) or 272.2K (winter).

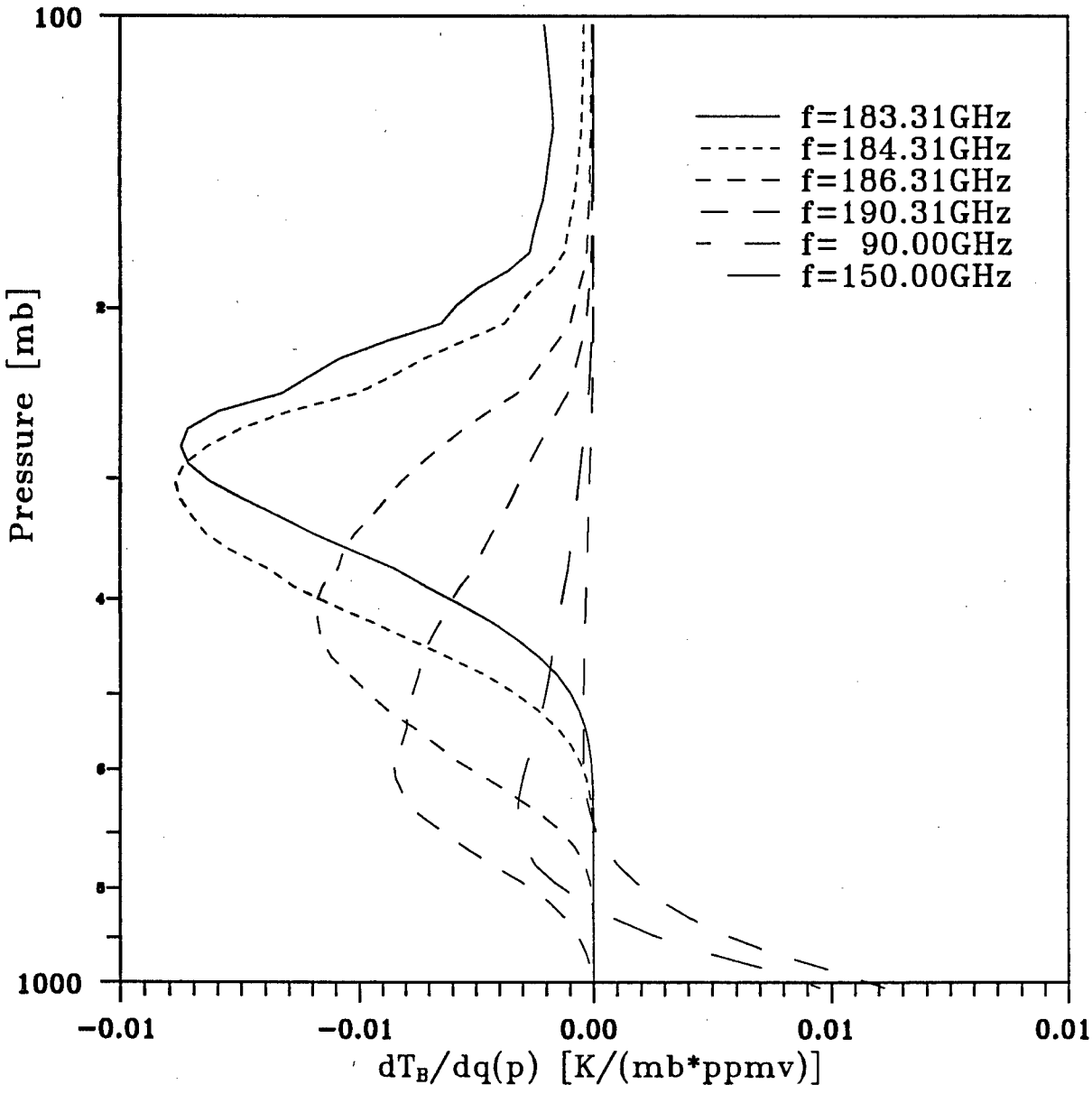

Fig.2.13. Variational derivatives of brightness temperature with respect to water vapor mixing ratio variations for different frequencies.
Atmospheric model – middle latitudes, summer;
$T_s=T_{1013}=294K$.

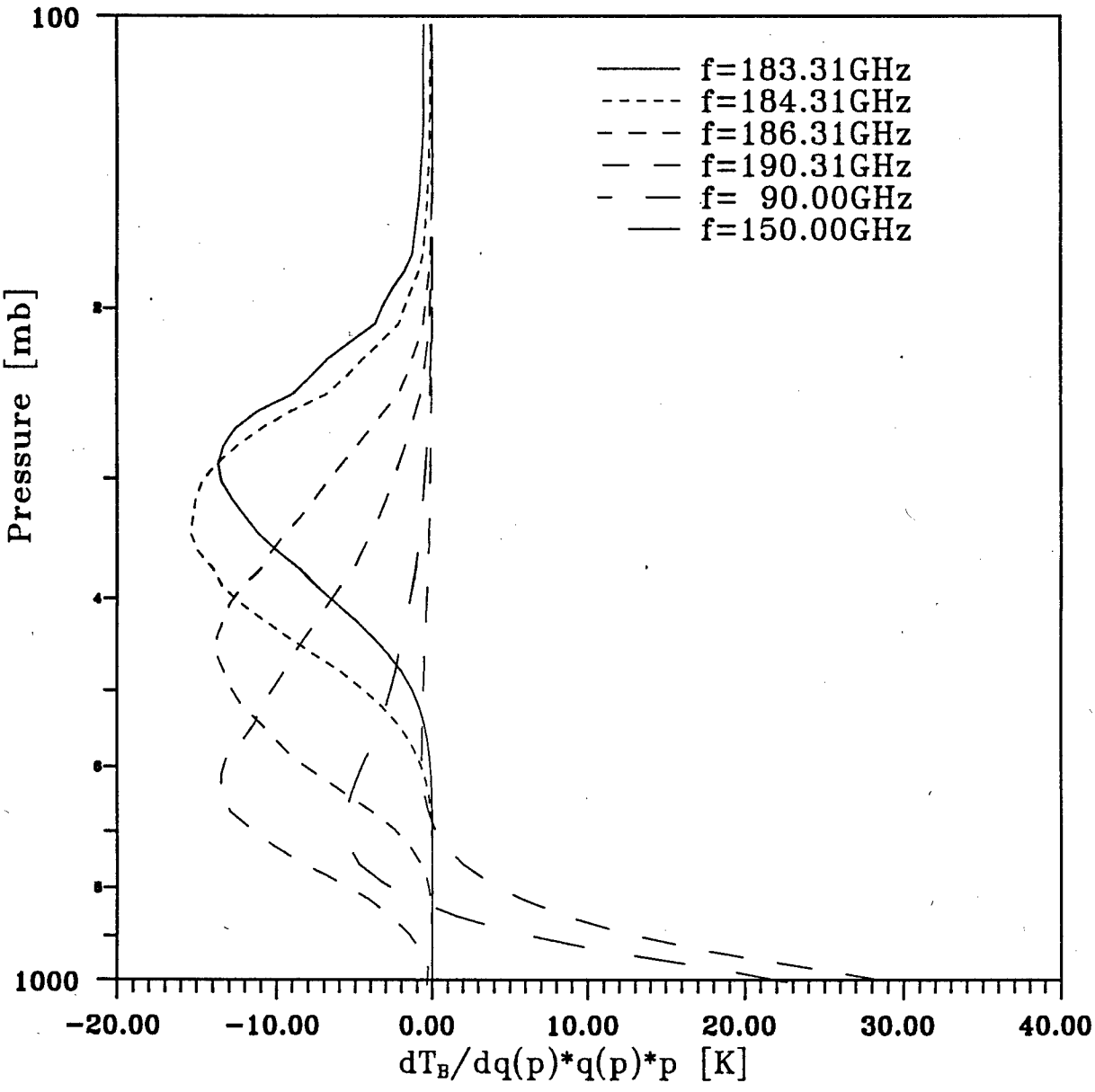

Fig.2.14. Relative humidity weighting functions for different frequencies.
Atmospheric model – middle altitudes, summer;
$T_s=T_{1013}=294K$.

corresponding the relative humidity weighting functions are given in Fig.2.15. It may be seen the strong dependence of the relative humidity weighting functions on the surface emissivity. Their values increase in three, when surface emissivity varies from 0.95 to 0.75. This effect is caused, evidently, by increasing the atmospheric contribution into outgoing radiance with decreasing the surface emissivity and may be analyzed quantitatively on the basis of Eqs. (2.5)-(2.6).

Fig.2.16 demonstrates also a marked dependence of the relative humidity weighting functions on the difference between near surface atmospheric temperature and surface one (ΔT). The increase of this difference from 5 to 10K results in relative growth of derivative values by tens of percentages.

To analyze an influence of different atmospheric parameters on the relative humidity weighting functions, we have fulfilled the calculations for various sets of simulated T(z) and q(z) profiles.

Fig.2.17 illustrates the influence on the relative humidity weighting functions due to a change of summer T(z) for middle latitudes by winter one, Fig.2.18 and 2.19 show the effect of the same change of q(z), and both T(z) and q(z) profiles, respectively.

Joint analysis of these three figures makes possible to conclude the following:

1.Temperature profile effects the relative humidity weighting functions noticeably for all three examined channels. At some levels, the derivative values may vary by the factor of two.

2.Humidity profile influences the relative humidity weighting functions very strongly. It is observed the variations of derivative values by several orders of magnitude, the shifts of derivative maxima by values about 100 mb and the change of derivative signs due to humidity profile variations.

3.The joint variations of T(z) and g(z) amplify mutually these effects.

These results demonstrate that inverse problem with respect to humidity profile is strongly nonlinear.

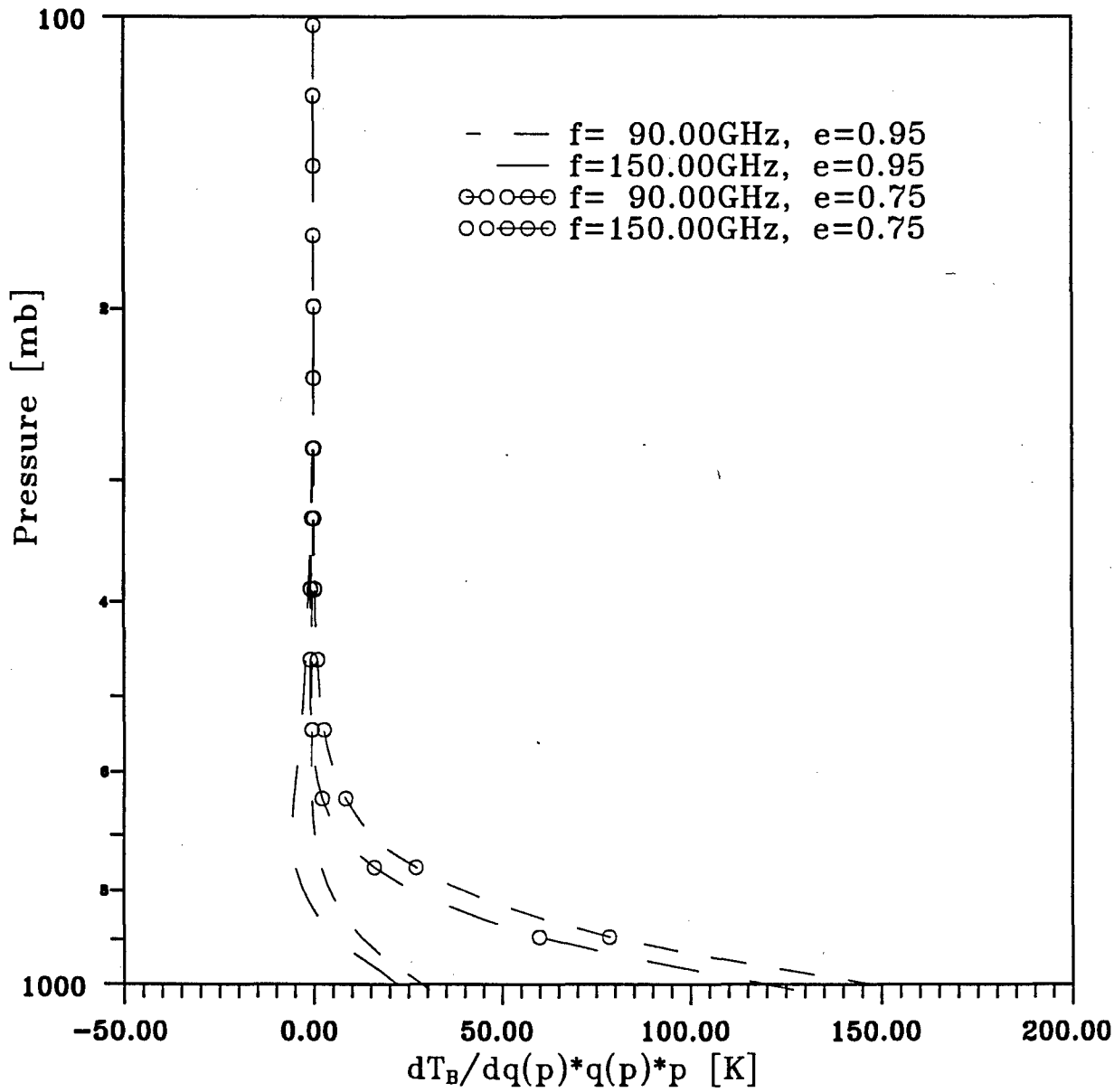

Fig.2.15. Influence of surface emissivity on relative humidity weighting functions for different frequencies. Atmospheric model – middle latitudes, summer; surface emissivity e = 0.95 (land), 0.75 (sea); $T_S=T_{1013}=294K$.

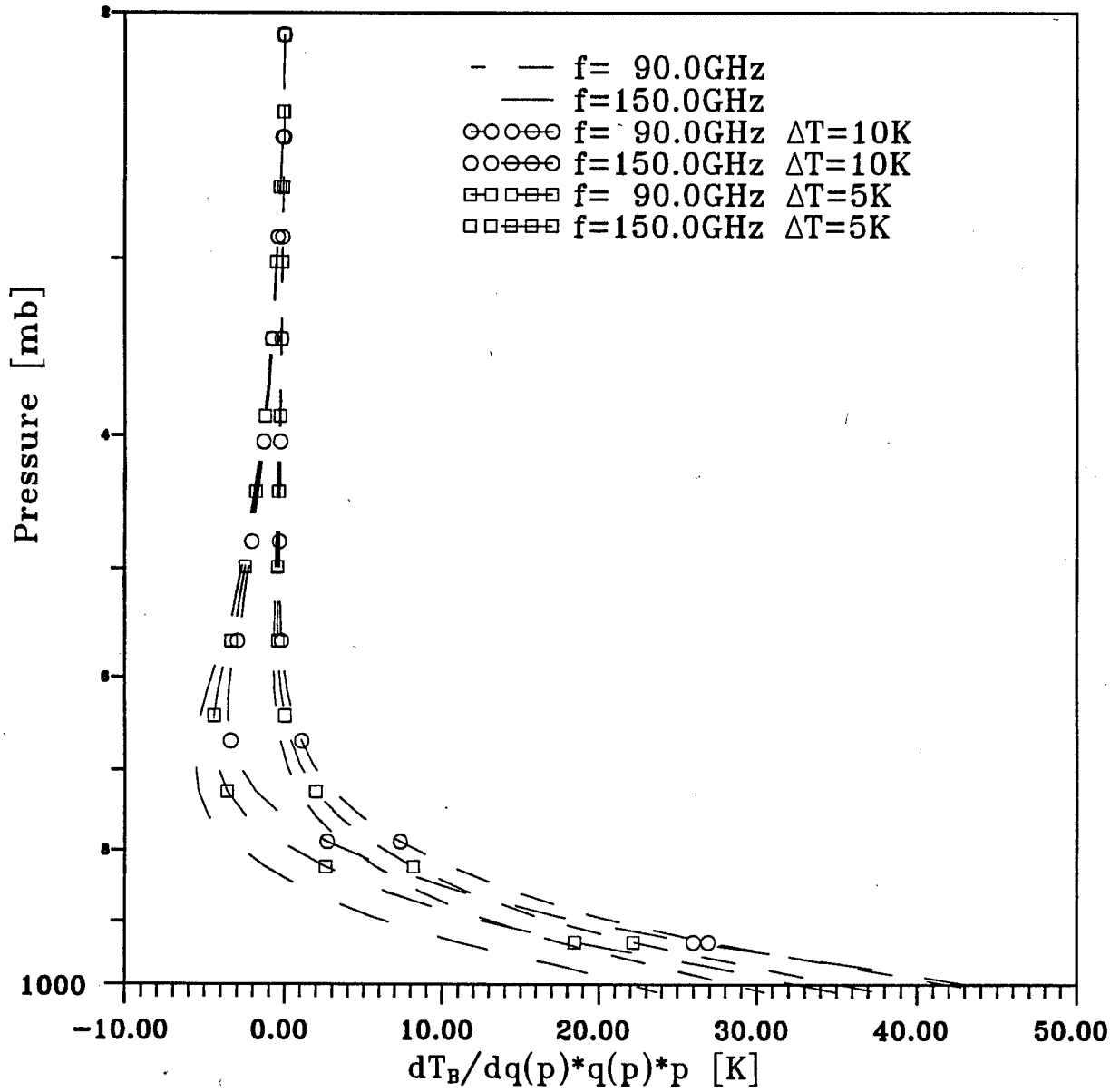

Fig.2.16. Influence of surface temperature variations (T) on relative humidity weighting functions for different frequencies.
Atmospheric model – middle latitudes, summer; T_{1013}=294K.

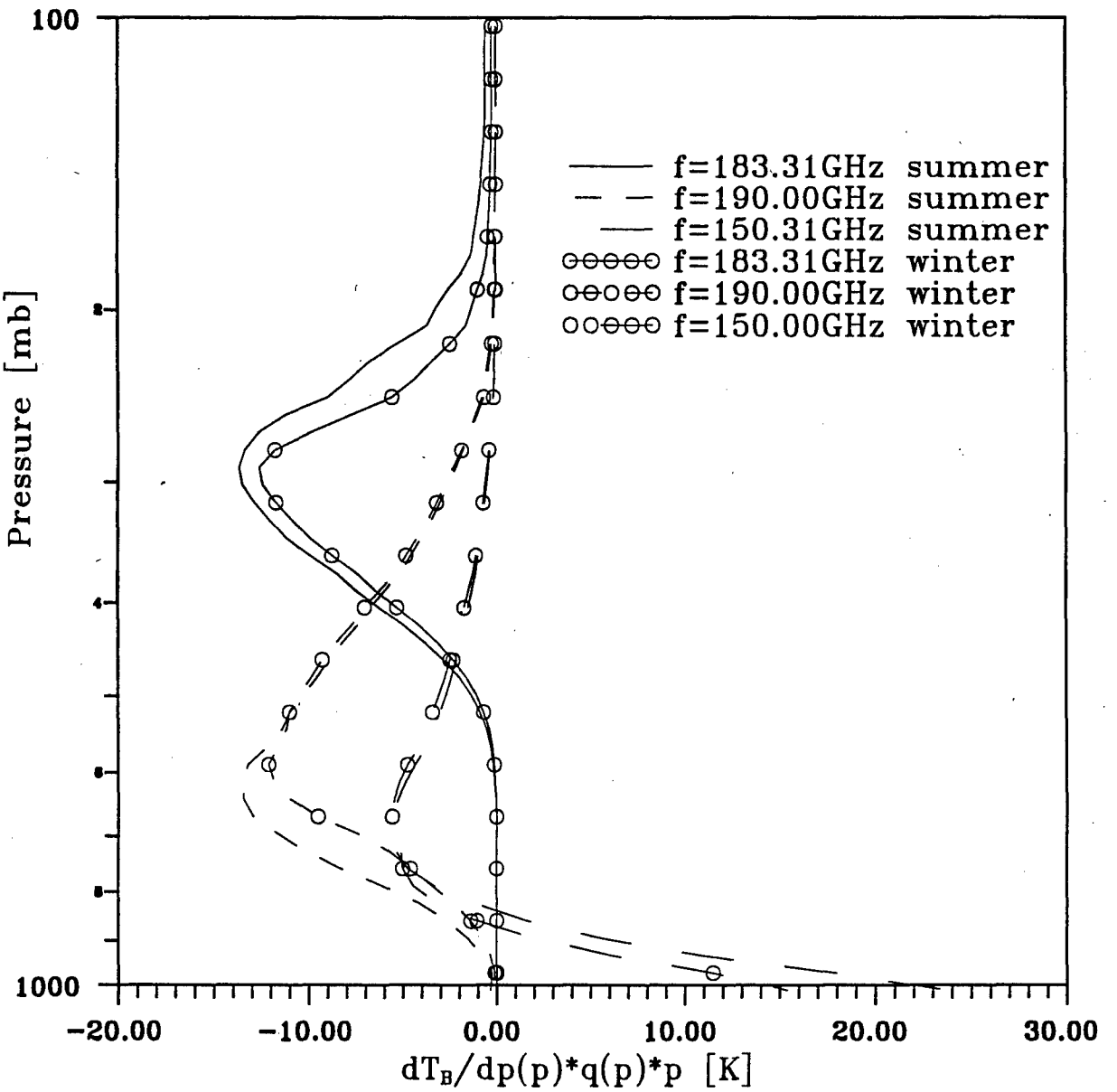

Fig.2.17. Influence of atmospheric temperature profile on relative humidity weighting functions for different frequencies.
Atmospheric model – middle latitudes, summer; $T_S=T_{1013}$.
Temperature profile corresponds to winter or summer model for middle latitudes.

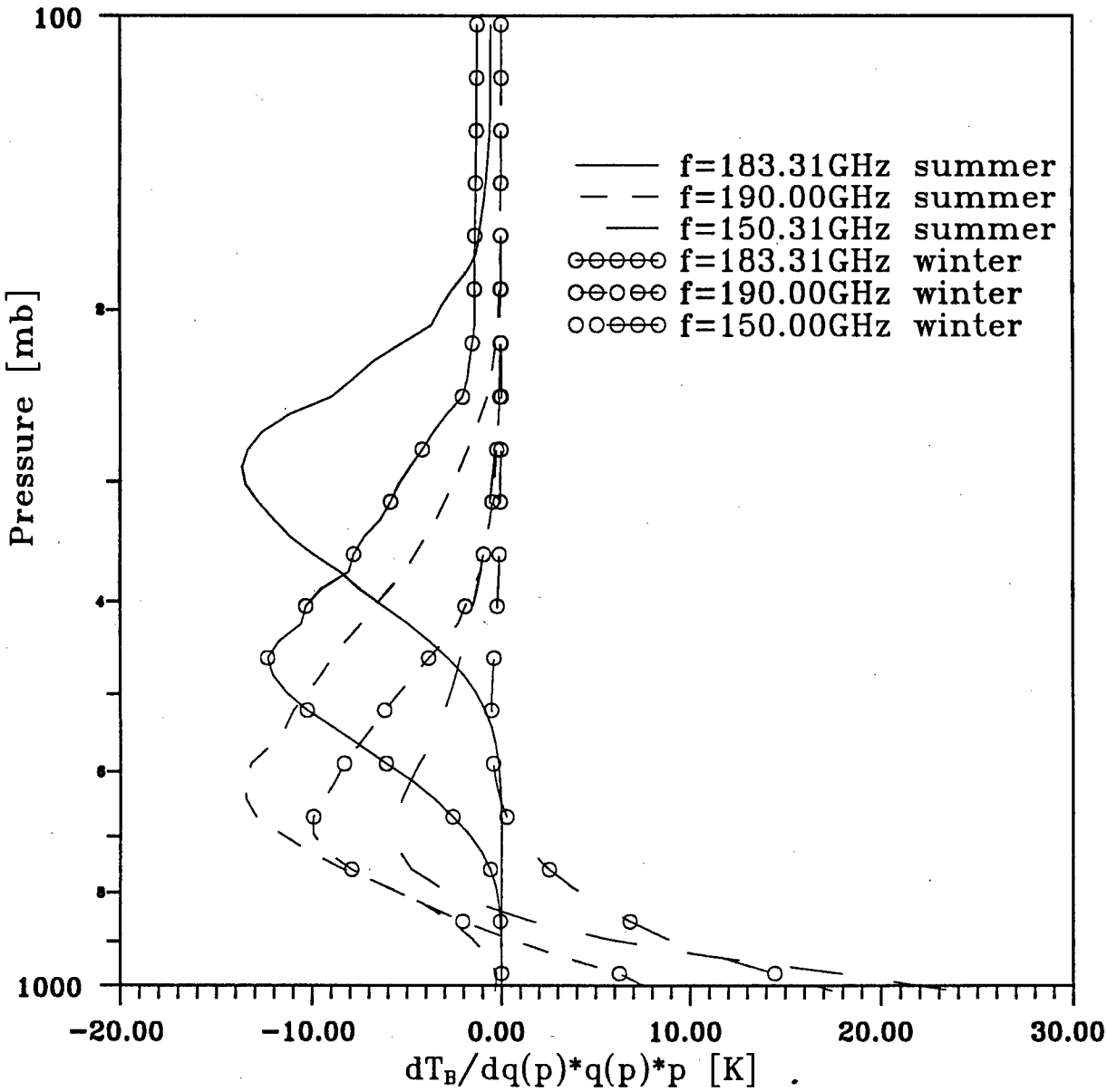

Fig.2.18. Influence of atmospheric humidity profile on relative humidity weighting functions for different frequencies. Atmospheric model – middle latitudes, summer; $T_S=T_{1013}$.
Humidity profile corresponds to summer or winter models for middle latitudes.

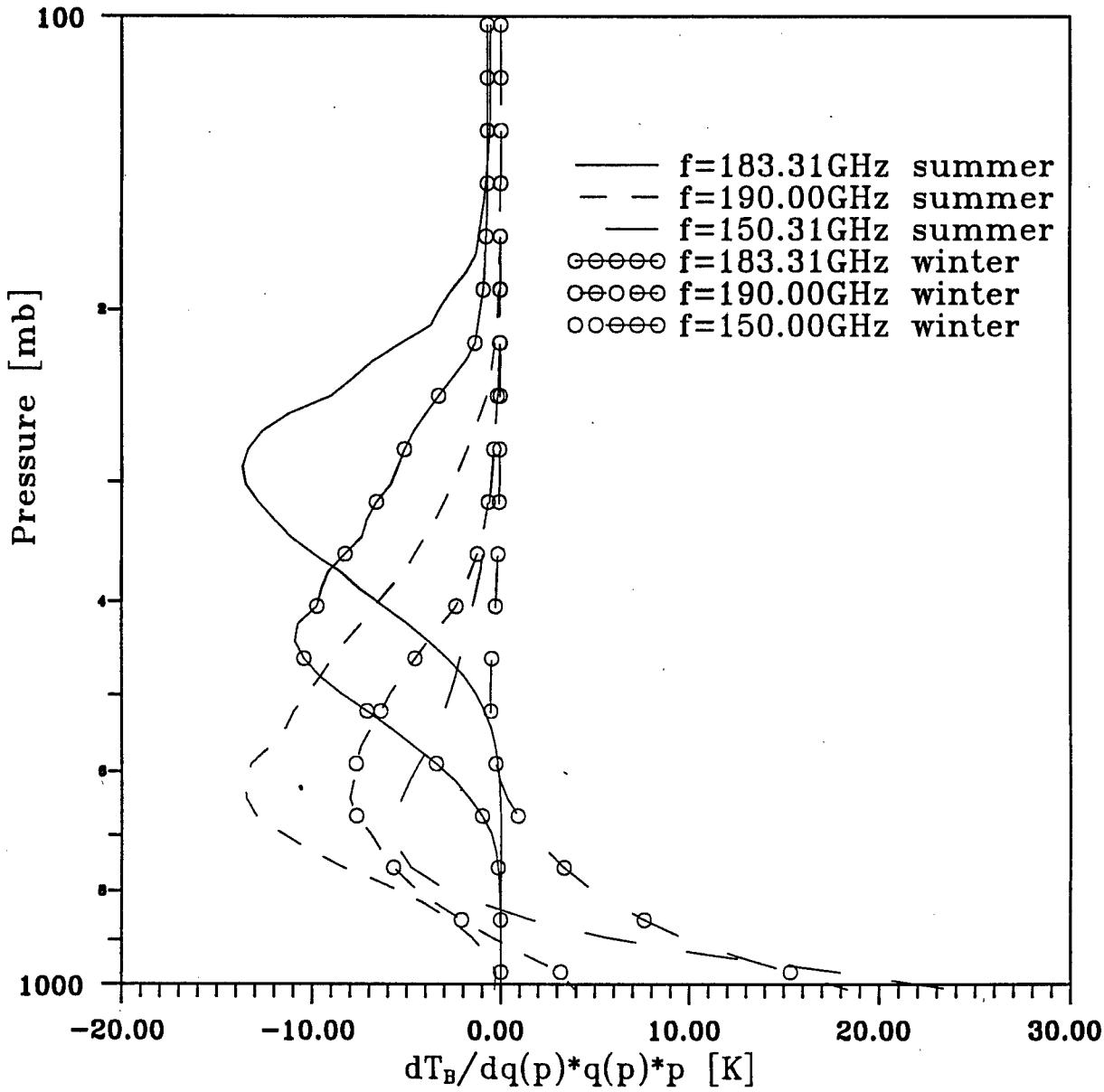

Fig.2.19.Influence of atmospheric model on relative humidity weighting functions for different frequencies. Atmospheric models–middle latitudes, summer or winter; $T_S=T_{1013}$.

3.CALCULATIONS OF INFORMATION CONTENT OF OUTGOING MICROWAVE RADIANCE MEASUREMENTS

3.1.Information content of remote sensing measurements

To compare the different spectral designs of the measurements, it is necessary to know the basics of the quantitative methods for estimation and comparison of the measurement efficiencies.

Let us consider the most-used lines of relevant approaches.

The inverse problem of remote atmospheric sensing is a solution of the operator equation:

$$\mathbf{y} = \mathbf{A}\mathbf{x} + \varepsilon \tag{3.1}$$

where **x** is the vector of sought parameters (atmospheric temperature and humidity profiles and surface temperature in the case discussed); **y** is the vector of quantities to be measured by spectral device; **ε** is the vector of measurement noise. The operator A describes the radiative transfer process and links the atmospheric state parameters x_i with radiative characteristics y_j measured by a device. (i=1,2,...m; j=1.2...n; where m is the number of parameters, describing the atmospheric state; n is the number of the measurements.)

In this treatment of the linear statistical method, **A** is assumed to be linear.

The every sets of the sought atmospheric parameters will be considered to belong to the vector space X. And the vector space Y will be considered to contain the sets of the measured values and measurement noise.

The noise ε is usually assumed to be distributed normally with the ensemble average $\bar{\varepsilon}$ and covariance matrix Σ:

$$\bar{\varepsilon} = E\varepsilon \equiv 0; \qquad \Sigma = E\varepsilon\varepsilon^{+} \tag{3.2}$$

where E is the sign of expectation value, and sign + refers to the matrix or vector transposition.

At present, the numerous methods to find a stable solution of the Fredholm equation of the first kind (3.1) have been developed. One of the commonly used inversion method is the statistic regularization techniques (method of optimal estimation) proposed independently by several authors (Strand and Westwater, 1968; Turchin et al., 1968; Turchin and Nozik, 1969; Rodgers, 1970, 1971, 1976, 1990).

To solve ill-posed problem (3.1) requires regularizing the equation on the basis of additional information about decision.

In the linear statistical method of the regularization, the decision is assumed to belong to an *a priori* statistics, defining the average vector of physical state parameters $\bar{x}$, and its covariance matrix **K** describing a natural variability of the sought parameter profiles:

$$\bar{x} = Ex; \quad \mathbf{K} = E(x - \bar{x})(x - \bar{x})^{+} \tag{3.3}$$

The covariance matrix **K** defines the valuation $\|x - \bar{x}\|_{K^{-1}}$ characterizing a departure of vector **x** from the statistics (3.3):

$$\|x - \bar{x}\|^{2}_{K^{-1}} = (x - \bar{x}, \mathbf{K}^{-1}(x - \bar{x})) \tag{3.4}$$

Then the estimate $\tilde{x}$ of regularized problem (3.1) can be obtained by joint minimizing the least-square fit to the measurements **y** and the least-square fit to the statistical mean $\bar{x}$:

$$\|y - A\tilde{x}\|^{2}_{\Sigma^{-1}} + \|\tilde{x} - \bar{x}\|^{2}_{K^{-1}} \Rightarrow \min \tag{3.5}$$

or, what is the same,

$$(y - A\tilde{x}, \Sigma^{-1}(y - A\tilde{x})) + (\tilde{x}, \mathbf{K}^{-1}\tilde{x}) \Rightarrow \min \tag{3.6}$$

(For simplicity in (3.6) and further we have neglected by the shift transformation of X and Y spaces, i.e. substituted, for example, $x - \bar{x}$ by x).

Minimizing (3.6) with respect to x yields:

$$\mathbf{G}\tilde{x} + \mathbf{K}^{-1}\tilde{x} = \mathbf{A}^{+}\Sigma^{-1}y \tag{3.7}$$

where $\mathbf{G} = \mathbf{A}^{+}\Sigma^{-1}\mathbf{A}$ is the Fisher matrix.

From (3.7) one can receive the following expressions for the retrieval estimate $\tilde{x}$ and its covariance error matrix **D**:

$$\tilde{x} = \bar{x} + (\mathbf{G} + \mathbf{K}^{-1})^{-1}\mathbf{A}^{+}\Sigma^{-1}y \tag{3.8}$$
$$\mathbf{D} = (\mathbf{G} + \mathbf{K}^{-1})^{-1}$$

To estimate the accuracy of the linear solution and the information content of the measurements, V.P.Kozlov (1966) have brought into existence the matrix **C**, named as "information matrix":

$$\mathbf{C} = \mathbf{KG} \tag{3.9}$$

If $\mathbf{u}_i$ and λ_i are the eigenvectors and eigenvalues of the matrix $\mathbf{C}$ ($\mathbf{Cu}=\lambda\mathbf{u}$), then the coefficients b_i in expansion of vector $\mathbf{x} = \sum_{i=1}^{m} b_i\mathbf{u}_i$ are incorrelated with each other and independently estimated values.

There exist a variety of approaches to estimate the information content of the measurements (Westwater and Strand, 1970; Houghton et al., 1986). We have used two definitions of information content proposed by Shannon (Shannon and Weaver, 1949) and Kozlov (Kozlov, 1966).

The information content, according to Shannon, may be regarded roughly as the number of bits needed to represent the number of distinct measurements that could have been made. This is computed as (Houghton et al., 1986):

$$I = 0.5 \sum_{1}^{m} \log_2(1+\lambda_i) \qquad (3.10)$$

The "information volume", according to Kozlov, is defined as (Kozlov, 1966):

$$V = \sqrt{\prod_{\lambda_i > 1} \lambda_i} \qquad (3.11)$$

Evidently, when calculating the information volume, we use only eigenvalues which are greater than 1 and correspond to the information components distinguished at given level of the measurement error. The point is that each atmospheric remote sensing measurement is practically unique, and statistical selection of the signal components which are smaller, than measurement error, is impossible. And consequently, the information volume, according to Kozlov, may be regarded as the number of atmospheric states distinguishable by used measurement device and may reach to very large magnitudes.

Another usefull measure of information content (named as "Kozlov factor") is the number of eigenvalues exceeding in magnitude 1. This factor is the quantity of independent information components that could have been derived from the measurements performed with given error.

It is evident, that in the case of uncorrelated measurement error (i.e. if $\Sigma = \sigma^2\mathbf{I}$, where $\mathbf{I}$ is the unit matrix), the above eigenvalues λ_i and eigenvectors u_i are connected with eigenvalues μ_i and vectors ϕ_i of the covariance matrix of measured quantity $\mathbf{K} = E(yy^+)$ by the simple relations:

$$\lambda_i = \mu_i/\sigma^2, \qquad \phi_i = \Sigma^{-1}\mathbf{A}u_i \qquad (3.12)$$

(In discussed case $\mathbf{K} = E(yy^+)$ is $\mathbf{K}_{T_BT_B} = E(T_BT_B^+)$.)

The above expressions for the information content estimations have been defined for the case of linear operator **A**. As a rule, in the atmospheric applications, the problem is described by linear approach only with some error. Nevertheless, in view of Eq.(3.12), we can use **K** matrix calculated with regard for nonlinear relations between outgoing radiance and atmospheric parameters to estimate the information content *I* and information volume *V*.

3.2.The basis for the calculations of outgoing microwave radiance information content

The radiative transfer model described in the Chapter 2 was used for calculations of covariance matrices of outgoing radiance in the terms of brightness temperature ($\mathbf{K}_{T_B T_B}$) in the 1-200 GHz spectral range.

To calculate $\mathbf{K}_{T_B T_B}$, it is necessary to have some simulated set of the atmospheric states correctly describing the real atmospheric and surface variabilities.

In particular, an empirical ensemble corresponding to a test area can be used as that set. One can also carry out a statistical simulation of the set using the values of average profiles and covariance matrices, generalizing the long-term seasonal observations in the test region.

Another method for forming the standard set has been proposed and successfully used in our work (Kozlov et al., 1983). This approach uses some ideas of classical theory of planning the experiment, in particular, the well-known Box theorem (Box, 1952). In the present study, to calculate $\mathbf{K}_{T_B T_B}$ we have utilized *a priori* set, formed by Kozlov et al. (1983) from "global" covariance matrices of temperature and humidity, constructed by Dr. Arking (Goddard Center of Space Investigation). The cross-correlations of these parameters have assumed to be equal to 0, that extends a statistical distribution.

As a result, we received the standard a priori set, consisting of 40 atmospheric models (temperature, humidity profiles) for quasi-statistical method. This set describes a priori statistics of the atmospheric state variations in a generally correct way (relatively to the first two moments of the distribution).

To estimate a range of applied atmospheric state ensemble, it is sufficient to mention, that the mean square variations of atmospheric temperature and humidity at different levels reach to 16.6K and 80%, respectively, and corresponding value for surface temperature variations is 16.9K. So, applied set is "very wide".

For the information content analysis, $\mathbf{K}_{T_B T_B}$ calculations were carried out for

monochromatic case and 1500 frequencies (so-called "the complete radiance experiment"). Their locations and amount in different intervals are given in Table 3.1.

Table 3.1

Frequency assignment for outgoing radiance calculations

Spectral range GHz	Absorber	Number of the points
40-85	O_2,H_2O	575
110 -130	H_2O	175
15 - 30	H_2O	125
175 -195	H_2O	125

The additional 500 measurement channels are distributed uniformly in all spectral range of 1-200 GHz.

As it follows from cited table, chosen frequencies cover oxygen absorption range, transparency windows and water vapor absorption lines.

3.3.Estimations of the number of independent information components

In Table 3.2 we give the first 30 eigenvalues μ_i of $\mathbf{K}_{T_B T_B}$ matrix calculated with regard for atmospheric temperature and humidity variations and surface emissivity equal to 0.95.

Table 3.2

The first eigenvalues μ_i (K^2) of $\mathbf{K}_{T_B T_B}$ matrix for the 1-200 GHz range.
(1500 channels; 40 different temperature and humidity profiles and surface temperatures; land, e = 0.95)

1	256467.69059
2	9458.45364
3	8967.11645
4	647.28262
5	546.44578
6	467.17321
7	264.37950
8	200.09120
9	91.15060
10	38.50167
11	13.75746
12	7.54997
13	3.10991
14	2.12617
15	1.61347
16	0.81480
17	0.47060
18	0.31865
19	0.24341
20	0.17757
21	0.12955
22	0.09117
23	0.07151
24	0.03988
25	0.03029
26	0.01810
27	0.01530
28	0.01178
29	0.01013
30	0.00644

It follows from these data, that 15 μ_i (for σ_{T_B}=1.0K), 18 μ_i (for σ_{T_B}=0.5K) and 29 μ_i (for σ_{T_B}=0.1K) comply with V.P.Kozlov criterion:

$$\mu_i > \sigma^2_{T_B}$$

where $\sigma^2_{T_B}$ is the random noise variance of outgoing radiance measurement in the

terms of T_B.

Similar $\mathbf{K}_{T_BT_B}$ and μ_i calculations for linear spectral model of surface emissivity of the sea ($\varepsilon(f)=a + bf$) result in the following number of independent components: 18 (for $\sigma_{T_B}=1.0K$), 22 (for $\sigma_{T_B}=0.5K$), and 31 (for $\sigma_{T_B}=0.1K$).

So the 1500 monochromatic spectral measurements simulating the complete radiance experiment contain a great deal of information about vertical temperature and humidity profiles of the atmosphere and underlying surface temperature T_s. It is worth to emphasize, that these calculations did not take into account the possible variations of surface emissivity.

The conducted calculations do not allow to separate the "information components" of matrix $\mathbf{K}_{T_BT_B}$ associated with the variations of different atmospheric parameters (T(z) and q(z)).

In this connection, we carried out the additional $\mathbf{K}_{T_BT_B}$ computations when varying T(z) (at $q(z)=\bar{q}(z)$) and q(z) (at $T(z)=\bar{T}(z)$) in turn. The corresponding eigenvalues (at surface emissivity equal to 0.95) are given in Table 3.3 and 3.4.

Table 3.3

The first eigenvalues μ_i (K^2) of $\mathbf{K}_{T_B T_B}$ matrix for the 1-200 GHz range.

(1500 channels; 40 different atmospheric temperature profiles and surface temperatures; the mean atmospheric humidity profile; land, e = 0.95)

1	254144.99630
2	8975.13144
3	2102.01714
4	547.25454
5	210.81622
6	127.15609
7	38.61295
8	13.68913
9	6.68457
10	2.25899
11	1.39076
12	0.68921
13	0.56537
14	0.32975
15	0.19811
16	0.09753
17	0.03694
18	0.02981
19	0.01202
20	0.00673

Table 3.4

The first eigenvalues μ_i (K^2) of $\mathbf{K}_{T_B T_B}$ matrix for the 1-200 GHz range.

(1500 channels; 40 different atmospheric humidity profiles; fixed surface temperature and the mean atmospheric temperature profile; land, e = 0.95)

1	7639.21629
2	820.94697
3	281.12041
4	68.05590
5	5.73913
6	0.33495
7	0.10836
8	0.04536
9	0.01694
10	0.01133
11	0.00672

The analysis of table data has showed the following:

1.The numbers of independent information components, inherent in outgoing radiance measurements over land and associated with only atmospheric and surface temperature variations, are 11, 14, and 19 at levels of measurement errors (σ_{T_B}) are 1.0K, 0.5K and 0.1K, respectively.

2.The numbers of independent information components, inherent in outgoing radiance measurements over land and associated with only atmospheric humidity profile variations, are 5, 6, and 10 at σ_{T_B} equal to 1.0K; 0.5K and 0.1K, respectively.

3.Replacing the land emissivity model by calm sea one only slightly increases (by 1-2) the number of distinguished independent components in the outgoing radiance spectrum.

4.The sum of independent component numbers of the covariance matrices calculated with regard for T(z) or q(z) variations individually is equal approximately to the number of those for $\mathbf{K}_{T_BT_B}$ covariance matrix considering these variations in combination. Apparently, the last is a result of neglecting the interconnection between atmospheric temperature and humidity when composing the *a priori* set of atmospheric state ensembles.

The principal conclusion from these first stage studies can be formulated in the following way. The complete radiance experiment contains a considerable amount of information about T(z) and q(z) profiles in terms of the principal components of the covariance matrix of outgoing brightness temperatures. Their number exceeds noticeably the number of SSM/T and SSM/T-2 measurement channels (12 channels).The number of independent components, which could be potential-derived from outgoing radiance spectra, has to make possible, in principle, to retrieve temperature and humidity profiles with high accuracy provided a low level of measurement noise (σ_{T_B}=0.1K). Table 3.5 summarizes the data about the number of the independent components for different calculation versions and error levels.

Table 3.5

Number of independent components at different calculation variants

No.	Calculation variant	σ_{T_B}, K		
		0.1	0.5	1.0
1.	T(z), T_s and q(z) variations, e=0.95	29	18	15
2.	T(z), T_s and q(z) variations, e(f)=a+bf	31	22	18
3.	T(z) and T_s variations, e=0.95	19	14	11
4.	T(z) and T_s variations, e(f)=a+bf	19	15	12
5.	q(z) variations, e=0.95	10	6	5
6.	q(z) variations, e(f)=a+bf	11	7	6

It is interesting to compare the information content of the complete radiance experiment with that of different specific satellite devices. For the correctness of comparison, the measurements by different devices were simulated without considering their finite spectral resolutions and for the monochromatic case. In our calculations, we used the means of monochromatic values in the centers of corresponding intervals for a measurement channel consisting of two or more spectral sub-intervals. The special study of this question has shown, that using the "monochromatic approach" for examined satellite devices do not bring the noticeable errors in calculations of the informative content.

In Table 3.6 the first eigenvalues μ_i of $\mathbf{K}_{T_B T_B}$ matrix, calculated using the above *a priori* atmospheric set, are given for a number of satellite devices.

Table 3.6

The first eigenvalues μ_i (K^2) of $\mathbf{K}_{T_B T_B}$ matrix for a number of satellite devices.

a) Land

Devices i	SSM/T	SSM/T-2	SSM/T + SSM/T-2
1	347.58	949.03	1297.23
2	175.79	127.87	179.11
3	8.40	11.30	149.27
4	4.25	1.03	10.39
5	0.58	0.45	8.78
6	0.15		5.87
7	0.0074		1.19
8			0.94
9			0.52
10			0.13
11			0.019
12			0.0034

b) Sea

Devices i	SSM/T	SSM/T-2	SSM/T + SSM/T-2
1	215.60	743.98	910.38
2	174.70	560.72	612.38
3	18.24	26.17	178.17
4	7.96	4.30	33.66
5	1.15	0.68	8.21
6	0.24		5.26
7	0.025		3.37
8			1.22
9			0.61
10			0.38
11			0.099
12			0.0064

An analysis of data of the table 3.6 let us make the following conclusions:

1.For radiometer SSM/T, the numbers of distinguished (according to Kozlov criterion) independent components in the covariance outgoing radiance matrix make up 4, 5 and 6 (for land) and 5, 5 and 7 for sea at RMS random errors σ_{T_B} of brightness temperature measurement equal to 1.0, 0.5 and 0.1K, respectively. Accounting for the vicinity of seventh eigenvalue for land to 10^{-2} (0.0074), it can be concluded, that all SSM/T channels at measurement error 0.1K are "informative" ones. At higher error levels (1.0 and 0.5K), radiometer SSM/T has the "redundant" measurement channels. Having in mind the values of informative

components given in table 3.5 (15, 18 and 29 for land), we can conclude that this fact testifies to non-optimal spectral positions of SSM/T channels.

2.For radiometer SSM/T-2, the numbers of informative components are 4, 5 and 5 (over sea and land) at error levels equal to 1.0, 0.5 and 0.1K. So, even at σ_{T_B}=0.5K, all SSM/T-2 channels are informative.

For a case of joint use of SSM/T and SSM/T-2 radiometers, the number of independent components is given in table 3.7.

Table 3.7

The number of independent components of outgoing radiance covariance matrix at joint use of SSM/T and SSM/T-2 radiometers

Measurement error, K	0.1	0.5	1.0
Land	11	9	7
Sea	11	10	8

As it follows from table 3.7, for combined remote sensing system of DMSP satellite (SSM/T and SSM/T-2), all the measurement channels are practically informative at σ_{T_B}=0.1K. At higher error levels (0.5 and 1.0K), the channels of this remote sensing system are not all informative. This fact, with accounting for data of table 3.5, testifies indirectly to non-optimal choice of the channels for temperature-humidity sounding by DMSP satellite. It is worth note, that these conclusions are concerned to examined "global ensemble" of atmospheric states and the cloudless atmosphere. Certainly, the inclusion of the variations of cloud and surface characteristics can influence this result.

3.4.Information characteristics of the measurements by different devices

Using calculated eigenvalues of outgoing radiance covariance matrix and the Eqs. (3.10)-(3.12), we have determined the information content I (by Shannon) and information volume V (by Kozlov) of different outgoing radiance measurements. The examples of these calculations at measurement RMS error of 0.1K are given in table 3.8.

(In the tables 3.8, 3.9 letter E denotes the following: for example, 0.346E28 = $0.346 \cdot 10^{+28}$).

Table 3.8

Information content I (according to Shannon) and information volume V (according to Kozlov) for different spectral designs of the measurements at σ_{T_B}=0.5K

	Land		Sea	
scheme of the measurements	I	V	I	V
1500 channels, all parameters are variable	74.2	0.249E+22	86.0	0.103E+26
1500 channels, temperature is variable	54.2	0.519E+16	54.8	0.819E+16
1500 channels, humidity is variable	25.8	0.307E+08	33.8	0.866E+10
SSM/T all parameters are variable	15.9	0.375E+05	17.0	0.801E+05
SSM/T-2 all parameters are variable	15.1	0.256E+05	17.7	0.181E+06
SSM/T + SSM/T-2 all parameters are variable	26.7	0.532E+08	29.6	0.383E+09

From these data it can be drawn the following conclusions:

1.Information content of the "complete radiance experiment" (1500 measurements in the 1-200 GHz spectral range) is essentially higher than those of SSM/T and SSM/T-2 radiometer measurements (both using those individually and in combination).

2.Information content of outgoing radiance measurements over water surface with respect to vertical atmospheric and humidity profiles is higher than that over land.

The information data given in table 3.8 does not account for essentially different number of outgoing radiance measurements in the complete radiative experiment (N_1=1500) and for SSM/T and SSM/T-2 radiometers (N_2). But it is evident, that increasing a number of the measurements (even in the same spectral channels) decreases practically a level of random measurement errors (in relation of N_1/N_2 for the random error variance). In this connection, we give table 3.9 representing the measurement information content according to Shannon and Kozlov with accounting for different number of the measurements in various experiment designs. In the Table 3.9, σ_{T_B} for different devices are calculated from $\sigma_{T_B}(N_2) = \sigma_{T_B}(N_1)\sqrt{\frac{N_2}{N_1}}$ and correspond to $\sigma_{T_B}(N_1)$=0.4K.

Table 3.9

Information content I and information volume V
for different spectral designs of measurements.
(A priori σ_{T_B} for 1500 channels - 0.4K, for other designs
σ_{T_B} is given in the first column of the table)

	Land		Sea	
scheme of the measurements	I	V	I	V
1500 channels, all parameters are variable	81.4	0.343E+24	94.2	0.301E+28
1500 channels, temperature is variable	59.4	0.213E+18	60.1	0.378E+18
1500 channels, humidity is variable	28.1	0.142E+09	36.5	0.517E+11
SSM/T all parameters are variable σ_{T_B} = 0.026 K	42.0	0.427E+13	44.3	0.210E+14
SSM/T-2 all parameters are variable σ_{T_B} = 0.024 K	37.0	0.143E+12	39.9	0.101E+13
SSM/T + SSM/T-2 all parameters are variable σ_{T_B} = 0.035 K	66.7	0.102E+21	72.6	0.317E+22

Table 3.9 demonstrates, that information content is noticeably higher in the "complete radiance experiment" than in the DMSP temperature-humidity sounding system. For example, information contents by Shannon are 81.4 (over land), 94.2 (over sea) and 66.7 (over land), 72.6 (over sea) for the "complete radiance experiment" and for simultaneous SSM/T+SSM/T-2 measurements, respectively.

So, the principal result of performed studies consists in revealing the fact, that DMSP temperature-humidity sensing system does not make possible to receive all available information about atmospheric temperature and humidity profiles contained in outgoing microwave radiation spectra.

In conclusion it is necessary to note, that we have carried out the similar information content analysis for 20-channel AMSU radiometer to be launched to space flight in 1996. The calculations have shown the noticeable preference the information characteristics of AMSU in comparison with those of SSM/T+SSM/T-2 system. But the information content of AMSU measurements is appreciably smaller than that of the "complete radiance experiment".

4.ANALYSIS OF POTENTIAL ACCURACY OF TEMPERATURE AND HUMIDITY MICROWAVE REMOTE SOUNDING

4.1.Mathematical basis of estimating the potential accuracy of remote sensing

In the case of linear operator **A** (see Part 3.1), the solution of the inverse problem may be represented according to (3.8) as:

$$\tilde{\mathbf{x}} = \bar{\mathbf{x}} + (\mathbf{G} + \mathbf{K}^{-1})^{-1}\mathbf{A}^{+}\Sigma^{-1}\mathbf{y}$$

Then we can write the following expression for the error of inverse solution:

$$\delta\mathbf{x} = ((\mathbf{G} + \mathbf{K}^{-1})^{-1}\mathbf{G} - \mathbf{I})\mathbf{x} + (\mathbf{G} + \mathbf{K}^{-1})^{-1}\mathbf{A}^{+}\Sigma^{-1}\varepsilon \qquad (4.1)$$

here $\mathbf{G} = \mathbf{A}^{+}\Sigma^{-1}\mathbf{A}$ is the Fisher information matrix, **K** is the covariance matrix of the *a priori* variability of atmospheric parameter vector **x**, **I** is the unit matrix, Σ is the noise covariance matrix.

It is easily seen, that the first term in Eq.4.1 does not depend on concrete realization of the random measurement error ε, and the second - on the sought vector of atmospheric parameters **x**. Therefore, it is the practice to call the first term as systematic, or null-space error component (Rodgers, 1990), and the second term - as random component. As those are independent random values, the covariance error estimate matrix **D** (see formula (3.9)) may be represented as the sum of their covariance matrices:

$$\mathbf{D} = \mathbf{D}_R + \mathbf{D}_S \qquad (4.2)$$

here

$$\mathbf{D}_R = (\mathbf{G} + \mathbf{K}^{-1})^{-1}\mathbf{G}(\mathbf{G} + \mathbf{K}^{-1})^{-1} \qquad (4.3)$$

$$\mathbf{D}_S = ((\mathbf{G} + \mathbf{K}^{-1})^{-1}\mathbf{G} - \mathbf{I})\mathbf{K}((\mathbf{G} + \mathbf{K}^{-1})^{-1}\mathbf{G} - \mathbf{I}) \qquad (4.4)$$

where $\mathbf{D}_R$ and $\mathbf{D}_S$ are the covariance matrices of the random and systematic retrieval error components, respectively.

The expressions (3.8), (4.1) have been formulated for one-vector retrieval problem (i=1) (Strand and Westwater, 1968; Turchin and Nozik, 1969; Turchin et al., 1970; Rodgers, 1970, 1971, 1976). But in reality the retrieval problems are many-parametric ones, and separate studies of different retrieval problems present, as a rule, only a methodical interest, for example, to examine the maximum

possibilities of the retrieval methods. But even in these separate retrievals it is necessary to take into account not only measurement errors (noise errors) but "effective" noise due to the variations of other parameters, though the retrievals of those are not planned.

We will illustrate this fact by formulation of the unified atmospheric temperature (T) and humidity (q) profile retrievals (Pokrovsky and Timofeyev, 1972), because this problem relates just to microwave sensing of the cloudless atmosphere by spectrometers SSM/T-1, SSM/T-2. In this case, assuming a known emissivity of underlying surface we can formulate the inverse problem in the following way instead of Eq.(3.1):

$$\delta \mathbf{y} = \mathbf{A}_T\, \delta \mathbf{T} + \mathbf{A}_q\, \delta \mathbf{q} + \varepsilon \tag{4.5}$$

Then from (3.8) one can obtain for optimal statistical estimates of temperature, $\delta\tilde{T}$, and humidity, $\delta\tilde{q}$, variances :

$$\delta\tilde{\mathbf{T}} = (\mathbf{K}_{TT}\, \mathbf{A}_T^{+} + \mathbf{K}_{Tq}\, \mathbf{A}_q^{+})\, (\mathbf{A}_T\, \mathbf{K}_{TT}\, \mathbf{A}_T^{+} + \mathbf{A}_T\, \mathbf{K}_{Tq}\, \mathbf{A}_q^{+} + \mathbf{A}_q\, \mathbf{K}_{qT}\, \mathbf{A}_T^{+} + \mathbf{A}_q\, \mathbf{K}_{qq}\, \mathbf{A}_q^{+} + \Sigma)^{-1}\, \delta \mathbf{y} \tag{4.6}$$

$$\delta\tilde{\mathbf{q}} = (\mathbf{K}_{qq}\, \mathbf{A}_q^{+} + \mathbf{K}_{qT}\, \mathbf{A}_T^{+})\, (\mathbf{A}_T\, \mathbf{K}_{TT}\, \mathbf{A}_T^{+} + \mathbf{A}_T\, \mathbf{K}_{Tq}\, \mathbf{A}_q^{+} + \mathbf{A}_q\, \mathbf{K}_{qT}\, \mathbf{A}_T^{+} + \mathbf{A}_q\, \mathbf{K}_{qq}\, \mathbf{A}_q^{+} + \Sigma)^{-1}\, \delta \mathbf{y} \tag{4.7}$$

where $\mathbf{K}_{TT}$, $\mathbf{K}_{qq}$ and $\mathbf{K}_{qT}$,$\mathbf{K}_{Tq}$ are covariance and cross-covariance matrices of the sought parameters.

Analogously from (3.9) we can deduce for error matrices characterizing the accuracies of the retrieval methods:

$$\mathbf{D}_{TT} = \left\{ \mathbf{K}_{TT}^{-1} + (\mathbf{A}_T^{+} + \mathbf{K}_{TT}^{-1}\, \mathbf{K}_{Tq}\, \mathbf{A}_q^{+})\, [\mathbf{A}_q(\mathbf{K}_{qq} - \mathbf{K}_{qT}\, \mathbf{K}_{TT}^{-1}\, \mathbf{K}_{Tq})\mathbf{A}_q^{+} + \Sigma]^{-1}\, (\mathbf{A}_T + \mathbf{A}_q\, \mathbf{K}_{qT}\, \mathbf{K}_{TT}^{-1}) \right\}^{-1} \tag{4.8}$$

$$\mathbf{D}_{qq} = \left\{ \mathbf{K}_{qq}^{-1} + (\mathbf{A}_q^{+} + \mathbf{K}_{qq}^{-1}\, \mathbf{K}_{qT}\, \mathbf{A}_T^{+})\, [\mathbf{A}_T(\mathbf{K}_{TT} - \mathbf{K}_{Tq}\, \mathbf{K}_{qq}^{-1}\, \mathbf{K}_{qT})\mathbf{A}_T^{+} + \Sigma]^{-1}\, (\mathbf{A}_q + \mathbf{A}_T\, \mathbf{K}_{Tq}\, \mathbf{K}_{qq}^{-1}) \right\}^{-1} \tag{4.9}$$

Supposing $\mathbf{A}_q = 0$ and $\mathbf{K}_{Tq} = 0$, we can write the formulas (4.6), (4.8) for temperature profile retrieval (one-dimensional, idealized problem):

$$\delta\tilde{T} = \mathbf{K}_{TT}\,\mathbf{A}_T^{+}\,(\mathbf{A}_T\,\mathbf{K}_{TT}\,\mathbf{A}_T^{+} + \Sigma)^{-1}\,\delta y \tag{4.10}$$

$$\mathbf{D}_{TT} = \left\{\mathbf{K}_{TT}^{-1} + \mathbf{A}_T^{+}\Sigma^{-1}\mathbf{A}_T\right\}^{-1} \tag{4.11}$$

Comparing, for example, (4.6) and (4.10) one can realize that idealized approach suffers from:

- distortion of the operator of the inverse problem;
- lack of the term $\mathbf{A}_q(\mathbf{K}_{qq} - \mathbf{K}_{qT}\,\mathbf{K}_{TT}^{-1}\,\mathbf{K}_{Tq})\mathbf{A}_q^{+}$ presenting by itself an additional "effective" noise in the radiance measurements.

In our study we assume, that temperature and humidity profiles are independent, that exceeds the *a priori* statistical ensemble. This means that $\mathbf{K}_{qT} = \mathbf{K}_{Tq} = 0$. Then Eqs.(4.8) and (4.9) turn into:

$$\mathbf{D}_{TT} = \left\{\mathbf{K}_{TT}^{-1} + \mathbf{A}_T^{+}(\mathbf{A}_q\mathbf{K}_{qq}\mathbf{A}_q^{+} + \Sigma)^{-1}\mathbf{A}_T\right\}^{-1} \tag{4.8'}$$

$$\mathbf{D}_{qq} = \left\{\mathbf{K}_{qq}^{-1} + \mathbf{A}_q^{+}(\mathbf{A}_T\mathbf{K}_{TT}\mathbf{A}_T^{+} + \Sigma)^{-1}\mathbf{A}_q\right\}^{-1} \tag{4.9'}$$

From these equations it is evident, that the uncertainty of one atmospheric parameter influence on retrieval error of other parameter. In Eq.(4.8), for example, the term $\mathbf{A}_q(\mathbf{K}_{qq}-\mathbf{K}_{qT}\mathbf{K}_{TT}^{-1}\mathbf{K}_{Tq})\mathbf{A}_q^{+}$, added to covariance measurement matrix, represents by itself an "effective" noise contaminating temperature profile measurements because of the humidity profile uncertainties. In the case of neglecting the cross-correlations between temperature and humidity (4.8'), this effective noise is $\mathbf{A}_q\mathbf{K}_{qq}\mathbf{A}_q^{+}$.

The above studies of device measurement content (Chapter 3) and retrieval error have been based on the assumptions of linear relations between radiance and the sought atmospheric parameters. But the basic retrieval problems of the remote sounding are nonlinear. For example, in the 1-200 GHz spectral range, the dependence between outgoing brightness temperature and atmospheric humidity profile is essentially nonlinear. Formally the nonlinear problem can be written as a generalization of the linear problem (3.1):

$$\mathbf{y} = \mathbf{B}(\mathbf{x}) + \varepsilon \tag{4.12}$$

where **B** is nonlinear operator and

$$\bar{x} = Ex;\ \bar{\varepsilon} = E\varepsilon \equiv 0;\ \mathbf{K} = E(x - \bar{x})(x - \bar{x})^{+};\ \Sigma = E\varepsilon\varepsilon^{+}$$

And the best estimate (in the probability sense) $\tilde{\mathbf{x}}$ corresponding to measurement value **y** minimizes the sum of the following deviations:

$$\|\mathbf{B}(\tilde{x}) - y\|^{2}_{\Sigma^{-1}} + \|\tilde{x} - \bar{x}\|^{2}_{K^{-1}} \Rightarrow \min \tag{4.13}$$

The traditional way to solve a nonlinear problem is to reduce the task to the sequence of linear tasks by some form of the iteration. The iteration method is simply a matter of expanding the operator **B** as a Taylor series about a guessed value x_k:

$$\mathbf{B}(x) = \mathbf{B}(x_k) + \mathbf{A}(x - x_k) + o(x - x_k)$$

here **A** is variational derivative matrix of operator **B** at the point x_k, x_k is the solution estimate derived on the previous iteration step.
Then Eq.(4.13) reduces to:

$$\|\mathbf{B}(x_k)+\mathbf{A}(x_{k+1}-x_k)-y\|^{2}_{\Sigma^{-1}} + \|x_{k+1}-\bar{x}\|^{2}_{K^{-1}} \Rightarrow \min \tag{4.14}$$

By minimizing this equation one can derives some equivalent and useful in practice expressions for x_{k+1}:

$$x_{k+1}=(\mathbf{A}^{+}\Sigma^{-1}\mathbf{A} + \mathbf{K}^{-1})^{-1}(\mathbf{A}^{+}\Sigma^{-1}(y - \mathbf{B}(x_k) + \mathbf{A}x_k) + \mathbf{K}^{-1}\bar{x}) \tag{4.15-1}$$

$$x_{k+1}=\bar{x} + (\mathbf{A}^{+}\Sigma^{-1}\mathbf{A} + \mathbf{K}^{-1})^{-1}\mathbf{A}^{+}\Sigma^{-1}(y - \mathbf{B}(x_k) - \mathbf{A}(\bar{x}-x_k)) \tag{4.15-2}$$

$$x_{k+1}=x_k+(\mathbf{A}^{+}\Sigma^{-1}\mathbf{A} + \mathbf{K}^{-1})^{-1}(\mathbf{A}^{+}\Sigma^{-1}(y - \mathbf{B}(x_k))+\mathbf{K}^{-1}(\bar{x}-x_k)) \tag{4.15-3}$$

$$x_{k+1}=\bar{x} + \mathbf{K}\mathbf{A}^{+}(\mathbf{A}\mathbf{K}\mathbf{A}^{+} + \Sigma)^{-1}(y - \mathbf{B}(x_k) - \mathbf{A}(\bar{x}-x_k)) \tag{4.15-4}$$

It is easy to prove that the limit of decision sequence (if the process converges) is the solution of nonlinear problem (4.13).
Although Eqs. (4.15-1)-(4.15-4) are equivalent, the proper choice of applied formula can essentially simplify a development of relevant software.It should be

mentioned that similar iterative procedures were early developed by other means (for example, Marks and Rodgers, 1993; Polyakov and Rozanov, 1989).

In a number of cases, the above algorithm does not give a convergent sequence of $\{x_k\}$ due to essential nonlinearity of the operator **B**. To resolve the problem, authors of the paper (Marks and Rodgers, 1993) have proposed to use the known Marquard algorithm of the functional minimizing, that gives the following iterative scheme:

$$x_{k+1}=x_k+(\mathbf{A}^+\Sigma^{-1}\mathbf{A}+\mathbf{K}^{-1}+c\mathbf{I})^{-1}(\mathbf{A}^+\Sigma^{-1}(y - \mathbf{B}(x_k))+\mathbf{K}^{-1}(\bar{x}-x_k)) \qquad (4.16)$$

where c is an adjusting coefficient, **I** is the unit matrix.

We have proposed (Polyakov, 1995) the approach somewhat different from the above (and stated further) to solve this problem. It gives the expression (4.18), similar to (4.16), but having a simple physical sense and some advantages in using. This approach is the following.

In the case of iterative process divergence, it is the most reasonable to restrict the solution variations at each iterative step by means of adding the limiting term to minimize the expression (4.14), i.e.:

$$\|\mathbf{B}(x_{k+1})-y\|^2_{\Sigma^{-1}}+\|x_{k+1}-\bar{x}\|^2_{K^{-1}}+\|x_{k+1}-x_k\|^2_{L^{-1}} \Rightarrow \min \qquad (4.17)$$

Here **L** is some positive definite matrix. Needless to say, Eq.(4.17) is miningful only in iterative process.

If the iterative process converges, the last term in Eq.(4.17) tends to zero, whatever matrix we use. This matrix may even change from iteration step to step. In any case, the solution of (4.17) coincides with that of the problem (4.14).

Then the formula of the solution refinement similar to (4.15-3) is:

$$x_{k+1}=x_k+(\mathbf{A}^+\Sigma^{-1}\mathbf{A}+\mathbf{K}^{-1}+\mathbf{L}^{-1})^{-1}(\mathbf{A}^+\Sigma^{-1}(y - \mathbf{B}(x_k))+\mathbf{K}^{-1}(\bar{x}-x_k)) \qquad (4.18)$$

By analogy with matrix **K** characterizing the estimate deviation from the mean, matrix **L** is the covariance matrix of the estimate variation at each iterative step. Matrix **L** must be constructed with regard for natural atmospheric parameter variability and the degree of nonlinearity in the radiance-parameter dependencies. For example, in the examined task, the dependence between radiance and atmospheric temperature profile is close to linear, but that between radiance and atmospheric humidity profile is essentially nonlinear. So, matrix **L** may be a diagonal one with

large and small components, corresponding to temperature and humidity, respectively. In each specific case, it is appropriate to construct this matrix on the basis of special feature of the task and to fit its optimal components by numerical simulation.

4.2.Numerical estimation of the potential errors of the temperature and humidity retrievals

The above study of microwave measurement information content, presented in Chapter 3, has demonstrated an availability of additional information about T(p) and q(p) in the radiance compared to DMSP remote sensing measurements (SSM/T and SSM/T-2 radiometers).

To estimate quantitatively an accuracy of atmospheric temperature and humidity sounding, we have carried out the error matrix calculations using the basic statistical approach (Pokrovsky and Timofeyev, 1972). To this end, two designs of outgoing microwave radiance measurements were examined:

a)."Complete radiance experiment" - 1500 measurement channels in the whole spectral range of 1-200 GHz (see Table 3.1);

b).SSM/T and SSM/T-2 measurements (12 measurement channels).

The large volume of error matrix calculations has made possible to compare two experiment designs, to study the effects of random measurement errors, vertical resolution, and *a priori* statistics. Basic calculations were carried out for 54 atmospheric levels and two sets of *a priori* statistics: global and local (with decreasing all covariance matrix elements by half). The examples of the calculation results are given in Fig.4.1-4.10. It is necessary to remind, that when calculating the error matrices (Pokrovsky and Timofeyev, 1972), we define a potential sensing accuracy, *i.e.* minimal attainable error for examined measurement error levels. Other possible factors, which can increase the retrieval errors (radiative model errors, absolute calibration errors, etc.) are not taken into account. At last, let us note, that adduced data have to do with cloudless atmosphere and two surface types - land and sea. Surface emissivities are assumed to be known. In this connection, the errors analyzed can be named as "potential" ones.

Fig.4.1, 4.2 illustrate the potential errors of vertical temperature profile retrieval from outgoing radiance measurements in 1500 channels and from SMM/T and SMM/T-2 measurements, respectively, for three RMS measurement errors in the terms of brightness temperature σ_{T_B} (σ_{T_B}=0.1; 0.3; 1.0K). It can be seen from the

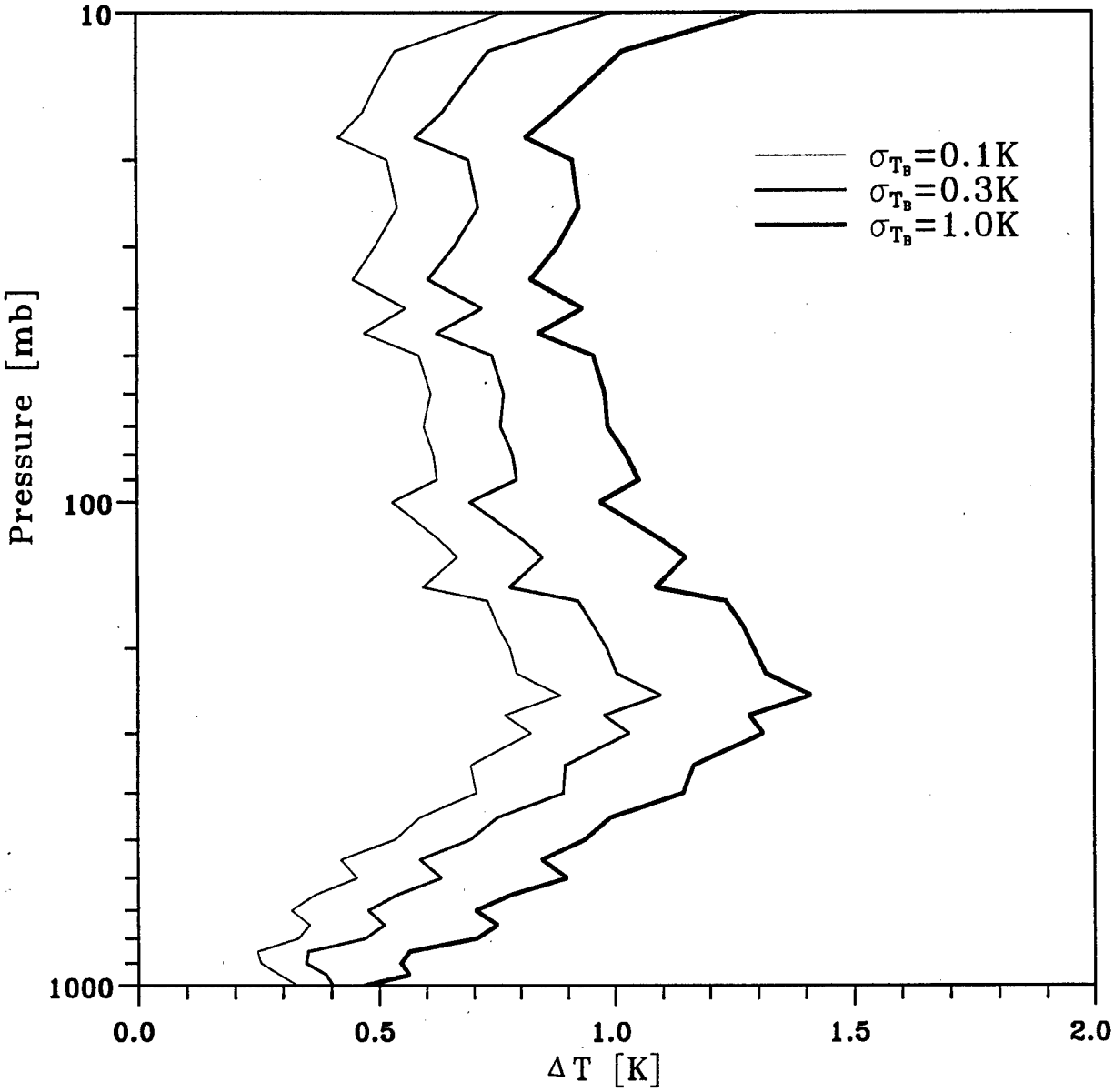

Fig.4.1.Potential errors of the temperature profile retrieval for the three levels of measurement errors σ_{T_B}.

1500 measurements, sea, global statistics.

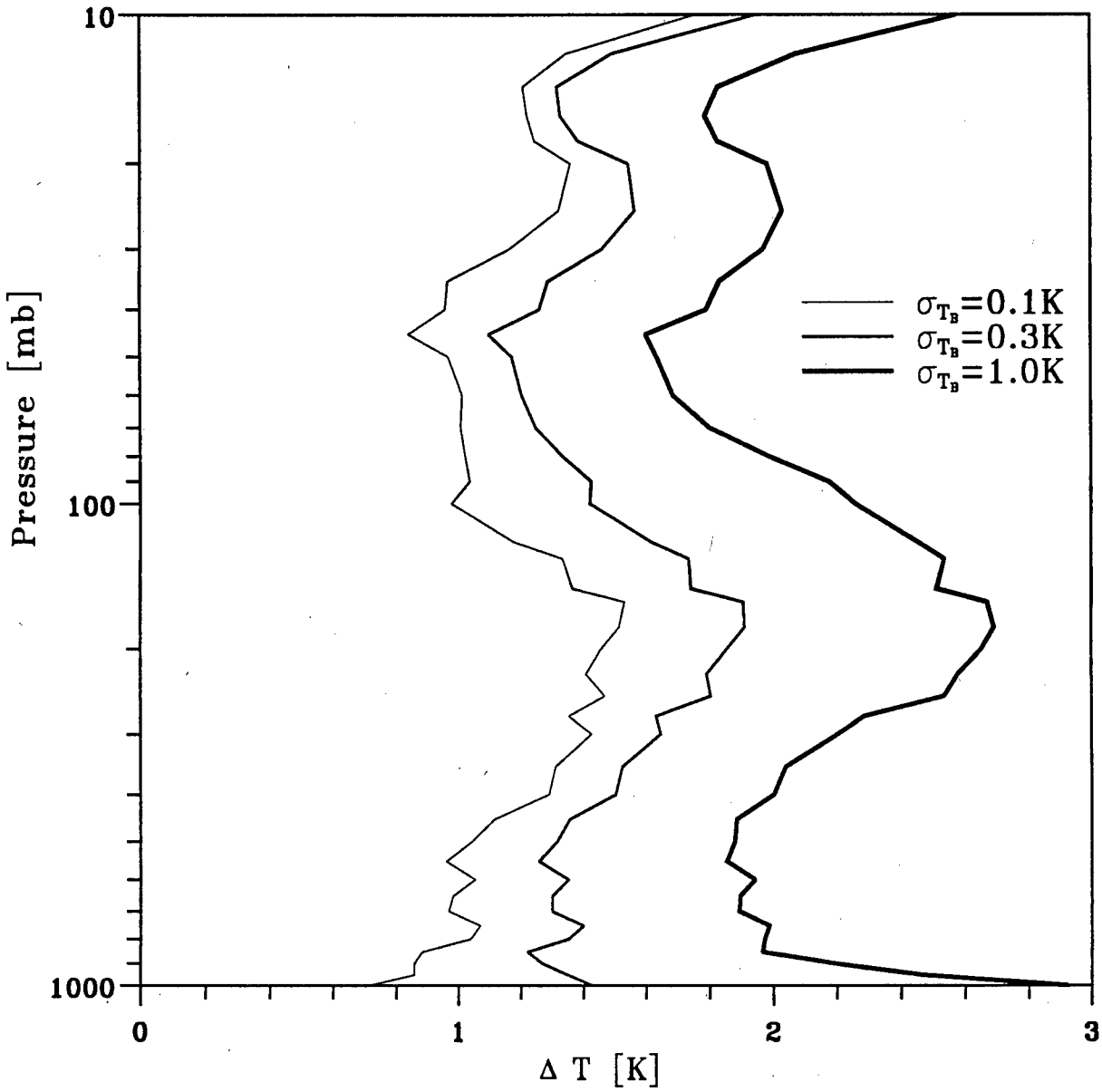

Fig.4.2.Potential errors of the temperature profile retrieval for the three levels of measurement errors σ_{T_B}.

SSM/T+SSM/T-2, sea, global statistics.

Figures, that retrieval errors decrease with increasing measurement accuracy. At σ_{T_B}=0.1K the complete radiance experiment makes possible to retrieve T(p) with the errors smaller than 0.9K in the wide pressure range (10-1000 mb). In the most part of this pressure range, the retrieval errors are 0.4-0.7K. At the same measurement error, SSM/T+SSM/T-2 system gives the maximal retrieval errors equal to about 1.3K in the 10-1000 mb pressure range.

At σ_{T_B}=1.0K, the complete radiance experiment allows to reach the accuracies equal to 0.5-1.4K in comparison with those of 1.6-3.0K for SSM/T+SSM/T-2 system. To compare more visually the retrieval errors of two experiment designs, those are given in Fig.4.3 at σ_{T_B}=0.3K. It is seen, that at some atmospheric levels (10-1000 mb), the retrieval advantages of the complete radiance experiment reach to 1.0K and to larger values at levels, which are higher than 10 mb. The last is a result of lacking the channels with high optical density in the SSM/T+SSM/T-2 system. The advantages of the complete radiance experiment for the 10-1000 mb layer can be clearly seen in Fig.4.4.

Thus, the calculations of potential accuracy of atmospheric temperature sounding confirm the above result, that outgoing microwave radiance contains the noticeable additional information (as compared with SSM/T+SSM/T-2 measurements) about atmospheric temperature structure.

An influence of the atmospheric humidity profile variations on the temperature sounding accuracy is illustrated by Fig.4.5. In this Figure, two profiles of T(p) retrieval errors are given: 1 - for a case of accounting for q(p) variations; 2 - for a case of known q(p). The effect of humidity profile variations is appreciable in the 200-1000 mb layer and can reach to 0.1-0.3K for the complete radiance experiment and to about 0.5K for SSM/T+SSM/T-2 system in the lower troposphere.

It is well-known, that accuracy of atmospheric temperature sounding depends on the initial guess and on "width" of *a priori* statistics used. Fig.4.6 demonstrates an influence of *a priori* statistics on the accuracy of atmospheric temperature sounding. It can be seen, that accuracy of the atmospheric temperature retrieval by use of "local" statistics at σ_{T_B}=0.3K is higher by 0.2-0.4K for the complete radiance experiment and by 0.3-0.7K for SSM/T+SSM/T-2 system . The smaller influence of *a priori* statistics on the retrieval with using 1500 radiance measurements is caused by the fact, that this experiment allows to obtain a greater information about the atmospheric temperature state and, as a consequence, *a priori* statistics slightly effects the retrieval results. It is interesting to note, that the accuracy of temperature profile retrieval at the 10-400 mb atmospheric layer by SSM/T+SSM/T-2 system with using local statistics is near to

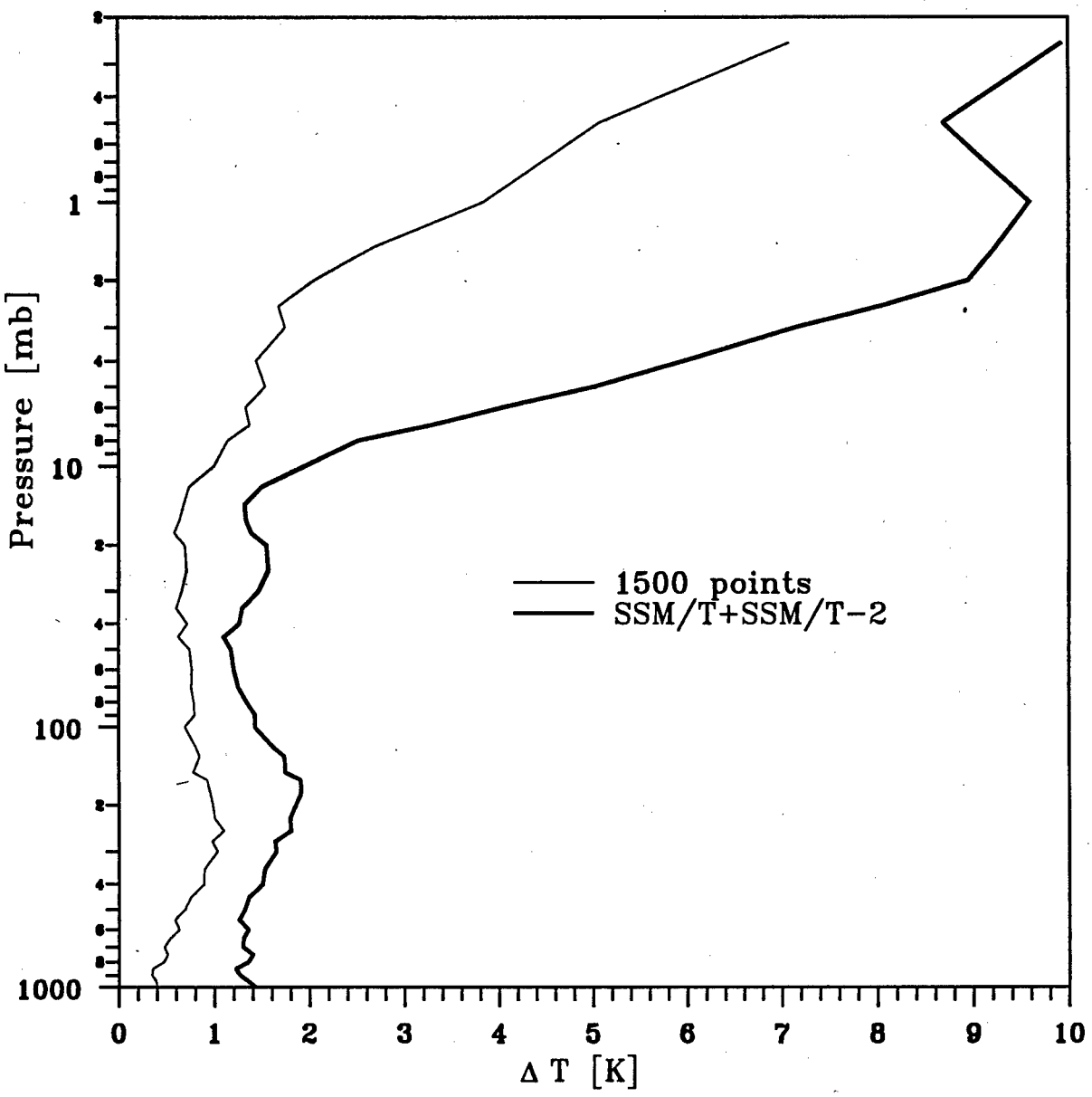

Fig.4.3.Potential errors of the temperature profile retrieval for two measurement designs: 1500 measurements and SSM/T+SSM/T-2. Sea, global statistics, measurement error-0.3K.

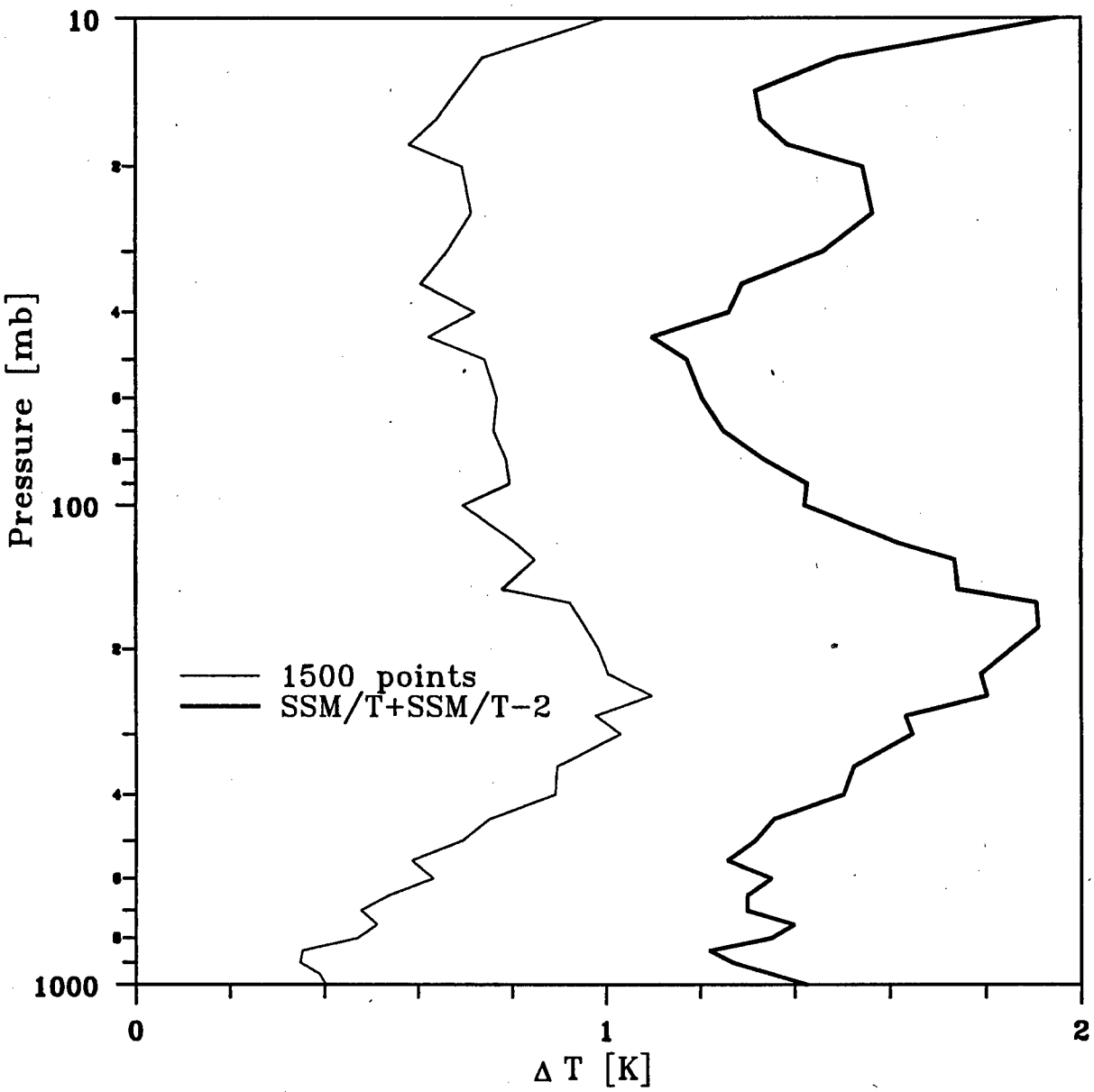

Fig.4.4.Potential errors of the temperature profile retrieval in the 10-1000mb layer for two measurement designs: 1500 measurements and SSM/T+SSM/T-2. Sea, global statistics, measurement error-0.3K.

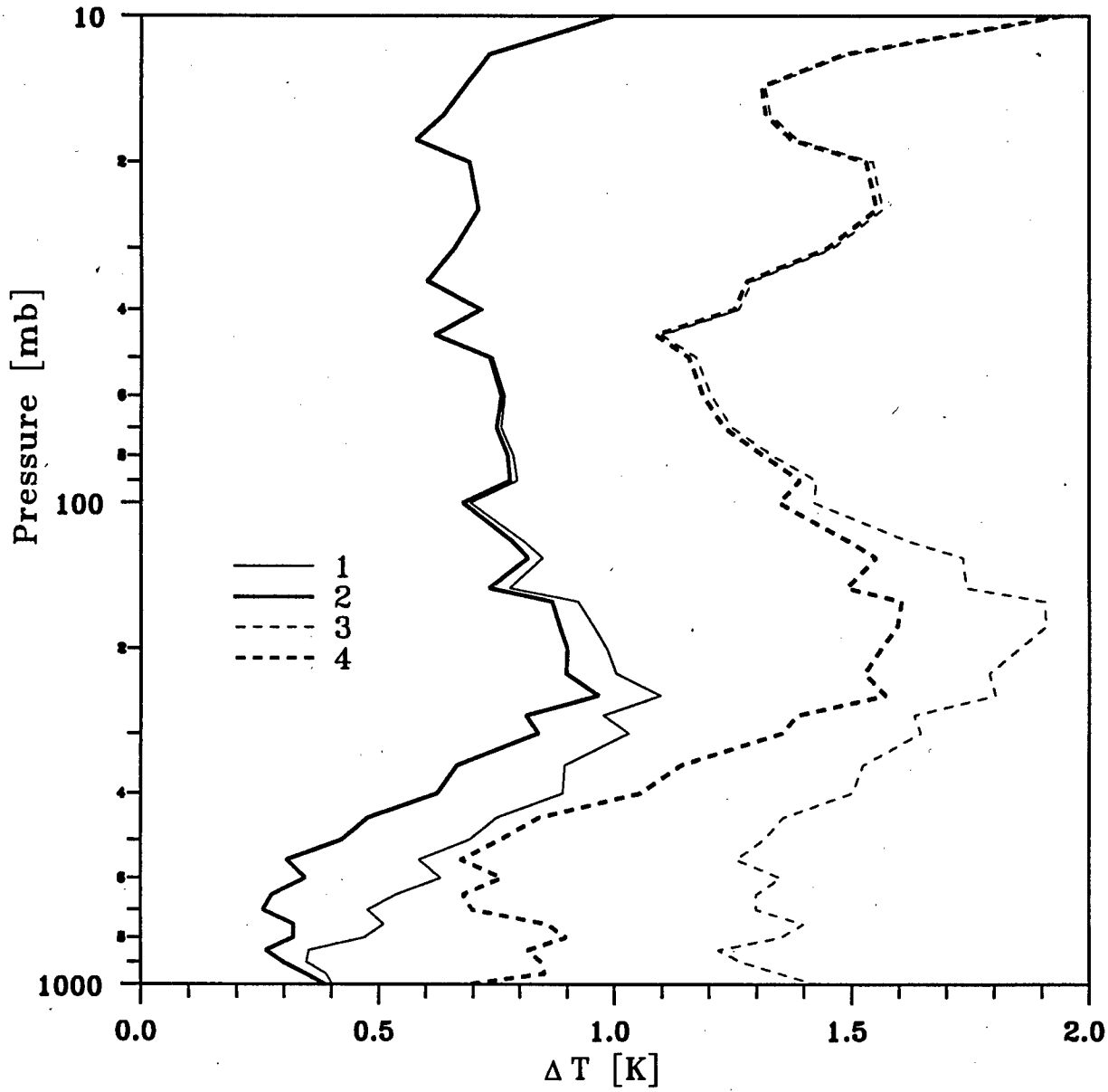

Fig.4.5.Potential errors of the temperature profile retrieval for the fixed and variable profiles of the atmospheric humidity.
Sea, global statistics, measurement error–0.3K.
1 – 1500 points, variable humidity
2 – 1500 points, fixed humidity
3 – SSM/T+SSM/T–2, variable humidity
4 – SSM/T+SSM/T–2, fixed humidity

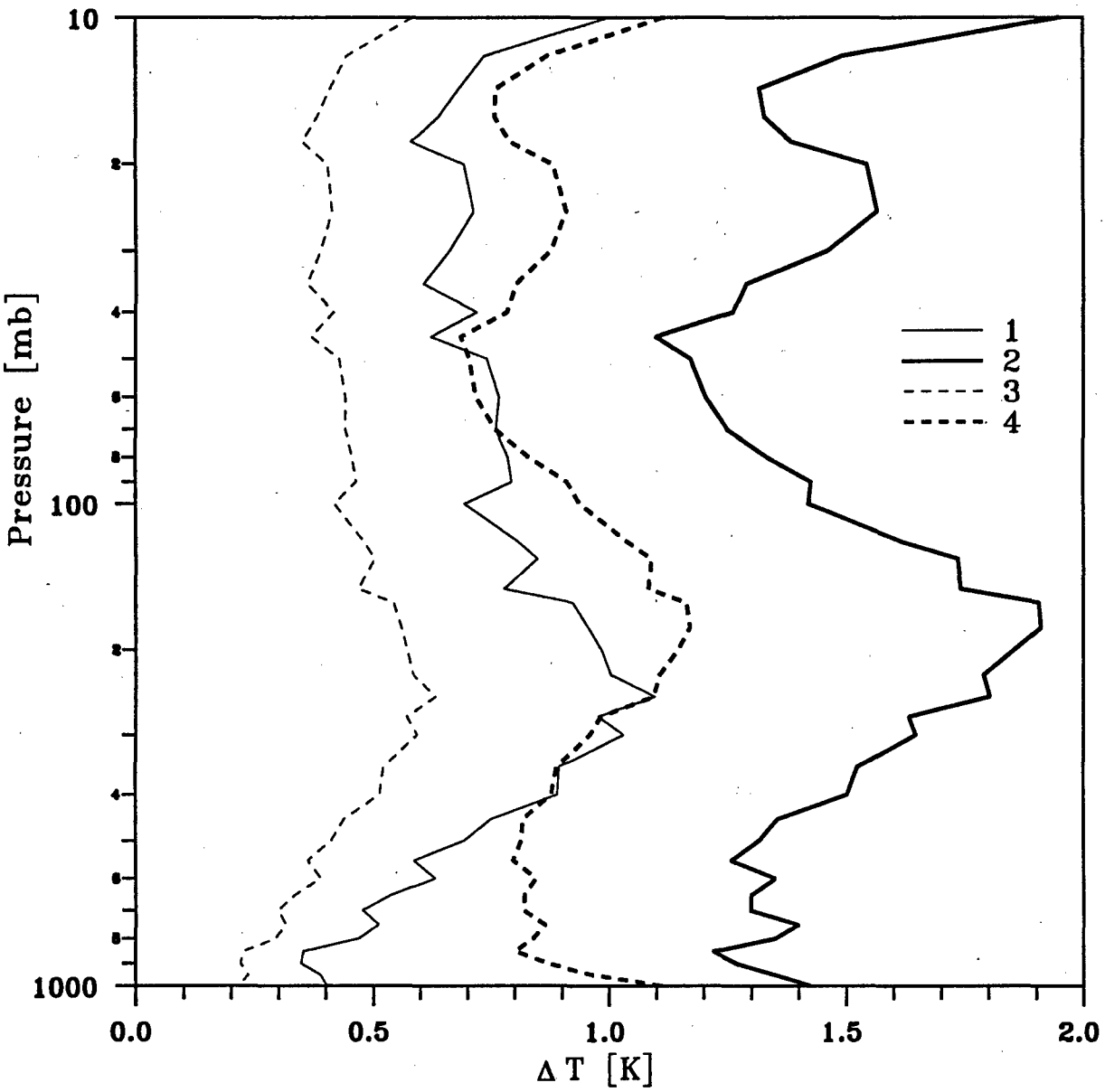

Fig.4.6.Potential errors of the temperature profile retrieval using global or local statistics. 1500 measurements and SSM/T+SSM/T-2. Sea, measurement error-0.3K.
1 - 1500 points, global statistics
2 - SSM/T+SSM/T-2, global statistics
3 - 1500 points, local statistics
4 - SSM/T+SSM/T-2, local statistics

that, accessible for complete radiance experiment using a global statistics. At the lower atmosphere, the complete radiance experiment gives the errors, which are noticeably smaller than those for SSM/T+SSM/T-2 measurements even for global statistics.

As it has been mentioned, the matrix error calculations were carried out for 54 atmospheric pressure levels. In a number of inverse problem, it is necessary to know the mean temperatures of some atmospheric layers. Thus, the operative system of the temperature sounding TOVS performs T(p) retrieval for 40 atmospheric pressure levels and gives the information about the mean virtual temperature (Reale et al., 1994). In Fig.4.7, we reproduce the temperature retrieval errors for two measurement designs (at σ_{T_B}=0.3K) and two vertical resolution. The retrieval accuracy in 18 layers is higher by 0.2-0.3K for both experiment designs in comparison with the attainable for 54 atmospheric levels. Effect of vertical averaging is slightly larger for the complete radiance experiment. It is evidently connected with the larger correlation between T(p) retrieval errors at different levels for SSM/T+SSM/T-2 system having only 12 channels in comparison with the complete radiance experiment involving 1500 measurements. It is important to emphasize, that the complete radiance experiment makes a possibility to retrieve the temperatures in 18 layers with high potential accuracies of 0.2-0.9K at σ_{T_B}=0.3K. In the most part of the examined 10-1000 mb atmospheric layer, the retrieval errors are about 0.5K. The corresponding errors for DMSP sounding system at the same measurement error are higher by 0.5-1.0K.

A joint influence of vertical averaging and *a priori* statistics on the accuracy of the mean temperature sounding in 18 atmospheric layers at σ_{T_B}=0.3K is demonstrated in Fig.4.8. It can be concluded, that complete radiance experiment (1500 measurements) with using local statistics allows to achieve the very high retrieval accuracy (0.2-0.6K) for average temperatures in 18 layers of the 10-1000 mb atmospheric range. The same retrieval accuracies for DMSP system are worse by 0.3-0.6K. Above this atmospheric range, the advantages of the complete radiance experiment achieve to 1-4K, that is due to an absence of optical dense measurement channels in the SSM/T+SSM/T-2 system.

An influence of surface emissivity on the temperature retrieval accuracy is demonstrated by Fig.4.9. This impact is incidental if the emissivity is known. The exception is the accuracy of temperature retrieval from SSM/T+SSM/T-2 measurements near underlying surface. In this case, the retrieval accuracy above land (e=0.95) is significantly better than that above sea. It is connected, in our opinion, with special shape of weighting function corresponding to the "transparent" measurement

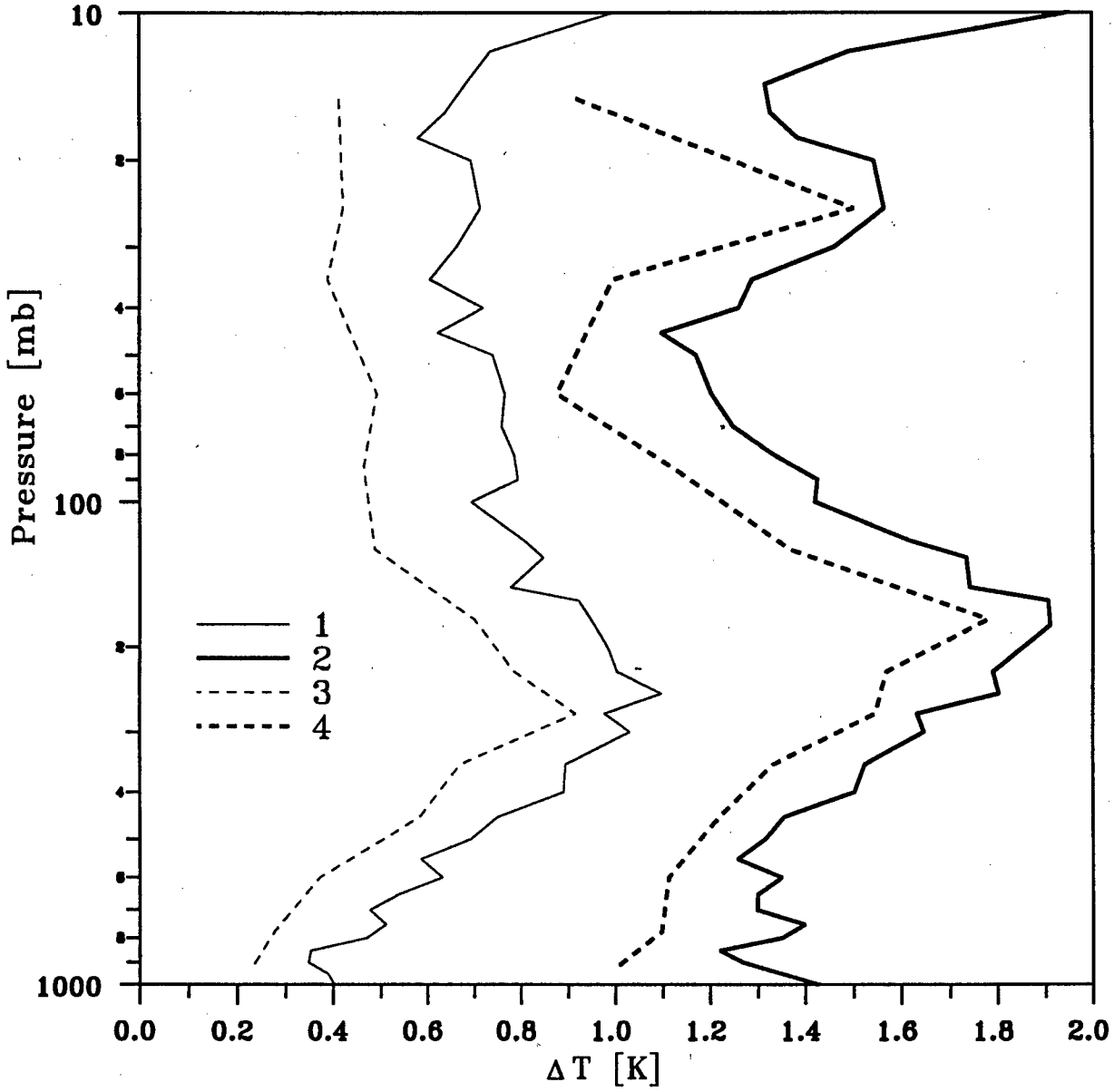

Fig.4.7.Potential errors of the retrieval of the temperature profile on 54 levels and the mean temperature in 18 atmospheric layers for two measurement designs: 1500 measurements and SSM/T+SSM/T-2.
Sea, global statistics, measurement error - 0.3K.
1 - 1500 points, 54 levels
2 - SSM/T+SSM/T-2, 54 levels
3 - 1500 points, 18 layers
4 - SSM/T+SSM/T-2, 18 layers

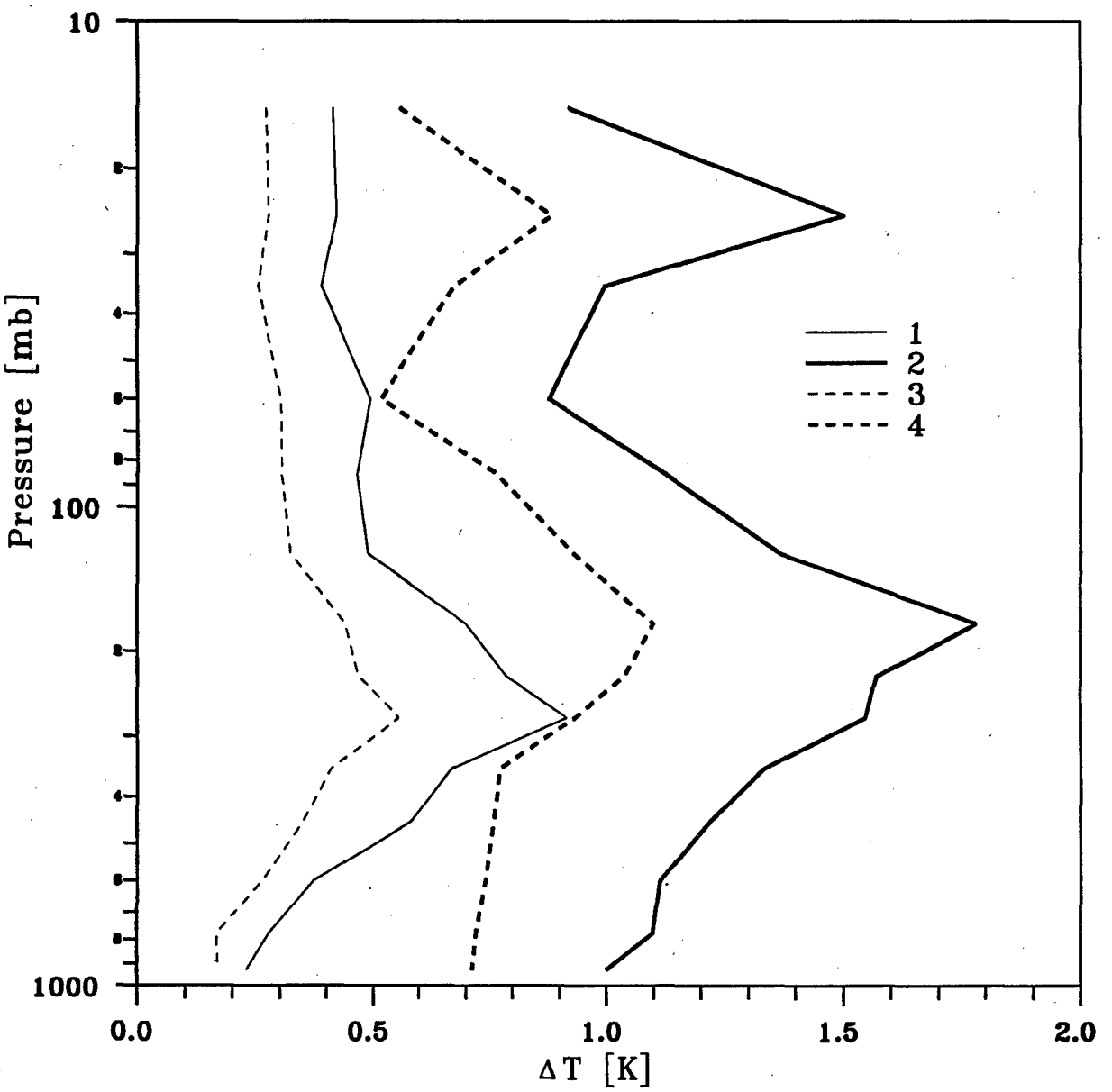

Fig.4.8.Potential errors of the mean temperature retrieval in 18 atmospheric layers using global or local statistics.
1500 measurements and SSM/T+SSM/T-2.
Sea, measurement error - 0.3K.
1 - 1500 points, global statistics
2 - SSM/T+SSM/T-2, global statistics
3 - 1500 points, local statistics
4 - SSM/T+SSM/T-2, local statistics

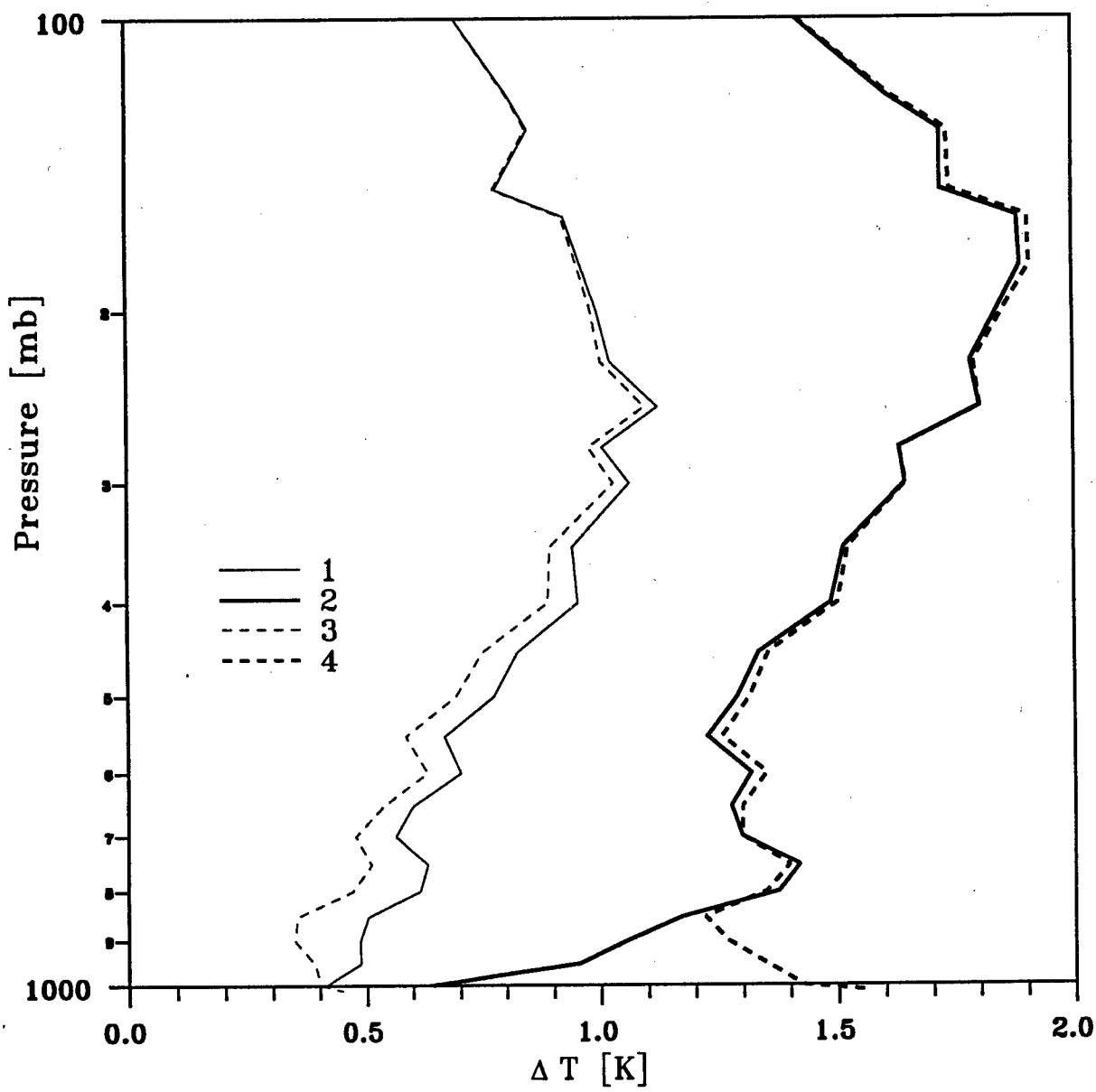

Fig.4.9.Potential errors of the temperature profile retrieval over land and sea for two measurement designs: 1500 measurements and SSM/T+SSM/T-2. Global statistics, measurement error - 0.3K.
1 - 1500 points, land
2 - SSM/T+SSM/T-2, land
3 - 1500 points, sea
4 - SSM/T+SSM/T-2, sea

channel of 50.500 GHz for SSM/T radiometer above sea surface (see Fig.2.8).

Fig.4.10 demonstrates the ratio between random and systematic (null-space) components in T(p) retrieval overall error (see Eqs. (4.3)-(4.4)) for examined experiment designs and σ_{T_B}=0.3K. It can be seen, that systematic retrieval error, caused by finite thickness of the temperature weighting functions, gives the maximal contribution. But these components are equal to 0.3-1.0K for the complete radiance experiment, and to 0.8-1.8K for the SSM/T+SSM/T-2 system.

The examples of similar calculations of atmospheric humidity retrieval accuracies for different designs of outgoing microwave radiance measurements are given in Fig.4.11-4.13.

In Fig.4.11 we reproduce the curves $\Psi(p) = \hat{\sigma}_q(p)/\sigma_q(p)$ for two examined experiment designs at σ_{T_B}=0.3K. (Here $\sigma_q(p)$ and $\hat{\sigma}_q(p)$ are *a priori* and *a posteriori* RMS uncertainties of atmospheric humidity profiles). By definition, $\Psi(p)$ function characterizes a residual uncertainty in retrieval atmospheric humidity profile with respect to *a priori* uncertainty.(A case of $\Psi(p)=0$ corresponds to absolutely exact retrieval of the humidity profile, $\Psi(p)=1$ - to the lack of information about q(p) in outgoing radiance measurements.). Fig.4.11 demonstrates the essential advantages of the complete radiance experiment in comparison with SSM/T+SSM/T-2 system. At a number of atmospheric levels, the $\Psi(p)$ functions corresponding to examined measurement designs differ by 0.1-0.2. If we turn to frequent-used relative retrieval error $\hat{\sigma}_q(p)/\bar{q}$ (here $\bar{q}$ is the mean atmospheric humidity profile), the complete radiance experiment and SSM/T+SSM/T-2 system give the retrieval errors of 5-10% and 10-30%, respectively. Cited data prove the above conclusion that SSM/T+SSM/T-2 measurements does not make possible to derive all available information about atmospheric humidity profiles contained in outgoing microwave radiance.

Dependence of humidity retrieval errors (in the terms of $\Psi(p)$ function) on measurement errors is given in Fig.4.12 for the complete radiance experiment. The accuracy of humidity sounding increases with measurement error decrease. It is especially observed in the 600-800 mb layer, that is connected with vertical behavior of humidity weighting functions.

The contribution of null-space and random components (at σ_{T_B}=0.3K) into overall error of atmospheric humidity profile retrieval (in the terms of $\Psi(p)$ function) demonstrates Fig.4.13. As well as for the case of atmospheric temperature profile retrieval (see Fig.4.10), the principal contribution is introduced by null-space errors caused by the finite thickness of humidity weighting functions.

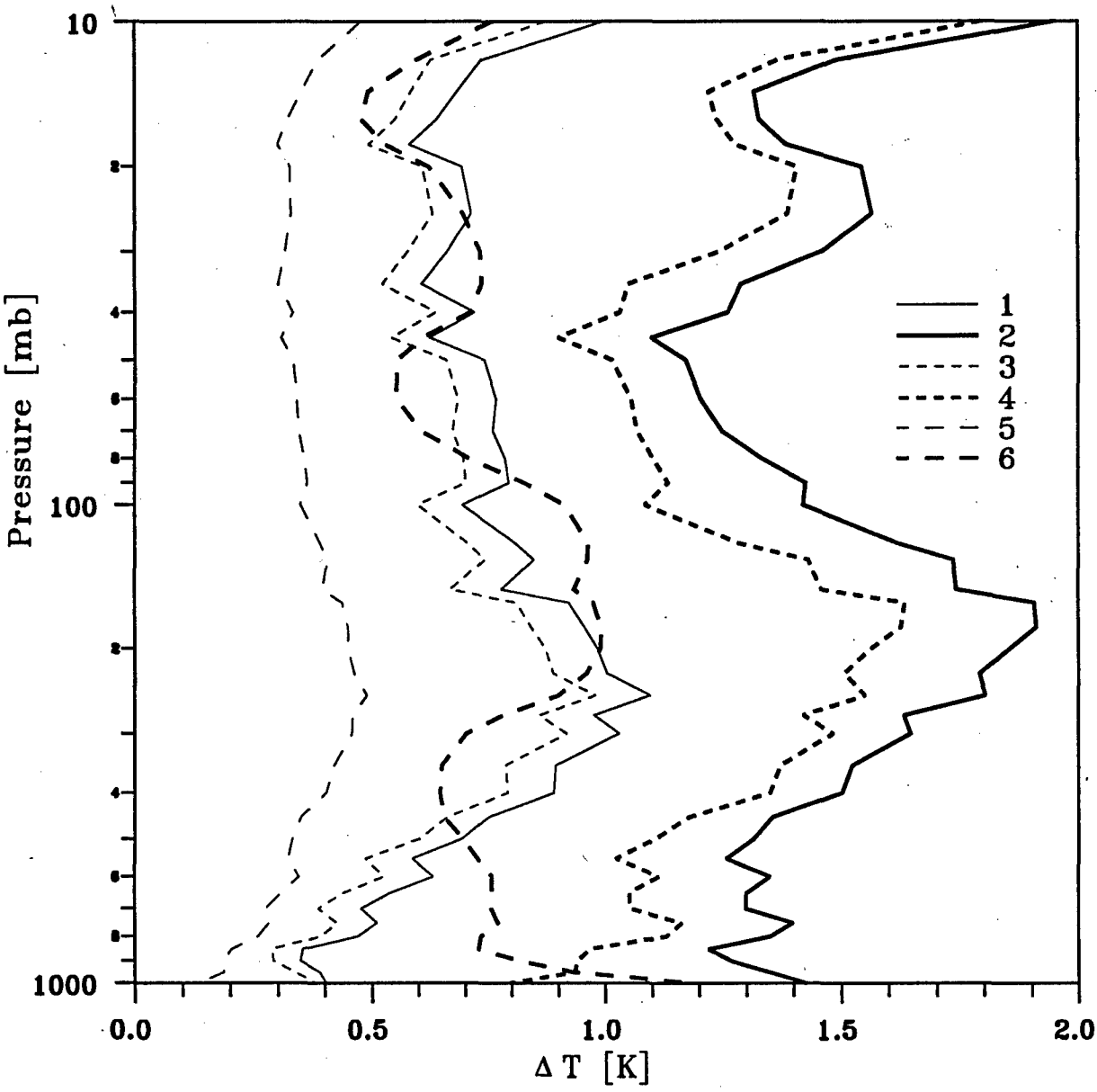

Fig.4.10.Potential errors (overall, null-space, random) of the temperature profile retrieval for two measurement designs: 1500 measurements and SSM/T+SSM/T-2. Sea, global statistics, measurement error - 0.3K.
1 - 1500 points, overall error
2 - SSM/T+SSM/T-2, overall error
3 - 1500 points, null-space error
4 - SSM/T+SSM/T-2, null-space error
5 - 1500 points, random error
6 - SSM/T+SSM/T-2, random error

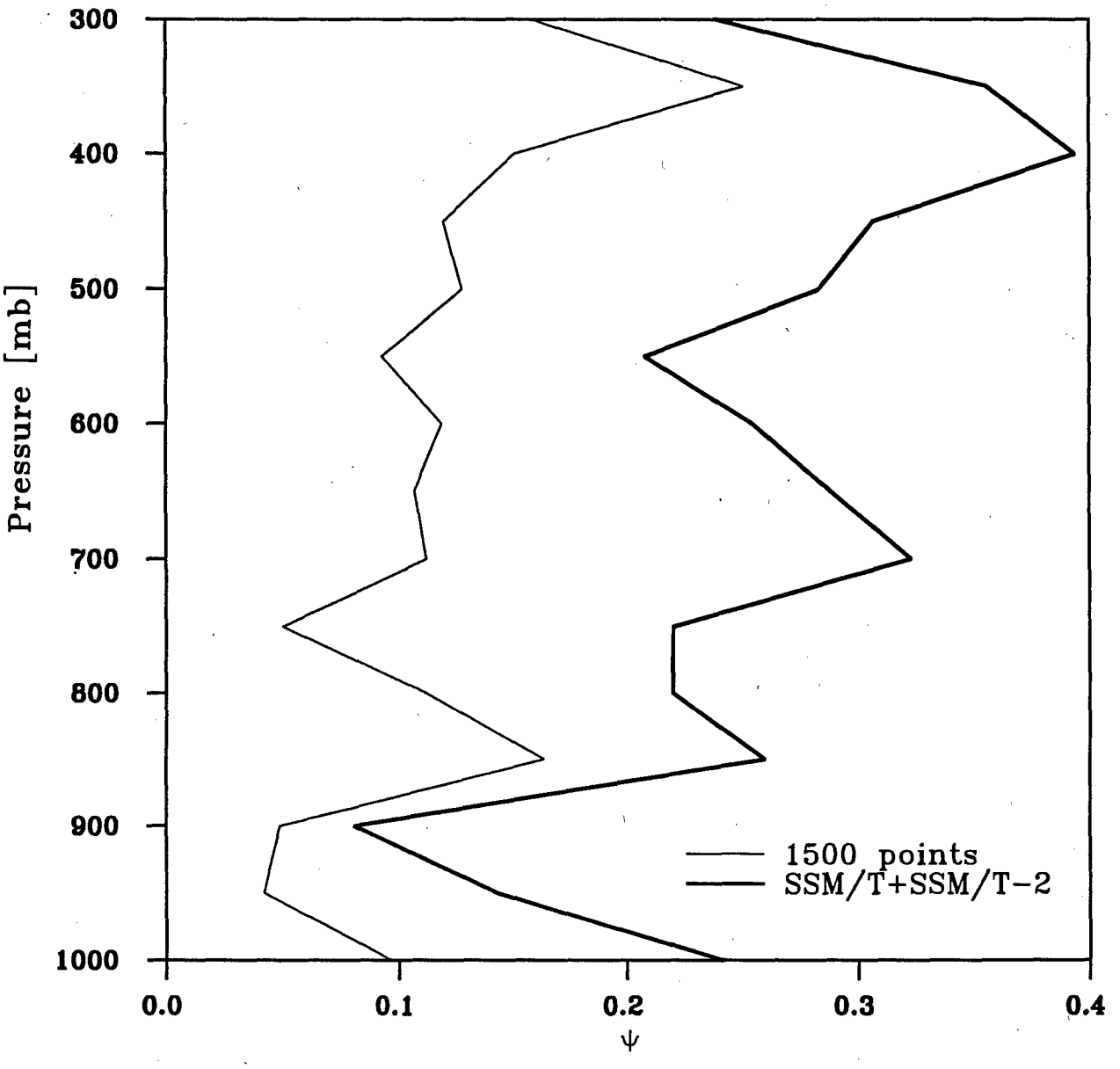

Fig.4.11.Function $\psi = \sigma_q(p)/\sigma_q(p)$ for two measurement designs: 1500 measurements and SSM/T+SSM/T-2. Sea, global statistics, measurement error - 0.3K.

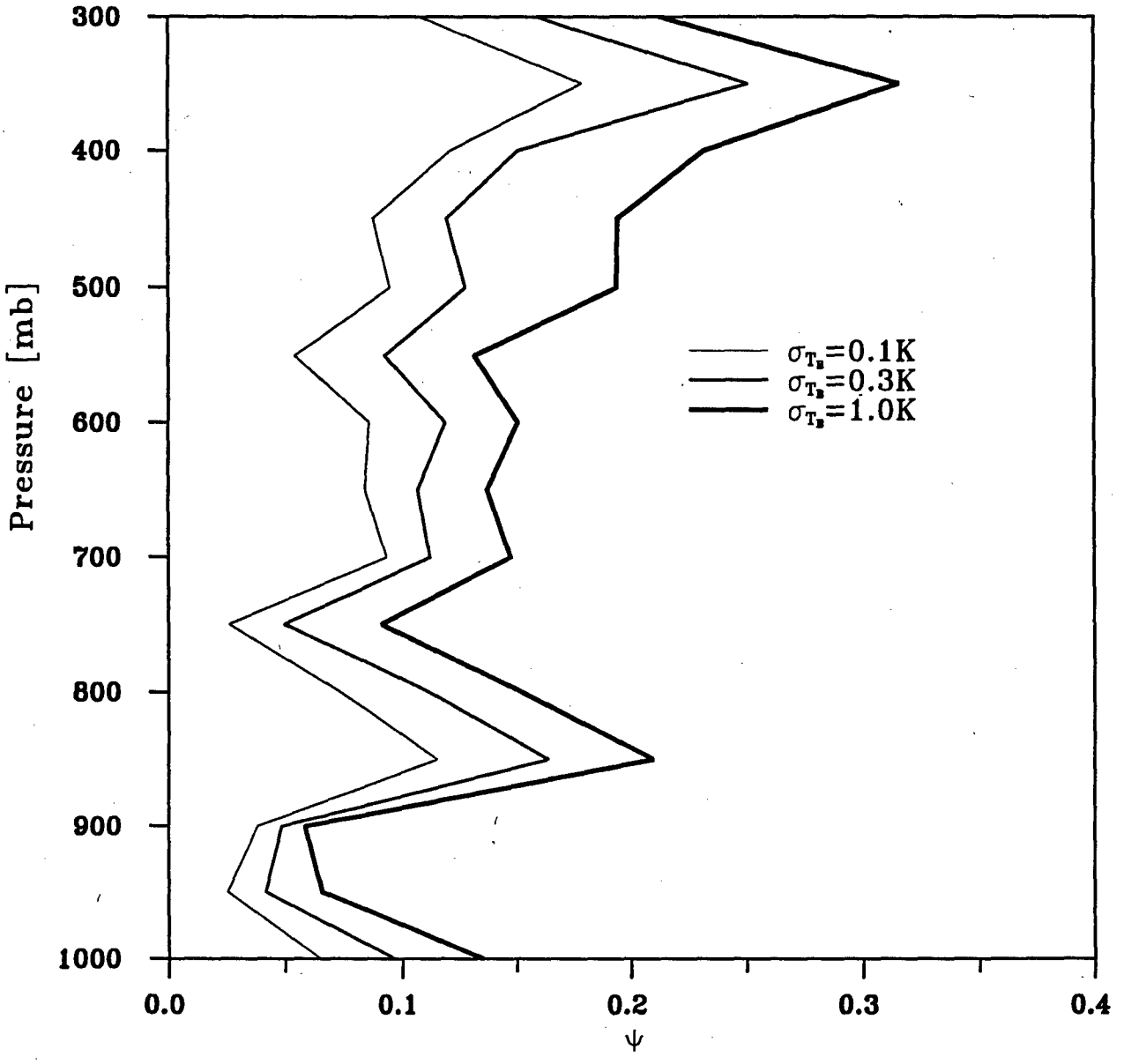

Fig.4.12.Function $\Psi=\sigma_q(p)/\sigma_q(p)$ at different measurement errors. Sea, global statistics, 1500 measurements.

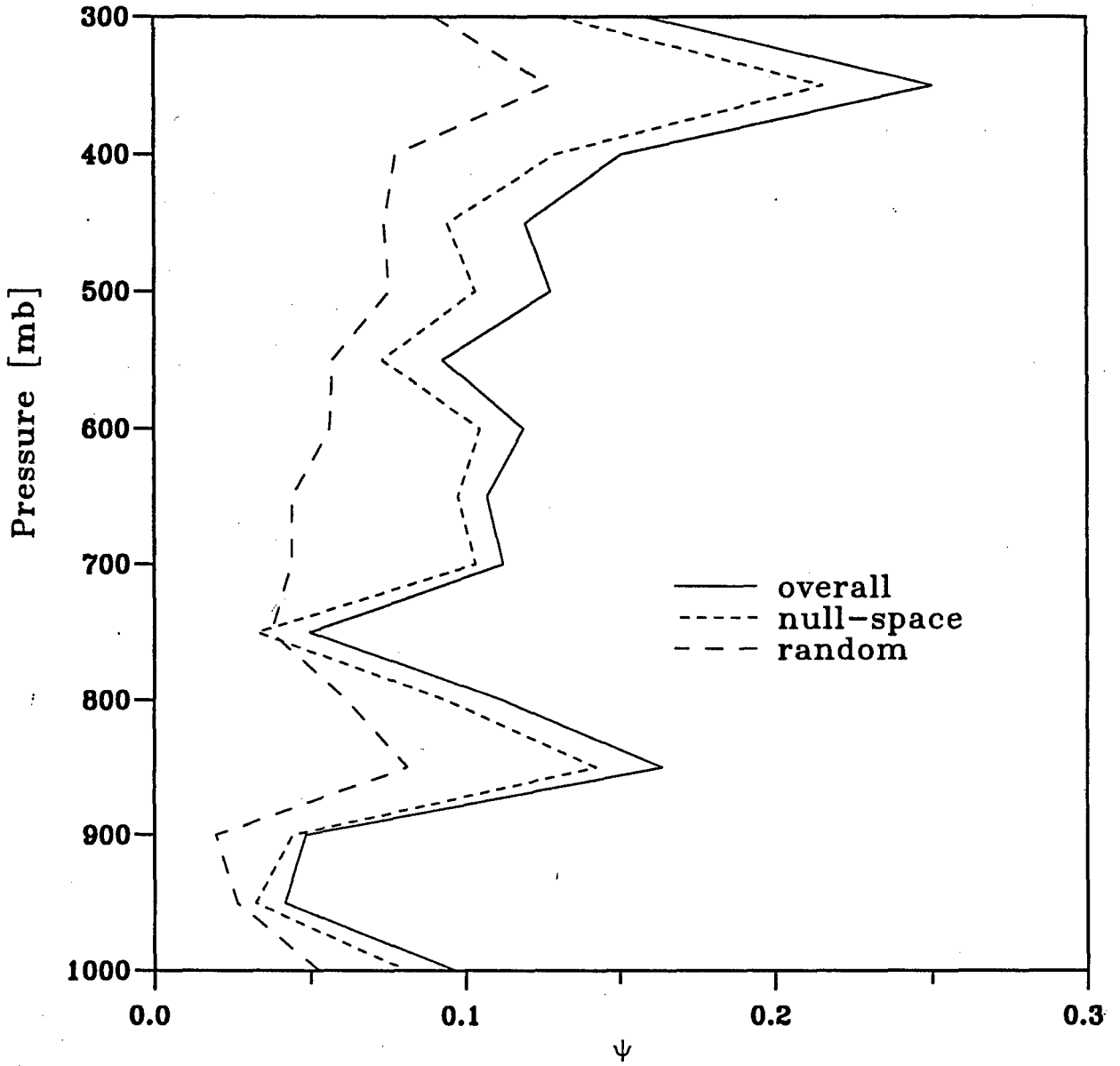

Fig.4.13.Potential errors (overall, null-space, random) of the humidity profile retrieval for 1500 measurements. Sea, global statistics, measurement error – 0.3K.

4.3.Numerical experiments on temperature-humidity sounding of the atmosphere

To illustrate the potential possibilities of the atmospheric temperature-humidity sounding for different designs of outgoing microwave radiance measurements, we have conducted the numerical experiments on the closed-loop scheme. The complete cycle of the numerical experiments includes the following steps:

1.For given model of atmospheric physical state, i.e. specific vertical temperature T(p) and humidity q(p) profiles, the brightness temperatures of outgoing radiance $T_B(f)$ are calculated by use of the radiative transfer model, described in Chapter 2.

2.The measurement errors are simulated by adding the $\varepsilon(f)$ values, produced by random-number generator and normally distributed with assigned variance $\sigma^2_{T_B}$, to the $T_B(f)$ values.

3.The joint estimates of atmospheric temperature and humidity profiles ($\tilde{T}(p)$ and $\tilde{q}(p)$) are retrieved by iterative method (formula (4.18)). All unknown parameters of the surface, namely, emissivity and surface temperature are derived simultaneously.

4.The retrieval errors are determined by comparison of the initial atmospheric profiles (T(p) and q(p)) with the estimates ($\tilde{T}(p)$ and $\tilde{q}(p)$).

It is necessary to note, that when solving the inverse problem, we have used the above iterative method, and the quasi-optimal estimates are defined, when the iterative process converges.

The examples of the temperature retrieval errors ($\Delta T(p)= T(p)-\tilde{T}(p)$) for different atmospheric models (σ_{T_B}=0.3K; the retrievals are carried out on 54 levels) are given in Fig.4.14-4.17 for two measurement designs (the complete radiance experiment and the SSM/T+SSM/T-2 system). The advantages of the complete radiance experiment in the temperature sounding are obvious on the most atmospheric levels. The errors of the temperature profile retrieval in the 10-1000 mb atmospheric layer do not exceed, as a rule, 1K for the complete radiance experiment. Those for the SSM/T+SSM/T-2 system may reach to 2-3K.

The influence of outgoing radiance measurement designs on the accuracy of humidity profile retrieval is illustrated by Figures 4.18-4.21. These Figures represent the initial q(p) profiles, the estimates $\tilde{q}(p)$ retrieved from the measurements simulating the complete radiance and DMSP experiments, and the mean atmospheric profile $\bar{q}(p)$. The advantages of the complete radiance experiment are especially

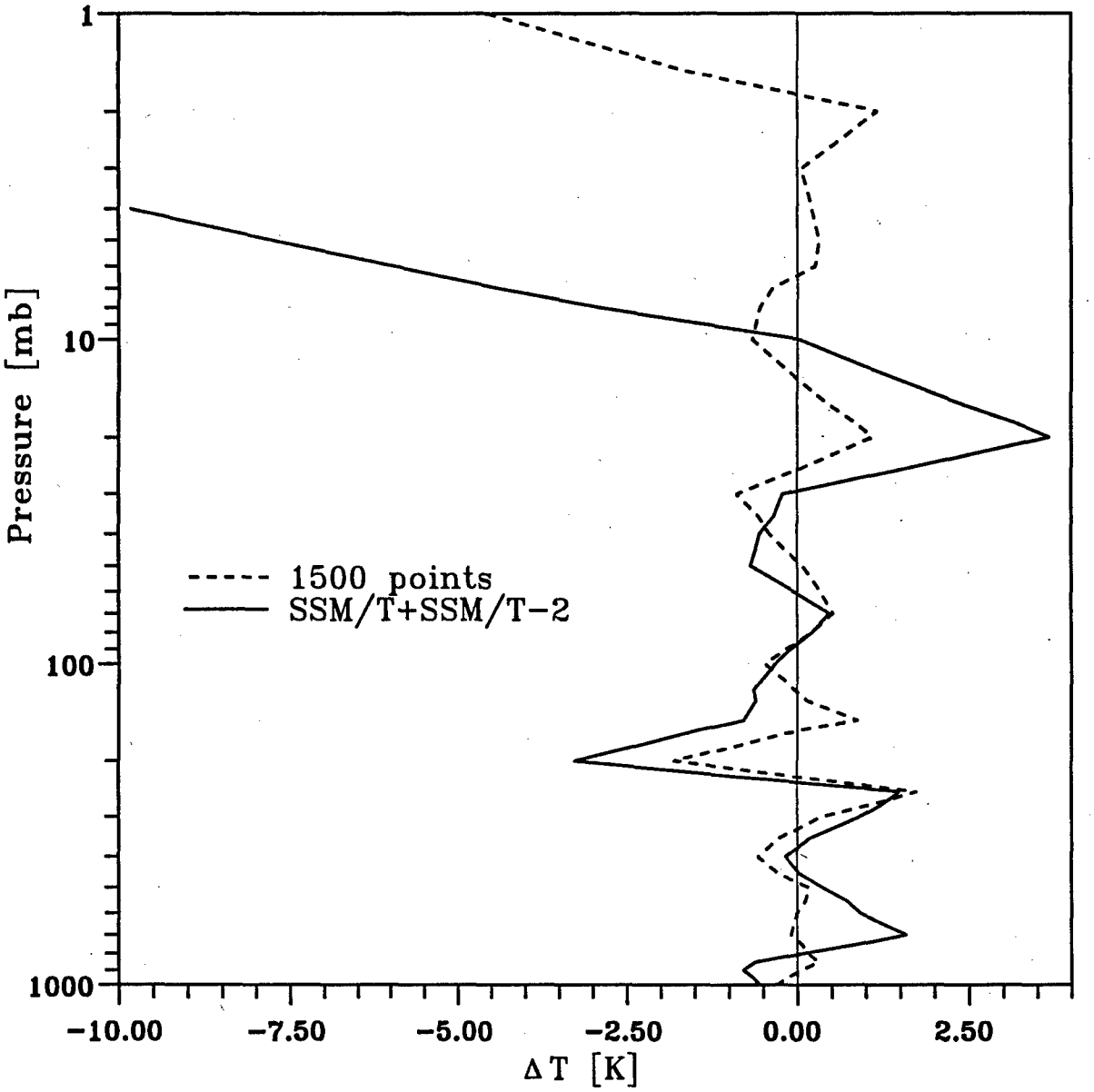

Fig.4.14.Temperature retrieval errors for two measurement designs: 1500 measurements and SSM/T+SSM/T-2 (numerical experiment).
Land, measurement error - 0.3K.

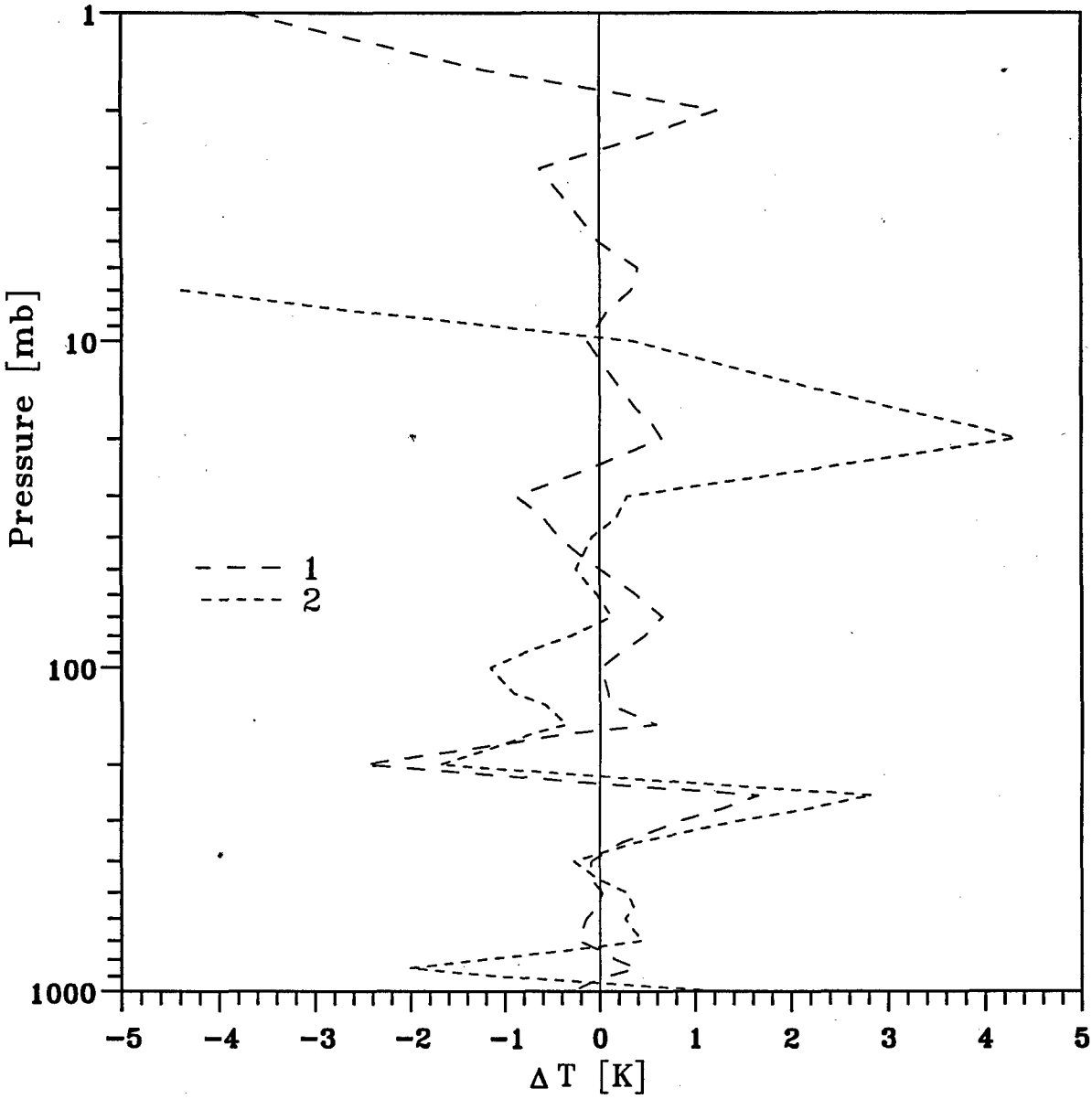

Fig.4.15.Temperature retrieval errors for two measurement designs: 1500 measurements and SSM/T+SSM/T-2 (numerical experiment). Land, measurement error - 0.3K.
1 - 1500 measurements
2 - SSM/T+SSM/T-2

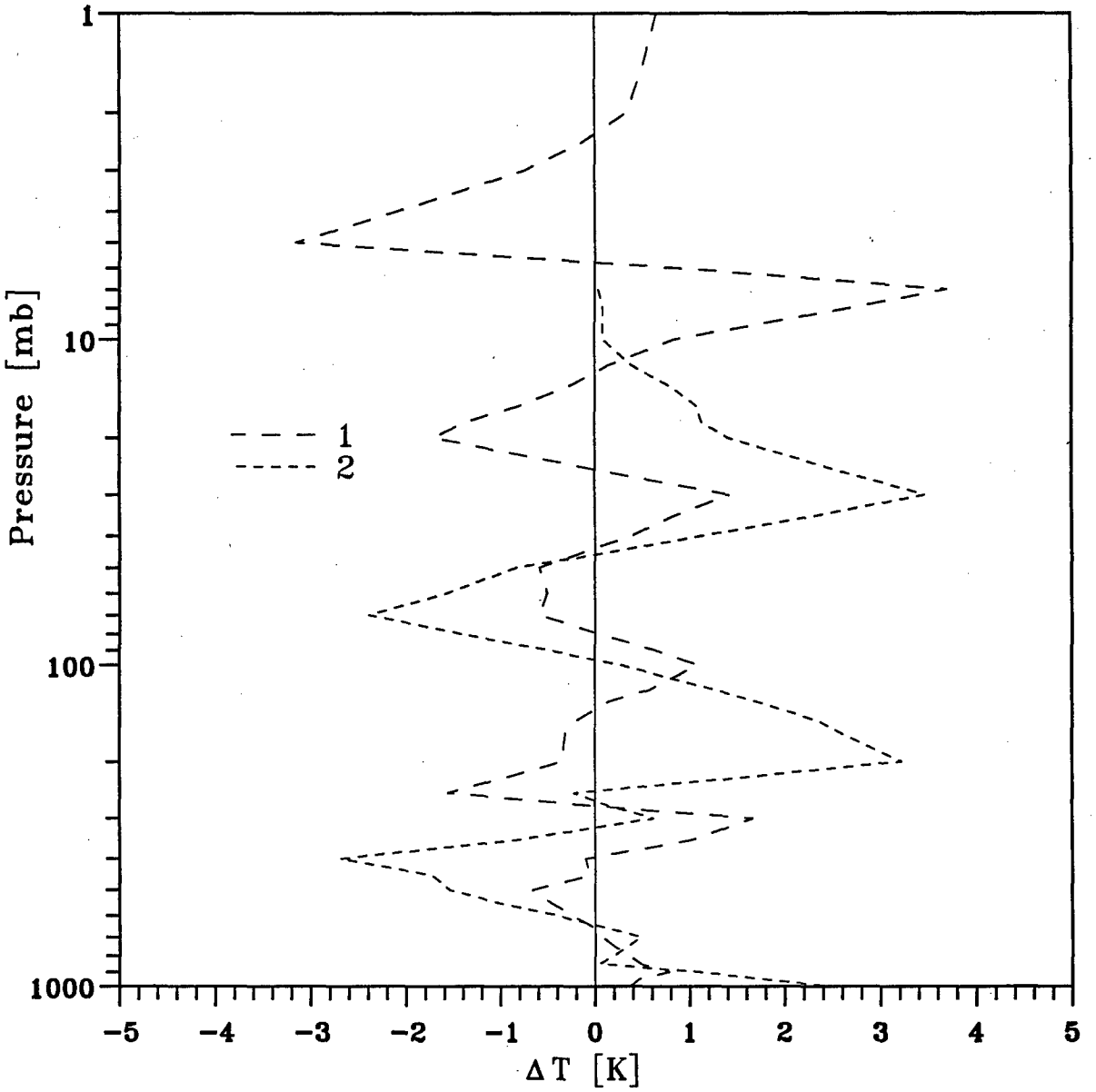

Fig.16.Temperature retrieval errors for two measurement designs: 1500 measurements and SSM/T+SSM/T-2 (numerical experiment). Land, measurement error - 0.3K.
1 - 1500 measurements
2 - SSM/T+SSM/T-2

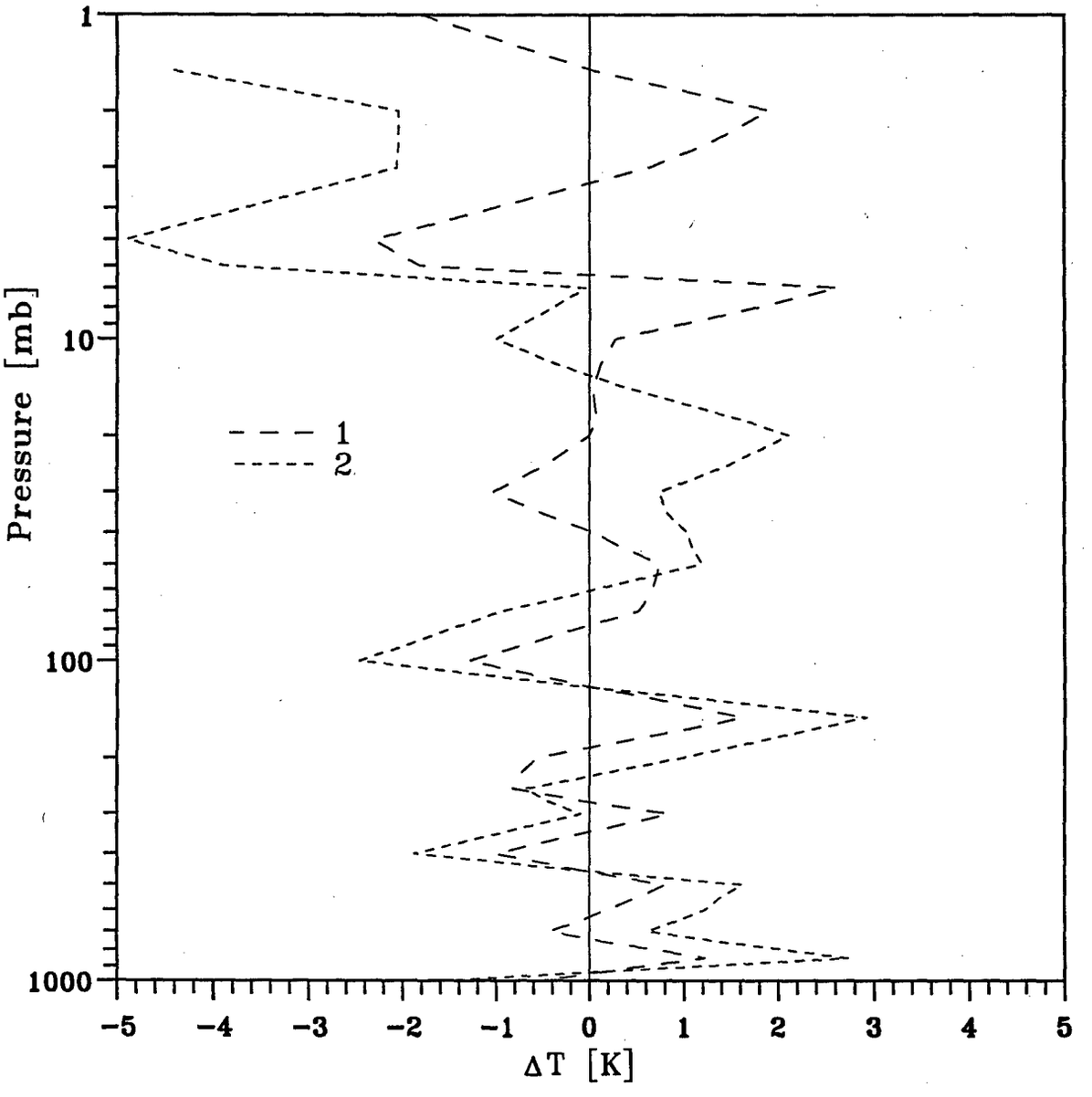

Fig.4.17.Temperature retrieval errors for two measurement designs: 1500 measurements and SSM/T+SSM/T-2 (numerical experiment). Sea, measurement error - 0.3K.
1 - 1500 measurements
2 - SSM/T+SSM/T-2

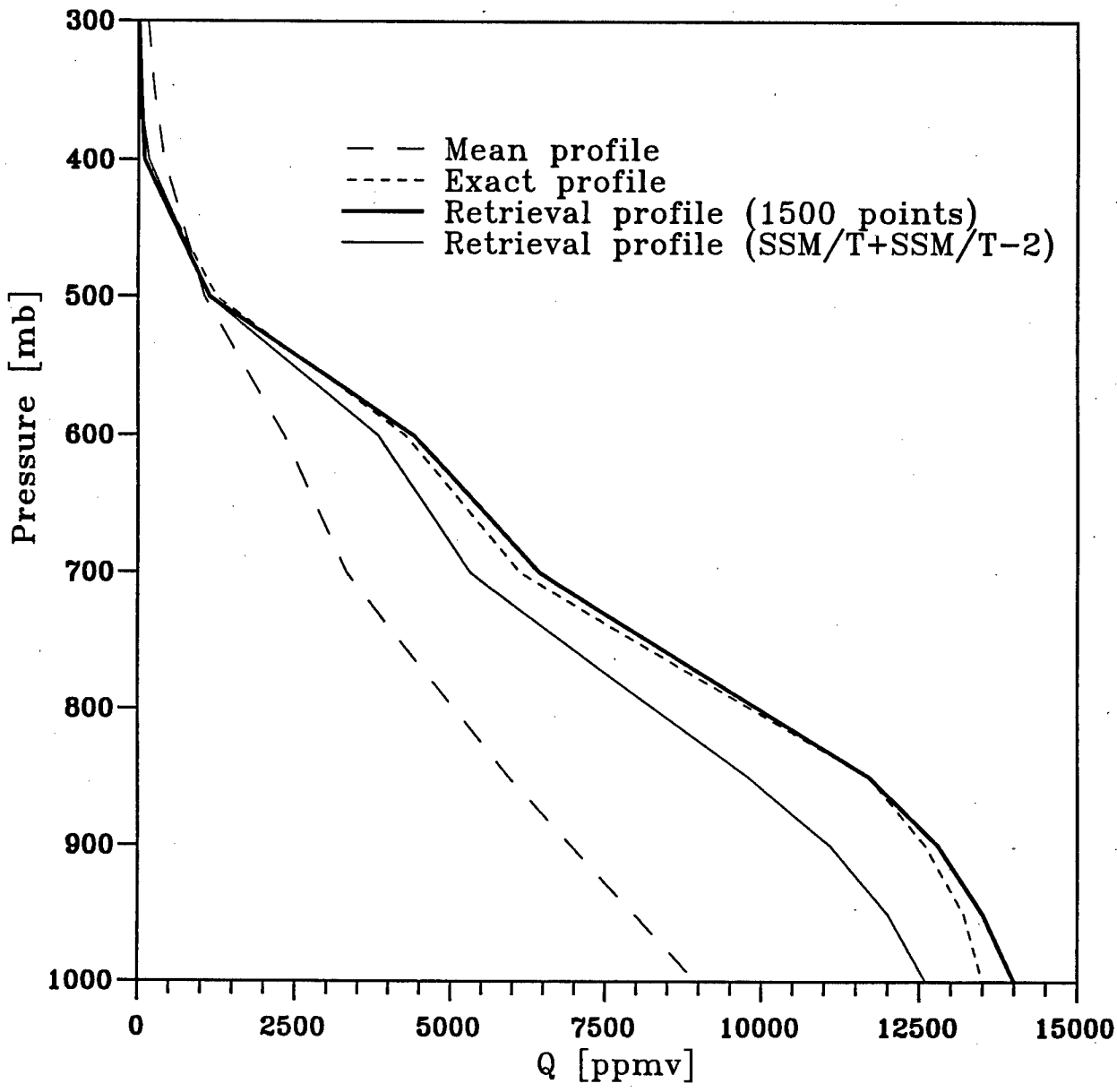

Fig.4.18. Humidity profile retrievals for two measurement designs: 1500 measurements and SSM/T+SSM/T-2 (numerical experiment).
Land, measurement error - 0.3K.

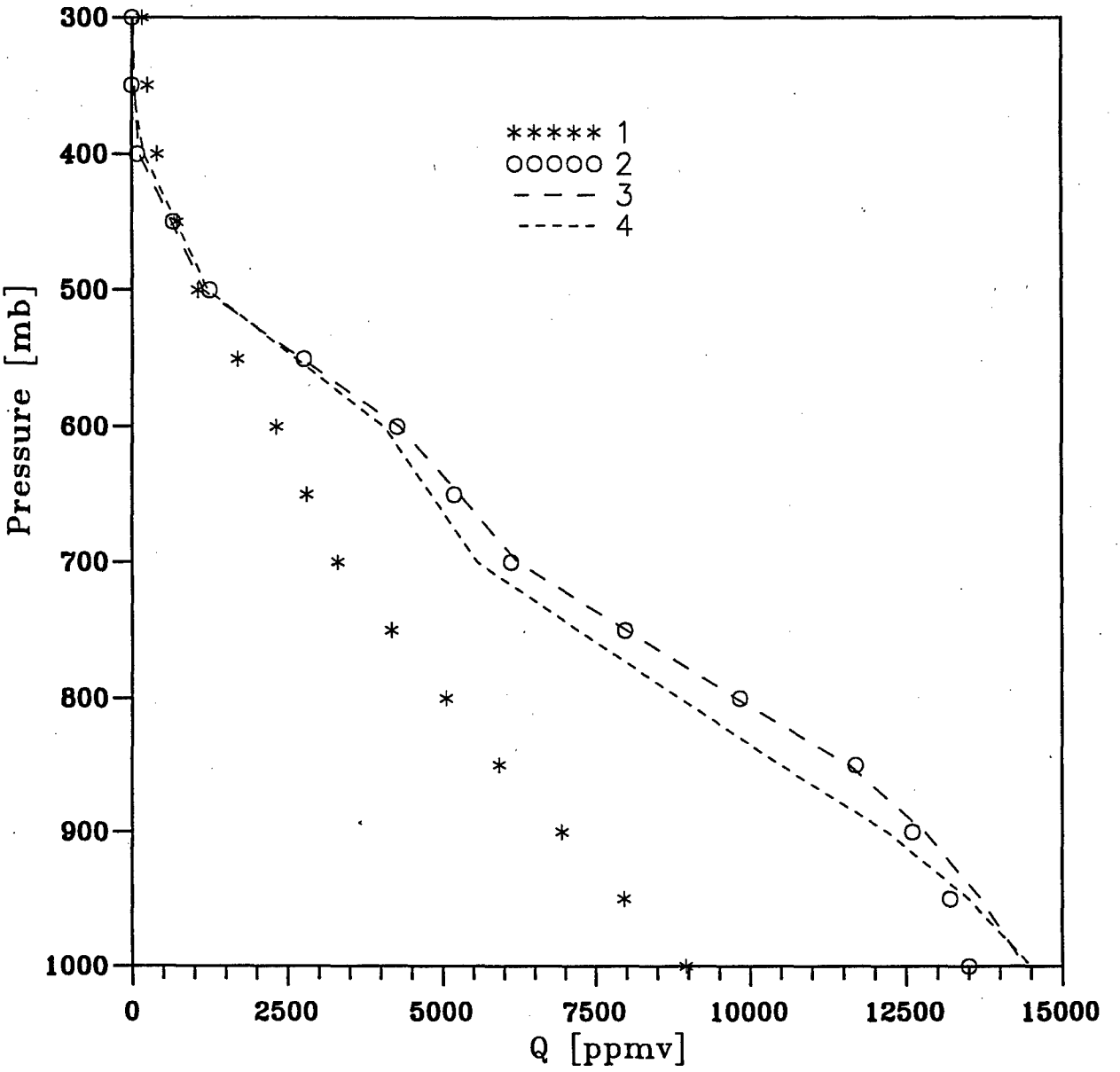

Fig.4.19.Humidity profile retrieval for two measurement designs: 1500 measurements, and SSM/T+SSM/T-2 (numerical experiment). Land, measurement error - 0.3K.
1 - the mean profile
2 - exact profile
3 - 1500 measurements
4 - SSM/T+SSM/T-2

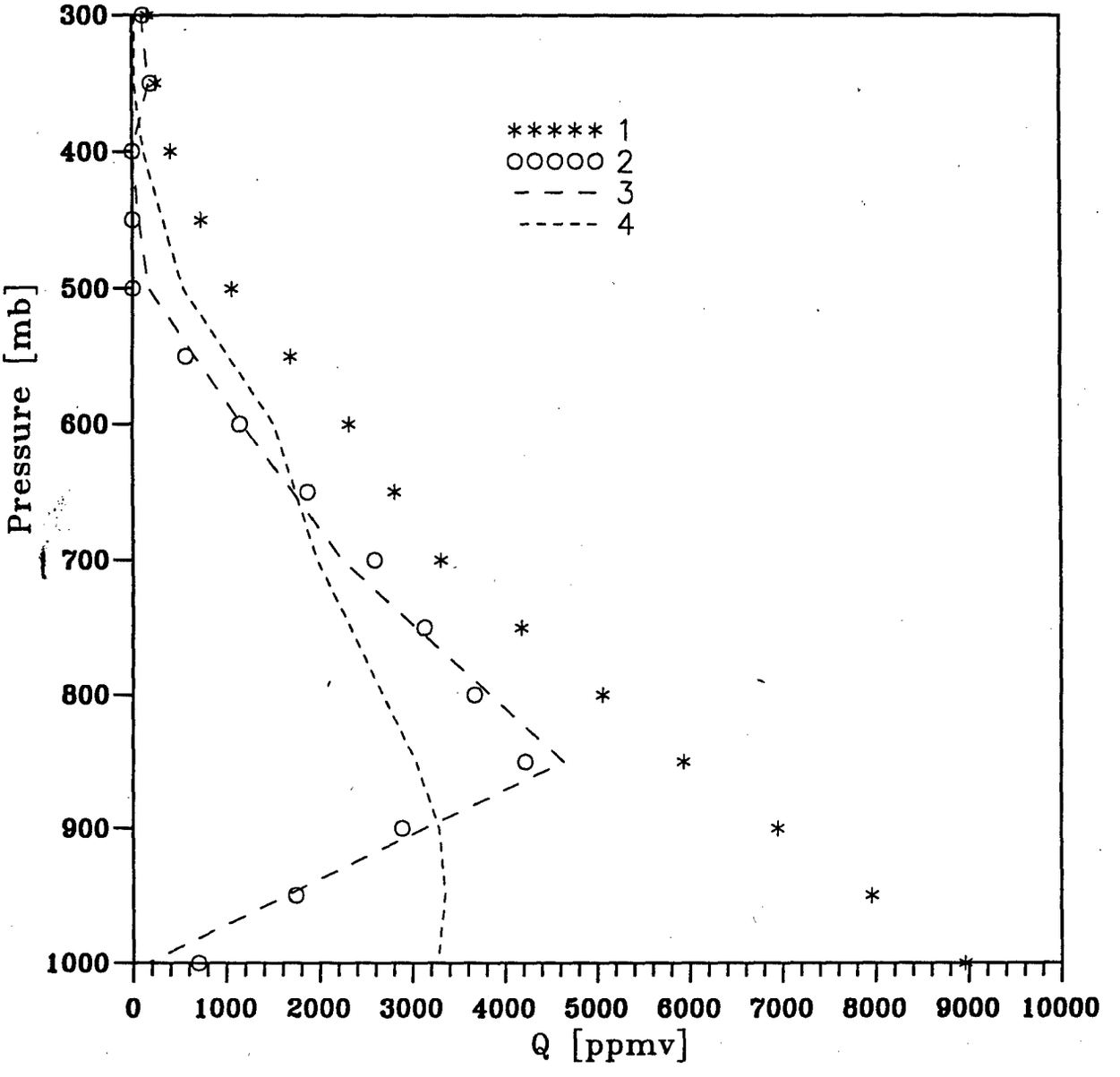

Fig.4.20.Humidity profile retrieval for two measurement designs: 1500 measurements and SSM/T+SSM/T-2. Sea, measurement error - 0.3K.

1 - the mean profile
2 - exact profile
3 - 1500 measurements
4 - SSM/T+SSM/T-2

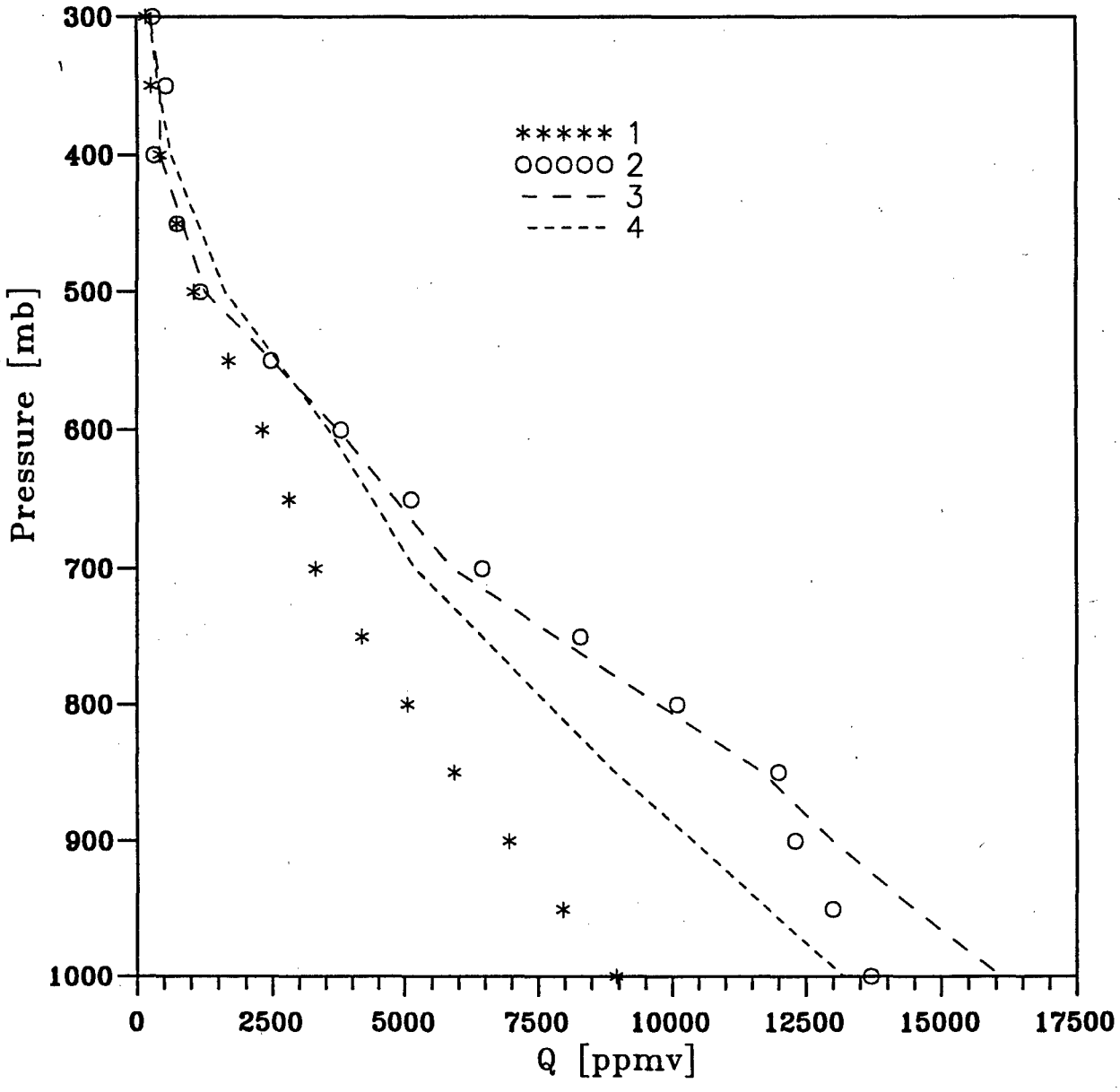

Fig.4.21.Humidity profile retrieval for two measurement designs: 1500 measurements and SMM/T+SMM/T-2 Land, measurement error - 0.3K.
1 - the main profile
2 - exact profile
3 - 1500 measurements
4 - SSM/T+SSM/T-2

revealed in Fig.4.19, 4.20. It is seen, that the complete radiance experiment allows to retrieve a relatively sophisticated vertical structure of q(z) profiles with high accuracy. The remote sensing system of DMSP satellite gives strongly smoothed $\tilde{q}(p)$ and, as a consequence, the errors of the humidity retrieval from the DMSP data are essentially larger.

Similar examples of the numerical experiments on atmospheric temperature retrievals in 18 atmospheric layers are given in Figures 4.22-4.24. The advantages of the complete radiance experiment are evident. In the most cases, the atmospheric temperature profile may be retrieved using the complete radiance experiment data with the errors which are less than 1K.

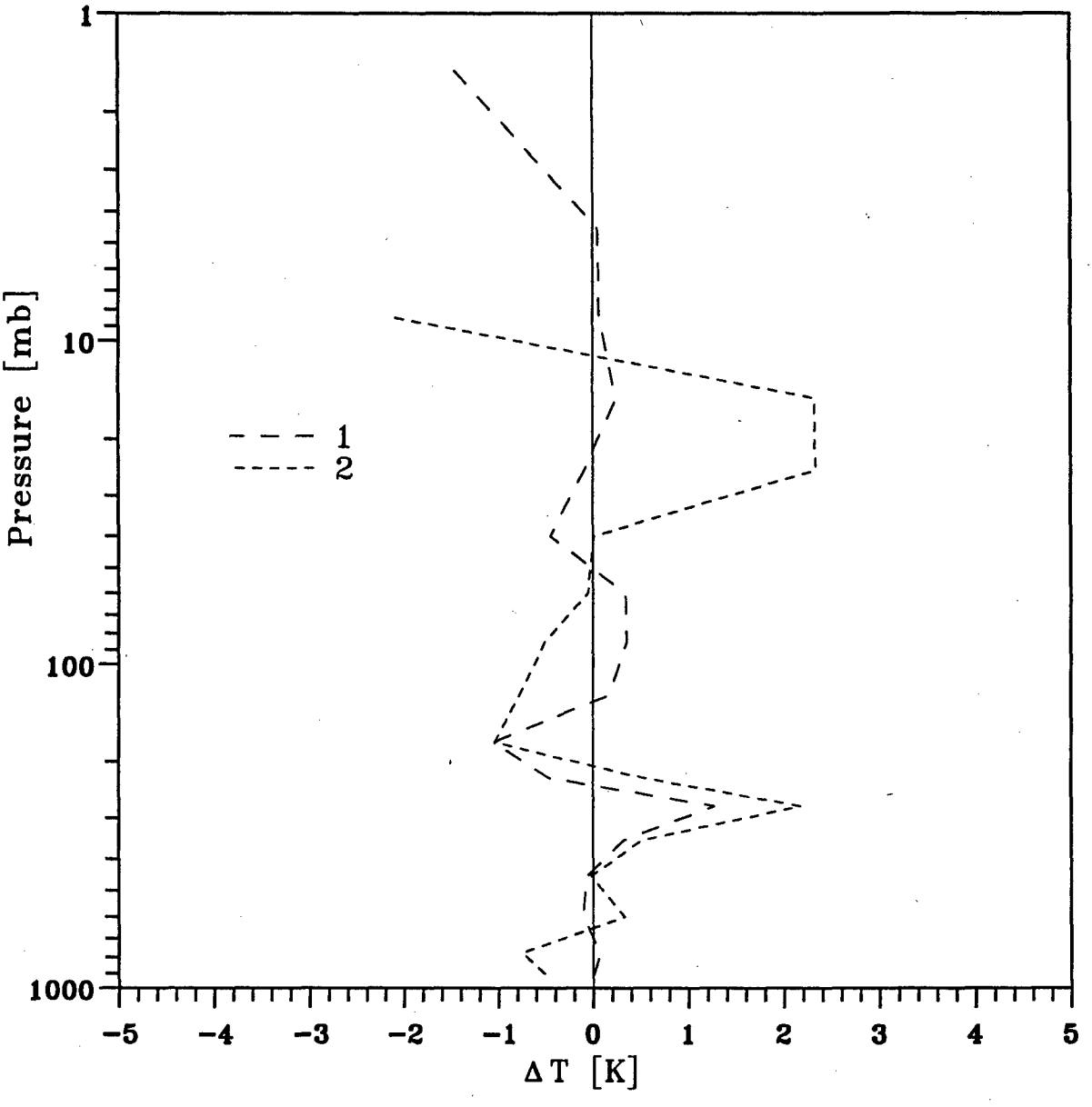

Fig.4.22.Errors of the temperature retrievals in 18 atmospheric layers for two measurement designs: 1500 measurements and SSM/T+SSM/T-2 (numerical experiment).
Land, measurement error - 0.3K.
1 - 1500 measurements
2 - SSM/T+SSM/T-2

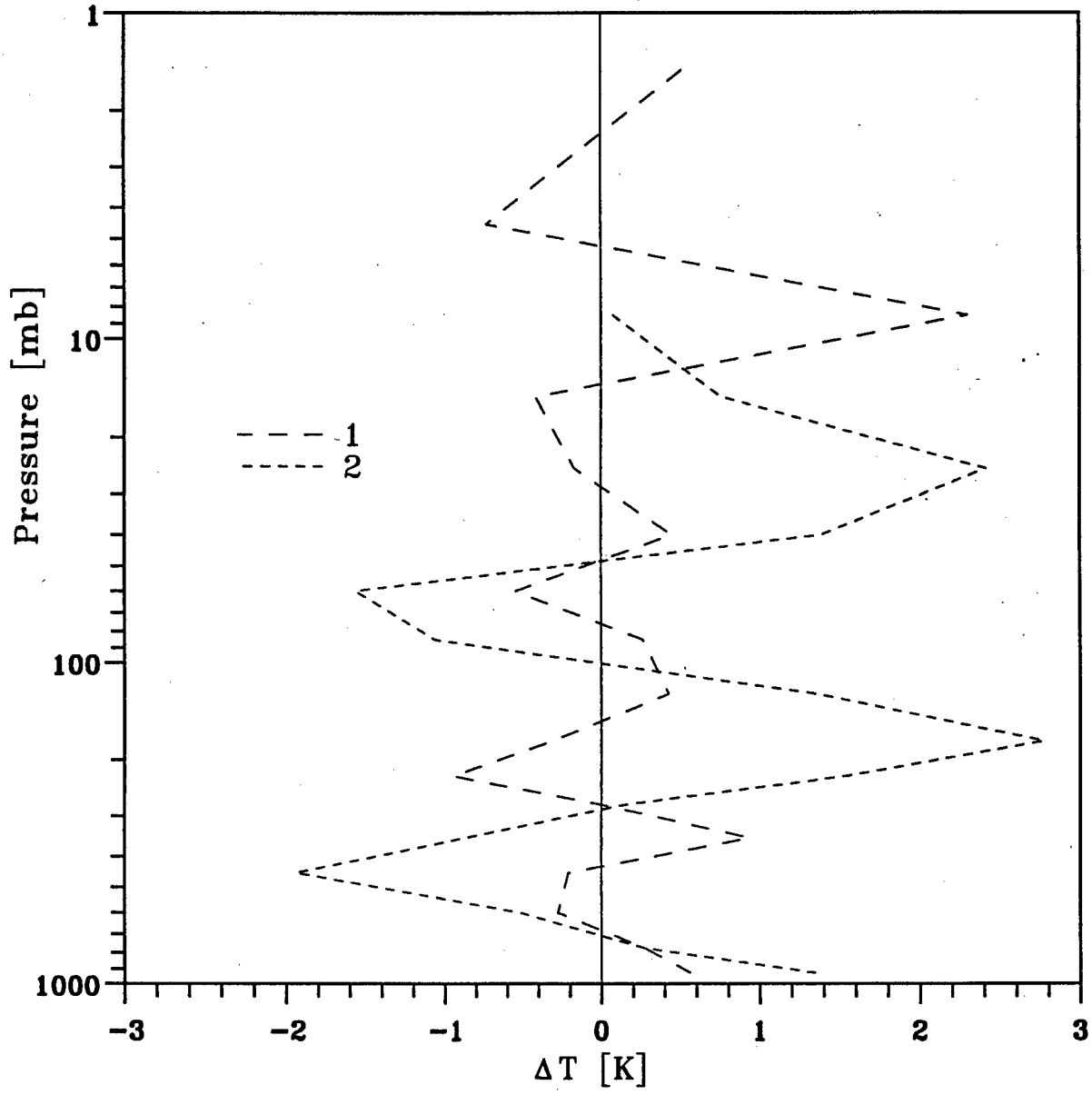

Fig.4.23.Errors of the temperature retrievals in 18 atmospheric layers for two measurement designs: 1500 measurements and SSM/T+SSM/T-2 (numerical experiment).
Land, measurement error - 0.3K.
1 - 1500 measurements
2 - SSM/T+SSM/T-2

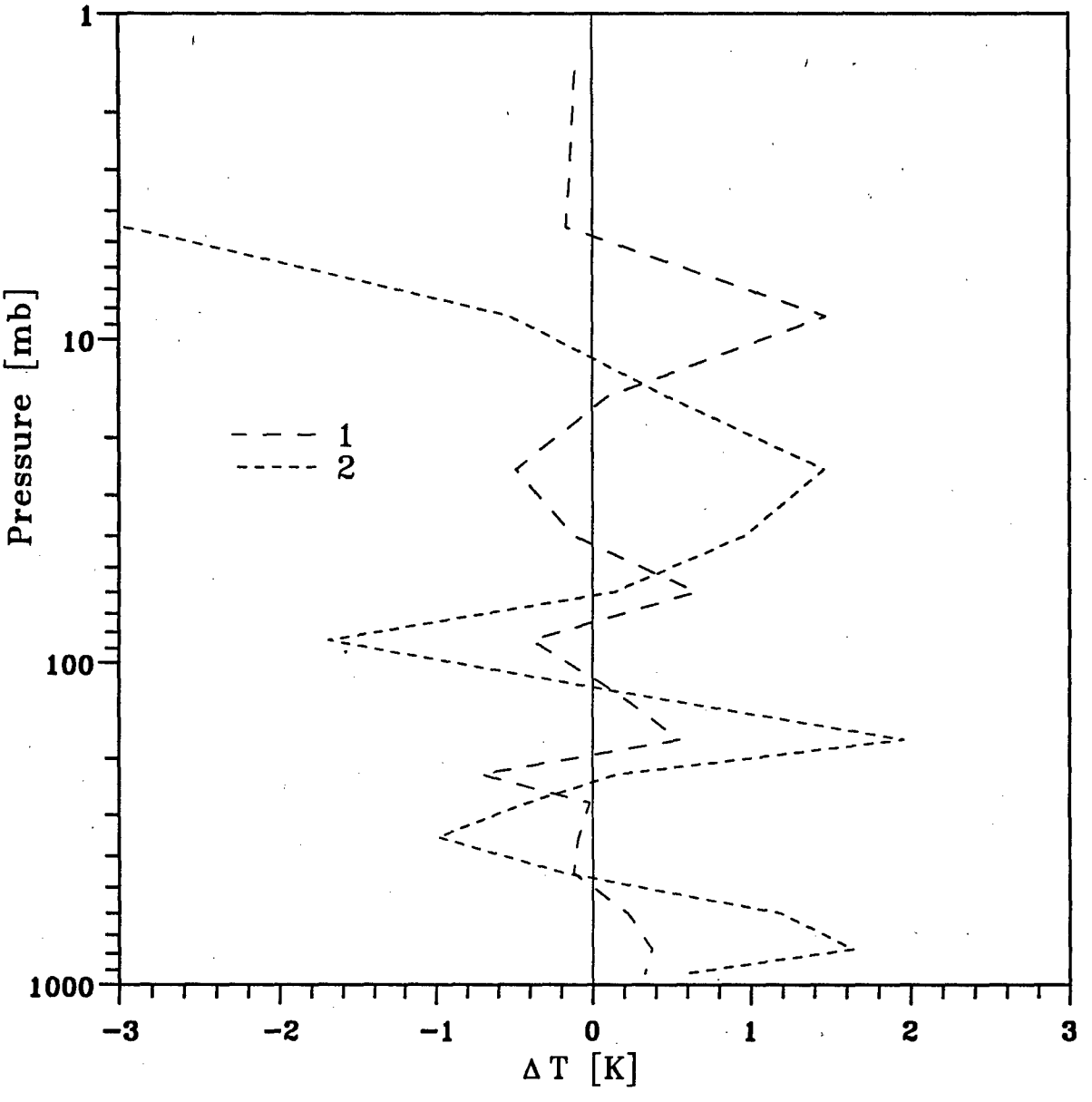

Fig.4.24. Errors of the temperature retrievals in 18 atmospheric layers for two measurement designs: 1500 measurements and SSM/T+SSM/T-2 (numerical experiment).
Sea, measurement error – 0.3K.
1 – 1500 measurements
2 – SSM/T+SSM/T-2

5.PRINCIPAL RESULTS AND CONCLUSIONS

The studies performed in the frame of the Special Contract SPC-94-4086 have given the following results:

1.A new code (MIT-SPbSU program) for calculations of outgoing microwave brightness temperatures $T_B(f)$ for a case of cloudless atmosphere has been developed. Liebe's (1993) algorithm of accounting for atmospheric radiative characteristics is assumed as a basis of this program. Distinctive characteristic of this program is a possibility to account the variational derivatives of brightness temperature with respect to different physical parameters of atmosphere and underlying surface (atmospheric vertical temperature and humidity profiles, surface emissivity).
Performed comparisons of T_B values calculated by MIT-SPbSU code and independent data have demonstrated a high quality of the developed program. Dependencies of T_B variational derivatives with respect to different parameters of atmospheric state have been analyzed. It is shown, for example, that a problem of atmospheric humidity remote sounding is essentially nonlinear.

2.The software meant for the solution of the inverse problems and for the calculations of error estimates of temperature-humidity satellite sounding in the 1-200 GHz spectral range has been developed. This code is based on the known iterative method (Polyakov and Rozanov, 1989; Marks and Rodgers, 1993), but it has been modified to retrieve the optimal, in the statistical sense, estimates of the solution.

3.The calculations of covariance matrices $\mathbf{K}_{T_B T_B}$ of outgoing microwave radiance for limited, but representative, ensemble of atmospheric states corresponding to global observations have been conducted. 1500 measurement channels in the 1-200 GHz spectral range with special channel choice are used to describe in detail the optical atmospheric characteristics and to simulate "the complete radiance experiment". The calculations of $\mathbf{K}_{T_B T_B}$ are carried out for two types of underlying surface - sea and land. The choice of the emissivity models employed for atmospheric studies has been justified by emissivity calculations for available part of examined range using the special developed code.

4.The eigenvalues and eigenvectors of outgoing radiance covariance matrices have

been calculated for two experiment designs - "complete radiance experiment" and experiment using SSM/T and SSM/T-2 measurements from DMSP satellite. According to Kozlov's criterion (Kozlov, 1966), a number of independent information components contained in outgoing radiance measurements has been defined for different measurement designs and error levels. It is shown, that for examined atmospheric parameter set, corresponding to the global observations, a number of independent measurement components ranges from 15 to 31 depending, first of all, on random measurement errors σ_{T_B} and surface type. So, for example, at σ_{T_B}=0.5K there is a possibility to "pick out" 18 (land) and 22 (sea) independent information components, caused by temperature and humidity variations, from outgoing microwave radiance spectra. These values essentially exceed the number of SSM/T and SSM/T-2 channels, intended for temperature and humidity sounding.

The additional calculations have demonstrated that the most part of independent information components is connected with temperature profile variations. But, the humidity profile variations form 6-8 independent information components in the space of measured signals.

Analysis of the eigenvalues of the radiance covariance matrices, corresponding to SSM/T and SSM/T-2 radiometer measurements shows, that there are 2-3 "redundant" measurement channels in SSM/T radiometer at σ_{T_B}=0.5-1.0K, and the same one channel for SSM/T-2 radiometer at σ_{T_B}=1.0K. This fact (with regard for performed information content analysis for "complete radiance experiment") justifies indirectly to non-optimal positions of DMSP spectral channels.

5.Information content of outgoing microwave radiance measurements has been defined by two criterions: according to Shannon and Kozlov. These calculations demonstrated the "information advantage" of the complete radiance experiment in comparison with SSM/T and SSM/T-2 measurements even with accounting for different number of measurement channels.

6.On the basis of the error matrix calculations, the temperature and humidity retrieval errors have been calculated for different experiment designs, measurement errors, "global" and "local" statistics, and 54 levels and 18 atmospheric layers. Analysis of the results has confirmed the principal conclusions received on the basis of information content calculations:

a).Accuracy of the temperature profile retrieval from the complete radiance experiment data is essentially better than that for SSM/T and SSM/T-2 measurements. In particular, at σ_{T_B}=0.3K, the retrieval errors for experiment with

1500 channels are smaller by 1.0K for a case of using global statistics.

b).Temperature retrieval errors decrease noticeably for both experimental designs if average temperatures in 18 atmospheric layers are defined and/or the local atmospheric statistics is used for the retrieval. In this case, for example, at σ_{T_B}=0.3K, the complete radiance experiment makes a possible to decrease a "potential" error to 0.3-0.9K in the 10-1000 mb layer. The minimal temperature retrieval errors which can be achieved using DMSP sounding system are greater by 0.7-1.0K.

c).Similar advantages of the complete radiance experiment are observed during humidity atmospheric sounding. At σ_{T_B}=0.3K, minimal potential errors of relative humidity profile retrieval are 5-15% and 10-30% in the 300-1000 mb atmospheric layer for 1500 measurements and SSM/T + SSM/T-2 measurements, respectively.

7.The numerical simulation of the satellite experiments on joint atmospheric temperature and humidity profile retrieval has been carried out. The analysis of the retrieval errors confirms the principal conclusions obtained as a result of the information content and potential accuracy studies.

Thus, performed numerical studies of information content of outgoing microwave measurements and the accuracy of atmospheric temperature and humidity sounding let draw the following main conclusions:

1.Outgoing microwave radiance spectra in the 1-200 GHz range contain a considerable quantity of information about vertical temperature and humidity atmospheric profiles. In the terms of independent information components, this information is characterized by 15-31 parameters depending on the levels of experimental errors. The main part of these components describes the temperature variations (11-21 parameters), the other (5-11 parameters) characterize the humidity profile variations.

2.A number of measurement channels of SSM/T + SSM/T-2 system of DMSP satellite is deficient to extract all existing information about atmospheric temperature and humidity profiles from outgoing microwave radiance spectra. Besides, the channel spectral locations are not optimal in a number of cases.

So the most important problem is to compute the optimal experiment designs for microwave radiometer with about 30 channels on the basis of recent methods of measurement condition optimization.

6.REFERENCES

Basharinov A.E., and A.M.Shutko, 1975: Simulation studies of the SHF radiation characteristics of soils under moist conditions. *NASA Tech.Transl., TTF-16.*

Bauer A., and M.Godon, 1991: Temperature dependence of water vapour absorption in line-wings at 190 GHz. *Journ. Quant. Spectr.Rad. Tran.*, **46**, 3, 211-220.

Becker G.E., and S.H.Autler, 1946: Water vapour absorption of electromagnetic radiation in the cm wave-length range. *Phys.Rev.*, **70**, 300-307.

Box G.E.P., 1952: Multifactor. Designs of first order. *Biometrica,* **39**, 1, 49-57.

Chedin A., H.Fisher, K.Kunzi, D.Spankuch, N.A.Scott, 1988: Report of the ITRA (Intercomparison of transmittance and radiance algorithms), *Intern.Radiation Commission, Univ. Maryland, USA.*

Choudhury B.J.,T.J.Schmugge, R.W.Newton, and A.Chang, 1979: Effect of surface roughness on microwave emission from soils. *Journ.Geoph.Res.,* **84**, 5699-5706.

Ferraro R., N.Grody and J.Kogut, 1986: Classification of geophysical parameters using passive microwave satellite measurements. *IEEE Trans.Geosci.Rem.Sens.,* **GE-24**, 6, 1008-1013.

Furashov N.I., V.Yu.Katkov, B.A. Svertlov, 1989: Submillimetre spectrum of the atmospheric water vapor absorption - Some experimental results. *ICAP 89, IEE Conf.Publ.*, 301, 310-311.

Godon M., J.Carlier, A.Bauer, 1992: Laboratory studies of water vapor absorption in the atmospheric window at 213 GHz. *J. Quant. Spectr. Rad. Tran.*, **47**, 4, 275-285.

Hollweg H.-D., V.S.Kostsov, G.Schlüssel, P.Schlüssel, Yu.M.Timofeyev, 1994: Interaction at mm and optical frequencies. *Interim Report. AO/1-2708/93/NL/NB, Universität Hamburg, Meteorologisches Institut, FRG, 7-th July.*

Houghton J.T., F.W.Tailor, C.D.Rodgers, 1986: Remote sounding of atmospheres. *Cambridge University Press.*

Isaacs R.G., G.Deblonde, 1987: Millimeter wave moisture sounding: The effect of clouds. *Radio Sci.,***22**, 3, 367-377.

Jackson T.J., and O'Neill, 1990: Attenuation of soil microwave emissivity by corn and soybeans at 1.4 and 5 GHz. *IEEE Trans.Geosci.Rem.Sens.,* **GE-28**, 978-990.

Jackson T.J., T.J.Schmugge,1991: Vegetation effects on the microwave emission of soils. *Rem.Sens.Environ.,* **36**, 203-212.

Kirdiashev K.P., A.A.Chukhlantsev, and A.M.Shutko, 1979: Microwave radiation on the earth's surface in the presence of vegetation cover. *Radio Eng.Electron.,* **24**, 256-264 (English Translation).

Klein L. and C.Swift, 1977: An improved model for dielectric constant of sea water at microwave frequencies. *IEEE J.Ocean.Eng.*, **OE-2**, 1, 104-108.

Konyate F., F.T.Ulaby, A.K.Fung, 1981: Microwave emission from a periodic soil surface. *Rem.Sens.Lab., Univ.Kansas Center for Res., AgRISTARS SM-K1-04180, Tech.Rep.*

Kozlov V.P., 1966: On vertical temperature profile retrieval from outgoing radiance spectrum. *Atmosph. Oceanic Phys.*, **2**, 10, 137-148, (English Translation).

Kozlov V.P.,Yu.M.Timofeyev, M.I.Trifonov, 1983: On optimization of conditions of outgoing radiation measurements in the problem of sea surface temperature remote sensing. *Sea Optics, Moscow, isd. Nauka,* 173-178, (in Russian).

Kuo C.C., D.H.Staelin, P.V.Rosenkranz,1994: Statistical iterative scheme for estimating atmospheric relative humidity profiles. *IEEE Trans.Geosci.Rem.Sens,* **32**, 2 254-259.

Leschansky Yu.I., G.N.Lebedeva, V.D.Shumilin, 1971: Dielectric properties of sand and clay soils in the centimeter, decimeter and meter band. *Radiophysics*, **14**, 562, (in Russian).

Liebe H.J., 1981: Modeling attenuation and phase of radio waves in air at frequencies below 1000 GHz. *Radio Science*, **16**, 1183-1199.

Liebe H.J., 1985: An updated model for millimeter wave propagation in moist air. *Radio Science*, **20**, 1069-1089.

Liebe H.J., 1987: A contribution to modeling atmospheric millimeter-wave properties. *Frequenz.*, **41**, 31-36.

Liebe H.J., 1988: Atmospheric attenuation and delay rates between 1 GHz and 1 THz. *Conference on Microwave Propagation and Marine Boundary Layer, Monterey, California, USA.*

Liebe H.J., 1989: MPM - an atmospheric millimeter wave propagation model. *Int.J.Infrared Millim.Waves*, **10**, 631-650.

Liebe H.J. and G.A.Hufford, 1989a: Modeling millimeter-wave propagation effects in the atmosphere. *AGARD Conference Proceeding No 454, Atmospheric propagation in the UV, Visible, IR and mm-wave region and related system aspects*, 18-1 - 18-13.

Liebe H.J., T.Manabe, G.A.Hufford, 1989b: Millimeter-wave attenuation and delay rates due to fog/cloud conditions. *IEEE Trans. Antten. and Propagat.*, **AP-37**, 1617-1623.

Liebe H.J., G.A.Hufford, R.O.DeBolt, 1991: The atmospheric 60 GHz oxygen spectrum: modeling and laboratory measurements. *US Department of Commerce, NTIA Report 91-272.*

Liebe H.J., G.A.Hufford, M.G.Cotton, 1993: Propagation modeling of moist air and

suspended water/ice particles at frequencies below 1000 GHz. *AGARD Conference Proceedings 542,* 3-1 - 3-10.

Marks C.J.M. and C.D.Rodgers, 1993: A retrieval method for atmospheric composition from limb emission measurements. *J.Geoph.Res.*, **98**, D8, 14939-14953.

Mingelgin U., 1974: The microwave dispersion spectrum of O_2. *Mol.Phys.*, **28**, 1591-1602.

Pokrovsky O.M., Yu.M.Timofeyev, 1972: General statistical approach to solution of inverse problems of atmospheric optics. *Meteor. and Hydrol.*, 1, 72-81, (in Russian).

Polyakov A.V. and V.V.Rozanov, 1989: Iterative method to solve the nonlinear inverse problem with using *a priori* information. *Trudi GosNICPR*, 33, 99-103, (in Russian).

Polyakov A.V., 1995: On the matter of using *a priori* statistical information for solving the non-linear inverse problems of atmospheric optics. *Submitted to Invest. Earth from Space* (in Russian).

Promes P.M., T.J.Jackson, P.E.O'Neill, 1988: Significance of agricultural row structure on the microwave emissivity of soils. *IEEE Trans.Geosci.Rem.Sens.*, **26**, 5, 580-589.

Pullianen J. et al., 1990: Study of microwave interaction with the earth's surface. *Final Report under ESTEC Contract 8447/89/NL/PB(SC).*

Reale A.L., M.W.Chalfaut, R.V.Wagoner, T.J.Gardner, L.W.Casey, 1994: TOVS Operational sounding upgrades: 1990-1992. *NOAA Technical Report NESDIS 76, Washington, D.C., March 1994.*

Rodgers C.D., 1970: Remote sounding of the atmospheric temperature profile in the presence of cloud. *Quart. J. R. Met. Soc.*, **96**, 654-666.

Rodgers C.D., 1971: Some theoretical aspects of remote sounding in the Earth's atmosphere. *J.Q.S.R.T.*, **11**, 6, 767-777.

Rodgers C.D., 1976: Retrieval of atmospheric temperature and composition from remote measurements of thermal radiation. *Rev. Geophys.and Space Phys.*,**14**, 609-624.

Rodgers C.D., 1990: Characterization and error analysis of profiles retrieved from remote sounding measurements. *J. Geoph. Res.*, **95**, D5, 5587-5595.

Rosenkranz P.W, 1975: Shape of the 5mm oxygen band in the atmosphere. *IEEE Trans.Antennas Propagat.*, **AP-23**, 498-506.

Sasaki Y., I. Asanuma, K.Muneyama, G.Naito, and T.Suzuki, 1987: The dependence of sea-surface microwave emission on wind speed, frequency, incidence angle, and polarization over the frequency range from 1 to 40 GHz. *IEEE*

Trans.Geosci.Rem.Sens., **25**, 2, 138-146.

Sasaki Y., I. Asanuma, K.Muneyama, G.Naito, and T.Suzuki, 1988: Microwave emission and reflection from the wind-roughened sea surface at 6.7 and 18.6 GHz. *IEEE Trans.Geosci.Rem.Sens.*, **26**, 6, 860-868.

Shannon C.E. and W.Weaver, 1949: The Mathemetical Theory of Communication. *The University of Illinois Press.*

Stankevich K.S., 1974: Absorption of sub-millimeter-range radio waves in a dry atmosphere. *Radiophys. Quantum Electron.*, **17**, 579-581, (English Translation).

Stepanenko V.D., G.G.Schukin, L.P.Bobulev, S.Yu.Matrosov, 1987: Passive Remote Sensing in Meteorology. *Hydrometeoizdat, Leningrad* (in Russian).

Stogryn A., 1971: Equations for calculating the dielectric constant of saline water. *IEEE Trans.Microwave Theory and Techn.*, **MIT-19**, 733-736.

Strand O.N., and E.R. Westwater, 1968: The statistical estimation of the numerical solution of a Fredholm integral equation of the first kind. *J.Assoc.Compt.Mach.*, **15**, 100-114.

Timofeyev Yu.M., 1974: Using infrared and microwave outgoing radiance to retrieve of atmospheric vertical humidity profile. *Problems of Atmospheric Physics*, 12, 38-44, (in Russian).

Timofeyev Yu.M., E.M.Shulgina, Yu.V.Plochenko, A.B.Uspensky, 1994: Microwave and millimeter wave temperature and humidity atmospheric sounding, Phase I: The analysis of state-of-the-art. *Interim Report on Special Contract SPC-94-4086.*

Tosellini F.(ed.), 1989: Applications of remote sensing to agrometeorology. *ECSE, EEC, EAEC, Brussels and Luxembourg,* 257-284.

Turchin V.F., M.S.Malkevich, I.A.Gorchakova, 1968: Applying of statistical regularization method to retrieve atmospheric vertical temperature profile. *Atmosph. Oceanic Phys.*, **5**, 5, (English Translation).

Turchin V.F., and V.Z.Nozik, 1969: Statistical regularization for the solution of some incorrect problem. *Atmosph. Ocean. Phys.* **5**, 56 (English Translation).

Turchin V.F., V.P.Kozlov, M.S.Malkevich, 1970: Applying the methods of mathematical statistics for solving ill-posed problems. *Progress in Physical Sciences*, **102**, 3, 345-386 (in Russian).

Ulaby F.T., R.K.Moore, A.K.Fung, 1982: Microwave Remote Sensing. Active and Passive, **I, II**. *Addison-Wesley, Reading, Mass.*

Ulaby F.T., R.K.Moore, A.K.Fung, 1986: Microwave Remote Sensing. Active and Passive, vol.**III**. *Artech House, Dedham,1065-2162.*

Wang J.R., R.W.Newton, J.W.Rouse, 1980: Passive microwave remote sensing of soil moisture: The effect of tilled row structure. *IEEE Trans.Geosci.Rem.Sens.*, **GE-18,**

296-302.

Waters J.W., and S.C.Wofsy, 1978: Application of high resolution passive microwave satellite systems to the stratosphere, mesosphere and lower thermosphere. *Ch.7 in High Spectral Resolution Passive Microwave Satellites, Applications Review Panel Final Report, Mass. Inst. Technol., Cambridge.*

Westwater E.R., and Strand O.N., 1970: Statistical information content of radiation measurements used in indirect sensing. *J.Atm.Sci.*, **25**, 12, 750-758.

Wilheit T.T., 1979: A model for microwave emissivity of the ocean's surface as a function of wind speed. *IEEE Trans. Geosci. Elect.*, **GE-17**, 244-249.

Wilheit T. and A.Chang, 1980: An algorithm for retrieval of ocean surface and atmospheric parameters from the observations of the scanning multichannel microwave radiometer. *Radio Sci.*, **15**, 3, 525-544.